DISCLAIMER

This report was prepared as an account of work sponsored by an agency of the United States Government. Neither the United States Government nor any agency thereof, nor any of their employees, makes any warranty, express or implied, or assumes any legal liability or responsibility for the accuracy, completeness, or usefulness of any information, apparatus, product, or process disclosed, or represents that its use would not infringe privately owned rights. Reference herein to any specific commercial product, process, or service by trade name, trademark, manufacturer, or otherwise does not necessarily constitute or imply its endorsement, recommendation, or favoring by the United States Government or any agency thereof. The views and opinions of authors expressed herein do not necessarily state or reflect those of the United States Government or any agency thereof. Reference herein to any social initiative (including but not limited to Diversity, Equity, and Inclusion (DEI); Community Benefits Plans (CBP); Justice 40; etc.) is made by the Author independent of any current requirement by the United States Government and does not constitute or imply endorsement, recommendation, or support by the United States Government or any agency thereof.

SANDIA REPORT
SAND2025-11078
Printed September 2025

Sandia National Laboratories

Fire and Thermal Experiments in Support of the Model Evaluation Protocol for LNG Facility Fires

Anay Luketa, Shane Adee, Ray Allen, and Alvaro Cruz-Cabrera

Prepared by
Sandia National Laboratories
Albuquerque, New Mexico
87185 and Livermore,
California 94550

Issued by Sandia National Laboratories, operated for the United States Department of Energy by National Technology & Engineering Solutions of Sandia, LLC.

Available to DOE and DOE contractors from
U.S. Department of Energy
Office of Scientific and Technical Information
P.O. Box 62
Oak Ridge, TN 37831

Telephone: (865) 576-8401
Facsimile: (865) 576-5728
E-Mail: reports@osti.gov
Online ordering: http://www.osti.gov/scitech

Available to the public from
U.S. Department of Commerce
National Technical Information Service
5301 Shawnee Rd
Alexandria, VA 22312

Telephone: (800) 553-6847
Facsimile: (703) 605-6900
E-Mail: orders@ntis.gov
Online order: https://classic.ntis.gov/help/order-methods/

ABSTRACT

The motivation for the experiments reported here pertains to the siting of Liquefied Natural Gas (LNG) facilities which requires assessing the potential adverse radiant thermal impacts of accidental fires on the public. The objective is to obtain data on jet fires, pool fires, fireballs, and concrete walls that could serve as thermal barriers for model validation. The fuels tested include ethane, ethylene, propane, and isopentane. The jet fires are considered moderate in scale with projected flame lengths up to 17.3 m and exit mass flow rates up to 2.3 kg/s. The pool fires and fireballs are considered large scale with a pool diameter of 5-m and maximum effective diameter up to 78 m, respectively. Measurements for the fire experiments include flame geometry, heat flux external to the fire, surface emissive power, and in the case of fireballs, rise height and duration. Data is also collected for model parameter inputs such as atmospheric conditions that include wind speed, wind direction, temperature, pressure, and relative humidity, as well as characteristics of the fuel supply conditions.

ACKNOWLEDGEMENTS

The authors would like to thank the Pipeline and Hazardous Materials Safety Administration (PHMSA) for sponsoring this work.

The authors would also like to thank the technologist team of:

- The Fire Science and Technology department that includes Carl Fitzgerald, Daniel Roybal, Donald McManaway, Travis Fitch, Marc Armijo, Randy Foster, Paul Garcia and Sean Altamirano

- The supporting technologists that include Dominica Toers-Bijns and Michael Montoya

- The photometric support by Michael Ludwig and Ed Bystrom

- The arming and firing operations team that include Wes Kuhns, Brent DeMone, Ben Sanchez, and Venner Saul for explosive applications.

CONTENTS

LIST OF FIGURES

LIST OF TABLES

ACRONYMS AND TERMS

Acronym/Term	Definition
DAQ	Data Acquisition System
DOT	US Department of Transportation
FDS	Fire Dynamics Simulator
IMDG	International Maritime Dangerous Goods
IMO	International Maritime Organization
IR	Infrared
ISO	International Organization for Standardization
LFL	Lower Flammability Limit
LN_2	Liquefied Nitrogen
LNG	Liquefied Natural Gas
LSC	Linear shaped charge
MAWP	Maximum Allowable Working Pressure
MEP	Model Evaluation Protocol
MWIR	Mid-Wave Infrared
N_2	Gaseous Nitrogen
NI	National Instruments
NIST	National Bureau of Standards and Technology
PHMSA	Pipeline and Hazardous Materials Safety Administration
SEP	Surface Emissive Power
TC	Thermocouple

This page left blank

1. INTRODUCTION

The motivation for the fire experiments reported here is related to the siting of Liquefied Natural Gas (LNG) facilities, which requires assessing the potential adverse radiant thermal impacts of accidental fires on the public. The assessment is conducted using models that predict heat flux as a function of distance. Per federal regulations with oversight by the Pipeline and Hazardous Materials Safety Administration (PHMSA), models must first be approved for use for such analysis. Part of the approval process involves comparison to experimental data as provided in a Model Evaluation Protocol (MEP) that includes large-scale pool fires, jet fires, and fireballs for LNG and processing fuels stored at facilities [1]. The MEP provides a methodology to assess a model's overall performance as well as criteria for a factor of uncertainty. The objective of the fire experiments reported here is to obtain data for model validation.

To carry out the objective, a series of jet fires, pool fires, and fireballs experiments are performed using fuels that include ethane, ethylene, propane, and isopentane. The fuels tested are involved in the processing of LNG and are stored at facilities. These types of fires can occur from accidental releases arising from various failure modes such as from fittings, valves, impact from machinery or tools, environmental hazards such as lightning, and other causes. In addition to the fire experiments, data on the thermal response of concrete walls that could serve as thermal barriers is collected. The motivation for the wall experiments is due to the potential for current LNG facilities requiring the installation of radiant thermal barriers to satisfy the factor of uncertainty criteria within the MEP. These facilities were built before the MEP for fires was developed, hence the potential need for thermal barriers.

For the fire experiments, the key measurements obtained for model comparison are flame geometry, heat flux external to the fire, surface emissive power, and in the case of fireballs, also rise height and duration. Data is also collected for model parameter inputs such as atmospheric conditions that include wind speed, wind direction, temperature, pressure, and relative humidity, as well as characteristics of the fuel supply conditions. The wall tests include collecting thermal response data for an insulated formed wall and an insulated masonry block wall.

The distinguishing features that classify these types of fires are whether the release and flow field is dominated by momentum or buoyancy forces, the mixing rate of fuel and oxidant relative to chemical reaction rates, flame shape, and duration. For diffusion flames, chemical reaction rates are orders of magnitude faster than the mixing rate of fuel and oxidant and thus the fuel consumption rate is termed 'mixing limited'. In contrast, the fuel consumption rate for premixed flames is not mixing limited since fuel and oxidant are already mixed. All the fires studied here are considered diffusion flames though they have different mixing rates.

Jet fires are high pressure releases that are momentum dominated and their duration can vary depending upon the size of the release and fuel reservoir. Due to the high-pressure release, their shapes are highly elongated, and their orientation can vary in angle between purely horizontal or vertical directions depending on the location of the release. Also, their fuel consumption rate is relatively high due to high mixing rates and large differences in release and atmospheric pressures that can result in sonic conditions. The main concern regarding jet fires is their ability to cause failure to nearby equipment due to thermal weakening from impingement. In contrast, the flow field of pool fires are buoyancy dominated and their release orientation is vertical.

Pool fires can result from spillage of fuel that can be either contained such as within a berm or uncontained allowing the fuel to spread freely. Their duration will depend upon the amount of fuel involved, wind conditions, and spillage surface. Higher wind speeds tend to increase the rate of

burning resulting in a shorter duration fire. The material comprising the spillage surface such as concrete, soil, rocks, or water will also affect the burn rate and hence duration. Their rate of fuel consumption is much lower than either jet fires or fireballs since turbulence induced mixing is much lower due to their lower momentum flow fields. Pool fires can cause thermal weakening to nearby equipment but typically will take longer to cause failure than a jet fire. They typically have larger thermal hazard zones compared to jet fires due to having a larger area of fuel supplying the fire. This results in a larger flame and hence greater area of thermal impact. Thus, the concern of thermal impact from pool fires is both near and far field.

Fireballs are high-pressure releases with flow fields initially momentum driven and then subsequently buoyancy driven. They can result from the over pressurization of a tank from rising temperatures induced by a nearby fire as well as from the breach of pressurized tanks. Their shape is approximately symmetrical in the vertical direction as they evolve due to the orientation of releases which are typically vertical or semi-spherical. In addition to thermal hazards, high-speed projectiles are thrown far distances from an over pressurized failed tank which can result in injury or death and damage to nearby equipment. Their fuel consumption rate is on the order of 10s of seconds due to the high rate of mixing by induced turbulence from large pressure differences and rapid phase change immediately upon release. The rapid phase change can result in a shock wave with the severity of damage dependent on the thermodynamic state and amount fuel released from a failed tank. The rapid phase change is due to an immediate change in thermodynamic state where the fuel is mostly in liquid form within the tank due to the tank's pressure and temperature but then rapidly converts to a state of atomized liquid and gas when released to atmospheric pressures. This results in rapid consumption of fuel and hence high heat release rates causing buoyancy forces to dominate as the fire evolves from the release point. At this point in its evolution the propagation of the fireball as it expands is at speeds on the order of 10 m/s which do not cause damaging overpressures. Due to the high buoyancy forces the fireball rises to relatively high heights. Fireballs are also characterized by very large effective diameters due to the high expansion in volume in changing from mostly a liquid to gaseous state.

The following first describes a description of the experimental set-up, followed by specification of the instrumentation, the results, comparison and discussion of the results, and a summary of key findings.

2. EXPERIMENTAL DESCRIPTION OF FIRE EXPERIMENTS

Table 2-1 provides the number of experiments performed for each fire type while Table 2-2 provides the amount of fuel used for each experiment. Table 2-3 provides the boiling points and density of the fuels. Note that ethane and ethylene are cryogenic fuels since their temperatures are below -90°C, while propane and iso-pentane are non-cryogenic fuels. The composition of the fuels is provided in the appendix, section A.3.

Table 2-1: Experimental matrix for fire experiments

	Fuels			
	Ethane	Ethylene	Propane	Iso-pentane
Fire type	Number of experiments			
Pool fire	1	1	1	1
Jet fire	1	1		1
Fireball	1	1		1

Table 2-2: Amount of fuel used for fire experiments.

Fuel	Amount m^3 (gallons)			Total Amount m^3 (gallons)
	Jet fires	Pool fires	Fireballs	
Ethane	1.6 (410)	9.7 (2570)	2.1 (560)	15.1 (3980)
Ethylene	1.3 (340)	5.7 (1510)	2.0 (535)	15.0 (3960)
Propane		5.7 (1515)		9.1 (2400)
Iso-pentane	1.6 (420)	5.3 (1400)	1.9 (490)	11.8 (3110)

Table 2-3: Boiling points and densities

Fuel	Normal Boiling Point (C)	Density* (kg/m3)
Ethane	-89.2	547
Ethylene	-104.2	568
Propane	-42.1	508
Iso-pentane	27.8	623

*As provided by supplier

Note that the original test matrix included an anhydrous ammonia pool fire and jet fire and a hydrogen sulfide jet fire. Past researchers have found that ammonia cannot maintain a stable flame due to its high ignition temperature (1100 K), relatively high lower flammability limit (LFL=16.6%), low flame propagation speed, low heating value, and low flame temperature [2] [3]. Evidence of this is flaring systems for ammonia at processing facilities which require special features to ensure the flame is maintained. These includes creating a premixed state, the use of a windshield to prevent dilution below the LFL, and multiple strategically placed pilot flames that must be continually active. An accident scenario would not have these features. Consequently, a jet fire and pool fire would be difficult to achieve. To confirm previous researcher's findings a small-scale test with ammonia was performed

using a 1'x1'x1' square gas burner. This exploratory test is described and discussed in the appendix, section A.2. It was found that the ammonia flame could not be sustained, thus the ammonia pool and jet fire were removed from the test matrix.

One of the combustion products of burning hydrogen sulfide is sulfur dioxide which is toxic if inhaled. To assess the extent that a sulfur dioxide cloud could travel, the computational fluid dynamics code, Fire Dynamics Simulator (FDS), developed by the National Institute of Standards and Technology (NIST) was used for simulating a hydrogen jet fire with a mass flow rate of 3 kg/s. The results indicate the cloud would impact the control room at the test facility thereby posing a significant safety hazard. Based on the simulation results the hydrogen sulfide jet fire was removed from the test matrix.

2.1. Experimental Configuration

The jet and pool fire experiments use the same fuel delivery system which involves using nitrogen to drive fuel out of a 20' International Organization for Standardization (ISO) container to a 3" diameter, 100' long pipeline. Each fuel is delivered by the supplier in separate ISO containers placed on a trailer chassis. The containers are approved by ASME Section VIII Div 1, the International Maritime Dangerous Goods (IMDG)/International Maritime Organization (IMO), and the US Department of Transportation (DOT). The ethylene and ethane are stored in ISO T-75 tanks which are rated for refrigerated cryogenic liquids and have a maximum allowable working pressure (MAWP) of 145 psig. The iso-pentane and propane are stored in an ISO T-11 (MAWP 58 psig) tank and ISO T-50 (MAWP 290 psig) tank, respectively.

Cryogenic fuels can cause brittle fracture in low carbon steels, thus metals rated for cryogens are required such as austenitic stainless steels (e.g. 304, 316), some aluminum alloys, and certain copper and nickel-based alloys. Thus, the fuel discharge and nitrogen supply systems are rated for cryogenic service. The pipeline is constructed of 3" diameter, schedule 40, 304 stainless-steel with a system MAWP of 600 psig @100F. A stainless-steel braided hose 8' in length, 3" in diameter, and MAWP of 720 psig, is part of the 3" piping system to allow for contraction and expansion during the ethane and ethylene tests. The piping and instrumentation diagram for the discharge line is provided in the appendix, section A.1. The piping and instrumentation are designed using the software package, UniSim Design®.

The nitrogen gas is produced via a vaporizer connected to a 1000-gallon cryogenic tank that contains liquefied nitrogen (LN_2). The LN_2 system is constructed of a combination of 1" and ½" stainless steel tubing and 1" 304 stainless steel, schedule 80, threaded piping and fittings, as well as cryogenic rated stainless-steel valves. In addition to being used to drive fuel out of the ISO tanks, the gaseous nitrogen is used to control pneumatic actuators and purge oxygen from the discharge line prior to testing. The LN_2 is used to cool the discharge line prior to releasing cryogenic fuels for all pool and jet fire experiments to reduce vapor production in the line during testing since the intent is to maintain a liquid state. The LN_2 is also used to pre-cool the concrete pool prior to release of cryogenic fuels for the pool fire experiments.

The nitrogen gas pressurizes the ISO container to about 20 psi above the current storage pressure but is maintained at a lower pressure than the MAWP. For the jet fires, the level of pressurization of the ISO container is based on providing adequate driving pressure to maintain a liquid state in the pipeline for the cryogenic fuels while achieving the desired fuel flow rates of approximately 3 kg/s.

The ISO container for ethane, the spherical LN_2 tank, vaporizer, and discharge line is shown in Figure 2-1. This is representative of the set up for all jet and pool fire tests, except for the iso-pentane jet fire. A close-up view of the ISO tank showing the hose connections for the fuel and pressurized N_2 is

shown in Figure 2-2. As shown in Figure 2-3, the discharge line is supported on stands with rollers to allow for free expansion and contraction that occurs due to the very low temperature of the cryogens. Corrugated steel sheeting is placed at locations where the pipeline is supported by the stands to allow for roller movement. To reduce vaporization of the cryogenic fuels, 4" thick FOAMGLAS® is placed around the discharge line. The FOAMGLAS® is then covered with a layer of insulation blanket followed by foil to provide thermal protection from the fires.

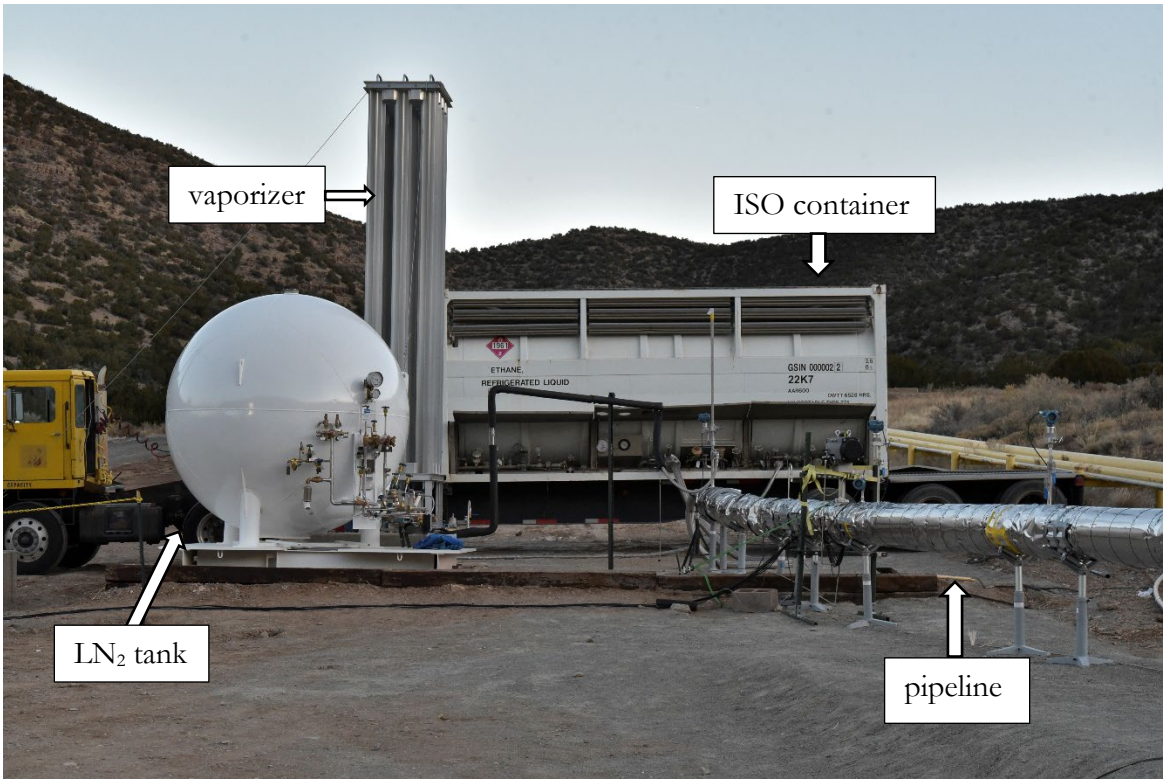

Figure 2-1: ISO container for ethane, spherical tank containing LN_2, and vaporizer.

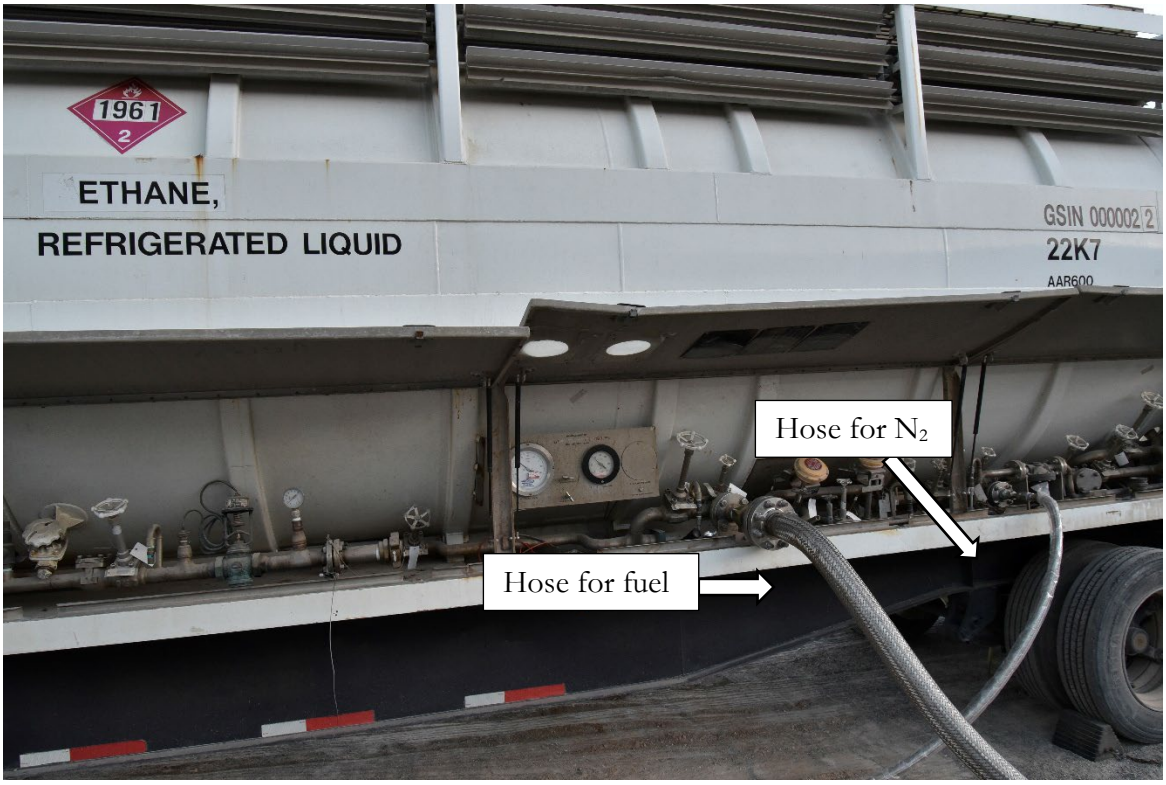

Figure 2-2: Flex hose connections for fuel supply and nitrogen.

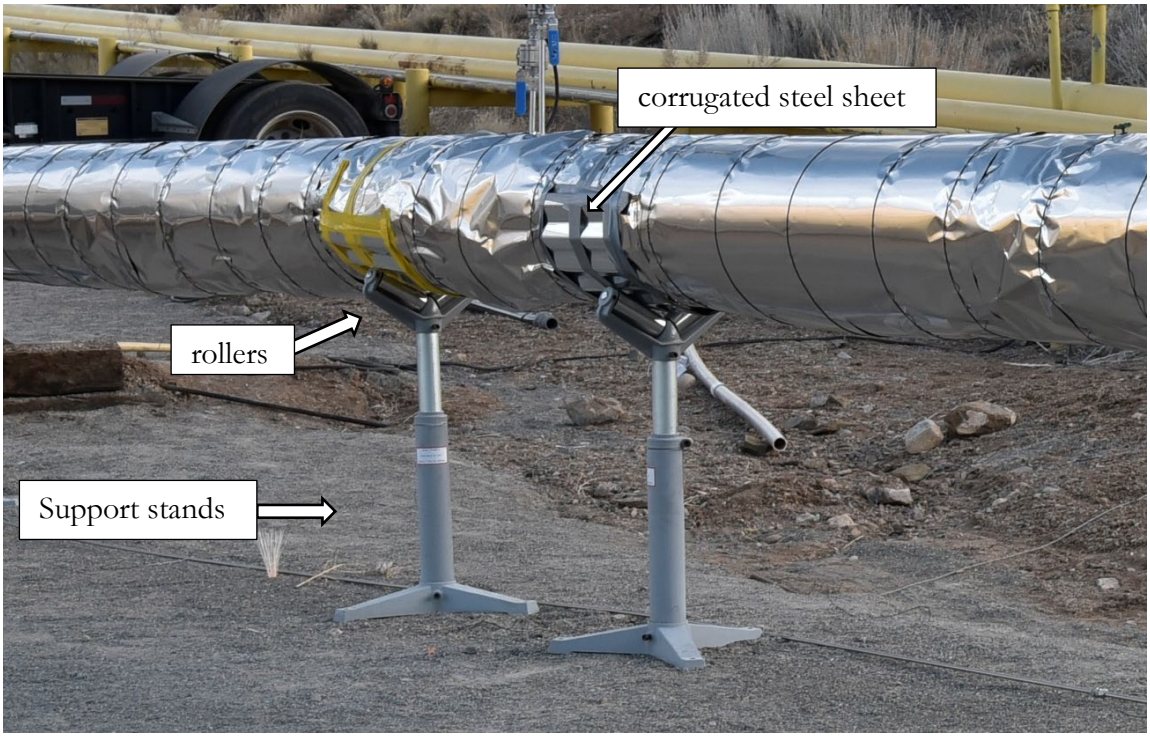

Figure 2-3: Pipeline support stands with rollers and corrugated steel sheet placed around pipe.

For the iso-pentane jet fire experiment, a propane tank is used to contain the fuel. Approximately 500 gallons of iso-pentane is transferred to a 1150-gallon vertical propane tank which is pressure rated for 250 psig. Utilizing the propane tank is necessary since the MAWP of the T-11 ISO container is 58 psig which is below the required pressure of approximately 100 psig to achieve the desired flow rate of 3 kg/s. Figure 2-4 shows the propane tank placed next to the LN_2 tank and vaporizer.

Figure 2-4: Arrangement of iso-pentane jet fire experiment with the 1150-gallon vertical propane tank next to the 1000-gallon spherical LN_2 tank and vaporizer.

The same discharge line and nitrogen system described above is utilized for both the jet and pool fire experiments but with some modifications. The jet fire tests are performed with a plate with a 5/8" diameter orifice placed at the end of the pipeline which is not in place for the pool fires (Figure 2-5). The distance from the ground to the orifice is approximately 3.4'. Another difference is that the pool fire tests require a 20' extension of 3" Schedule 40 stainless steel piping to the end of the discharge line. A 48" long, 3" diameter stainless-steel braided hose (MAWP 720 psig) is connected to this addition with the other end connected to a diffuser to prevent splashing (Figure 2-6). The diffuser is approximately 1' in diameter, 3.5' in height, and 2" above the bottom of the pool. The open pipe at its top which allows vapor to escape is approximately 3" in diameter and 1' in length.

Also shown in Figure 2-6 are three bubblers or diptubes which are used to indicate liquid level. The open end of the tube is placed vertically about 1/2" from the bottom of the pool and placed 1.5' from the edge of the pool to minimize the effect of turbulence induced by boiling at the side walls.

Compressed nitrogen gas is introduced into the diptubes to ensure that they are free of liquid and filled with gas. A pressure transducer is connected to the top of the diptube to measure the pressure of the nitrogen gas inside the tube which is equivalent to the hydrostatic pressure of the liquid fuel which is below 1 psi for anticipated fuel depths. The pressure measured by the pressure transducer is directly related to the height of the liquid column using a calibration curve developed by using water. The pressure is recorded at heights up to 10" in increments of 1" using water to generate a curve of pressure versus height. For a given pressure reading during testing the corresponding height on the calibration curve can then be identified. This calculated height is then multiplied by the ratio of the density of the fuel to the density of water to determine the height of the fuel.

Figure 2-5: Orifice at the end of the pipeline for the jet fire experiments.

Figure 2-6: Diffuser attached to pipeline for pool fire experiments.

All pool fire tests utilize a concrete pool due to the low temperatures of liquid ethane, ethylene, and propane. A carbon steel pan will undergo brittle fracture at temperatures below approximately -50°C. While a stainless-steel pan will not undergo brittle fracture at cryogenic temperatures, the thermal stresses resulting from the large temperature gradient introduced by the liquid cryogen and fire would jeopardize its structural integrity. The concrete pool is 16'5" (5-m) in diameter as shown in Figure 2-7 and has an inner and outer pool made of lightweight and normal concrete, respectively. The lightweight concrete acts as an insulator due to its thermal properties which reduces the rate of vaporization when introducing fuel into the pool.

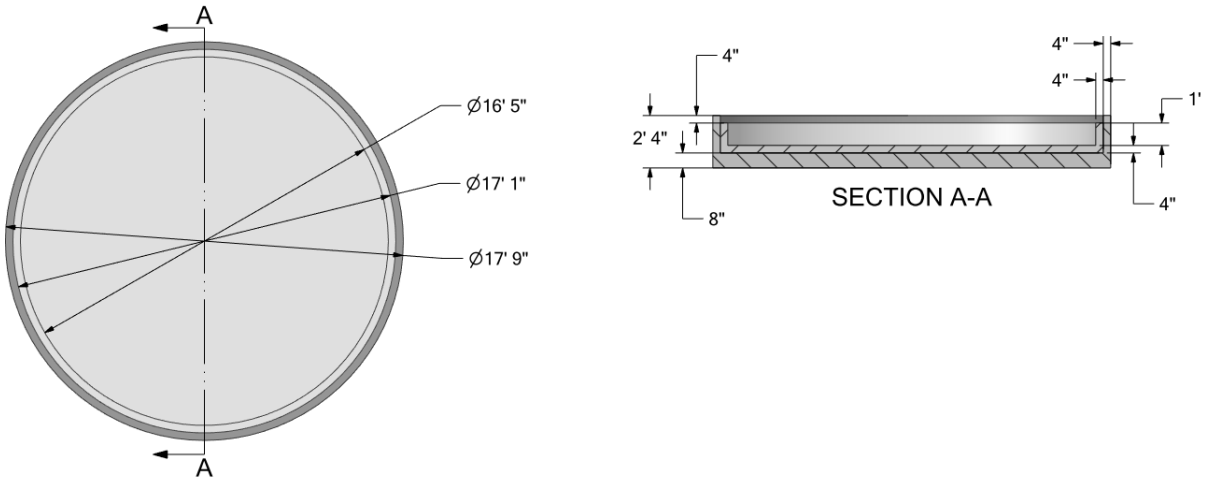

Figure 2-7: Concrete pool for pool fire experiments.

To carry out the fireball experiments, the pipeline infrastructure, N_2 storage tank, and vaporizer are dismantled and removed from the test site since these experiments require a different configuration. Refurbished tanks built in accordance with the American Society of Mechanical Engineers (ASME) pressure vessel code are used for the ethane and ethylene fireball experiments. These tanks are constructed with an inner tank (48" diameter) and an outer tank (60" diameter) and are vacuum sealed and insulated with loose-fill perlite to maintain a liquid state. They have a capacity of 900 gallons and are approximately 10' in height. Figure 2-8 shows one of the vertical cryogenic tanks as well as the tank used to contain LN_2. The iso-pentane experiment uses a new 1150-gallon vertical propane tank that is 48" in diameter, approximately 11' in height, and is single walled with no insulation. This is the same tank used to carry out the iso-pentane jet fire experiment. The cryogenic tanks and propane tank have a MAWP of 219 psig and 250 psig, respectively.

During fireball testing, the tanks are surrounded by concrete blocks and steel barricades to reduce the distance that fragments are thrown, and to prevent the tank becoming horizontal due to potential asymmetrical forces that occur during release. Also, one end of a chain is attached to one lifting lug on top of the tank and the other end attached to a 30,000 lb. concrete block to cause the tank lid to be thrown in a direction away from personnel and critical infrastructure after opening the tank with linear shaped charges as described in section 2.3.

Figure 2-8: Vertical cryogenic tank for fireball experiments and LN_2 tank.

2.2. Instrumentation

The following sections 2.2.1 through 2.2.6 provide a description of the data acquisition system, heat flux gauges, photometric equipment, flow rate instruments, pipeline pressure and temperature instruments, and weather instruments.

2.2.1. Data acquisition system

The data acquisition system (DAS) uses National Instruments hardware and LabView software. The system consisted of a PC with a data acquisition card connected to a National Instruments (NI) SCXI-1320 chassis. The chassis is a hardware component that serves as a housing for various types of modules, such as data acquisition (DAQ) devices, signal conditioning modules, and other specialized instruments. Modules are individual hardware components that can be inserted into the chassis and are designed for particular measurements. Through the chassis, modules can work together to create a complete measurement system. The module, SCXI-1125, is used to collect data from voltage, current, temperature, and pressure sensors and other input devices.

A high accuracy calibrator, Fluke 5730A, is used to verify that the system is reading the channels correctly and to quantify the system uncertainty due to cabling, electronics, and software using a known range of input voltages. The system measurement are errors then analyzed channel-by-channel. If any channel is found to be outside of tolerance, the data from that channel is excluded from the final analysis.

2.2.2. Heat flux gauges

A total of 40 heat flux gauges, manufactured and calibrated by Hukseflux, are used for each fire test series. The gauges are wide-angle with a field of view angle of 180° and measure both radiative and convective heat transfer and thus are total heat flux gauges. Their thermopile sensor uses a combination of Gardon and Schmidt-Boelter designs with a measurement range of 50 kW, a response time below 25 ms, a time constant of 63%, and a black coating with an emissivity above 0.95. Since they require water cooling, water in containers is supplied to groupings of five gauges using a submergible pump placed within each container during testing. Table 2-4 provides the measurement uncertainty for each gauge with a 95% confidence interval based on calibration from the manufacturer. For the heat flux gauges the DAQ system indicated a ±0.1% uncertainty.

Note that the sensivity coefficient which is a factor reported by the manufacturer for each gauge allowing for conversion of voltage readings to a heat flux based on calibration is applicable to incident radiation only and does not include convection. For heat flux gauges not in close proximity to the fire the convective contribution to the heat flux is small compared to the radiative contribution. However, for gauges near or in a fire, convection can become more significant due to flow induced by buoyancy forces. Also, for gauges in the fire or within close proximity soot can sometimes adhere to the face of the gauge because the water cooling keeps the gauge surface at a temperature where both soot and water vapor can foul the gauge. For gauges in the fire uncertainties can be up to ±39% for low wind conditions [4]. Potenially effected gauges are identified in section 3 which provides the results for each experiment.

The heat flux gauge arrangement and their distances from the release point (0, 0) for the jet fires experiments is provided in Figure 2-9 and Table 2-5, respectively. For the pool fire experiments, the heat flux gauge arrangement and their distances from the center of the pool (0, 0) is provided in Figure 2-10 and Table 2-6, respectively. Finally, the heat flux gauge arrangement and their distances from the

center of the release point (0, 0) for the fireball experiments is provided in Figure 2-11 and Table 2-7, respectively. This is the optimum arrangement for the fireball experiments given the limitations of the terrain surrounding the test facility and the gauge's measurement range. The gauges were aimed horizontal at 90° for the jet and pool fire experiments, and angled 45° upward from horizontal for the fireball experiments.

Table 2-4: Measurement uncertainty of heat flux gauges

Gauge number	Uncertainty (%) (radiation only)
1	5.7
2	5.6
3	5.7
4	5.7
5	5.6
6	5.5
7	5.4
8	5.8
9	5.6
10	5.5
11	5.7
12	5.5
13	5.5
14	5.4
15	5.5
16	5.4
17	5.7
18	5.8
19	5.4
20	5.4
21	5.5
22	5.5
23	5.6
24	5.5
25	5.6

Gauge number	Uncertainty (%) (radiation only)
26	5.7
27	5.7
28	5.4
29	5.7
30	5.6
31	5.5
32	5.8
33	5.5
34	5.6
35	5.8
36	5.7
37	5.6
38	5.6
39	5.7
40	5.4

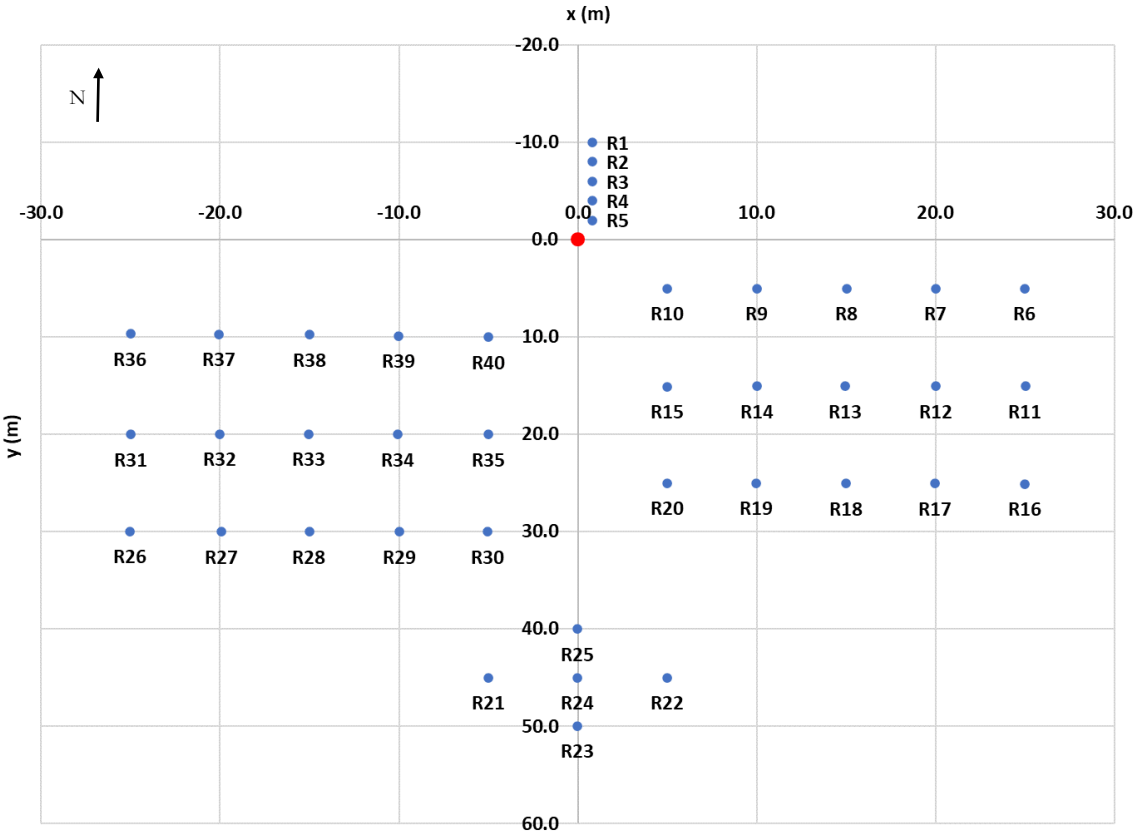

Figure 2-9: Layout of heat flux gauges for the jet fire experiments.

Table 2-5: Jet fire experiments: locations of heat flux gauges relative to center of release point

Heat flux gauge	x (m)	y (m)	z (m)
R1	0.8	-10.0	1.19
R2	0.8	-8.0	1.17
R3	0.8	-5.9	1.10
R4	0.8	-4.0	1.08
R5	0.8	-2.0	1.05
R6	25.0	5.0	0.67
R7	20.0	5.0	0.65
R8	15.0	5.0	0.59
R9	10.0	5.0	0.63
R10	5.0	5.0	0.60
R11	25.0	15.1	0.57
R12	20.0	15.0	0.56

Heat flux gauge	x (m)	y (m)	z (m)
R13	14.9	15.1	0.53
R14	10.0	15.1	0.47
R15	5.0	15.1	0.47
R16	25.0	25.1	0.45
R17	20.0	25.0	0.41
R18	15.0	25.0	0.41
R19	10.0	25.0	0.40
R20	5.0	25.0	0.38
R21	-5.0	45.0	-0.30
R22	5.0	45.0	-0.11
R23	0.0	50.0	-0.26
R24	0.0	45.0	-0.20
R25	0.0	40.0	-0.09
R26	-25.0	30.0	-0.34
R27	-19.9	30.0	-0.26
R28	-15.0	30.0	-0.16
R29	-10.0	30.0	-0.09
R30	-5.1	30.0	0.13
R31	-25.0	20.0	-0.12
R32	-20.0	20.0	-0.08
R33	-15.0	20.0	0.01
R34	-10.1	20.0	0.27
R35	-5.0	20.0	0.27
R36	-25.0	9.7	-0.05
R37	-20.1	9.7	0.04
R38	-15.0	9.8	0.08
R39	-10.0	9.9	0.48
R40	-5.0	10.0	0.32

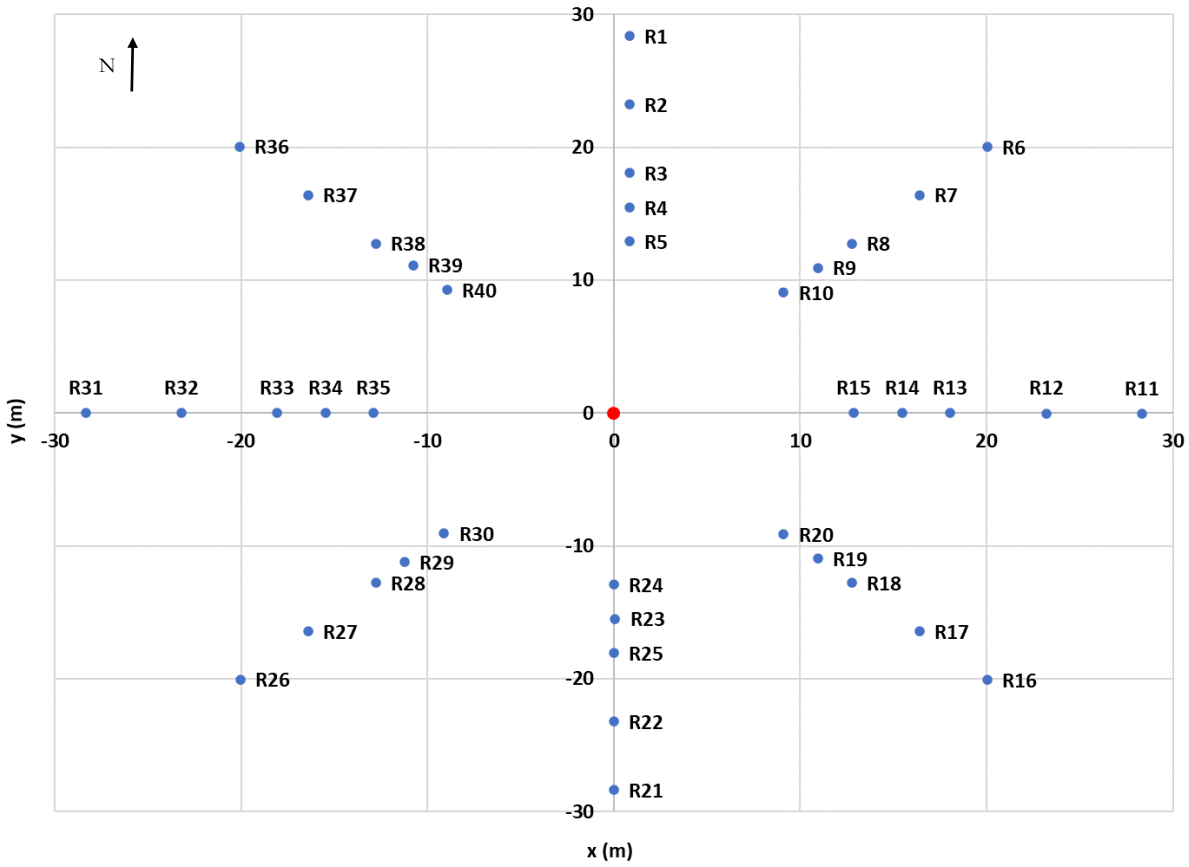

Figure 2-10: Layout of heat flux gauges for the pool fire experiments.

Table 2-6: Pool fire experiments: locations of heat flux gauges relative to center of pool

heat flux gauge	x (m)	y (m)	z (m)
R1	0.9	28.4	1.30
R2	0.8	23.2	1.21
R3	0.8	18.0	1.15
R4	0.9	15.5	1.11
R5	0.8	12.9	1.07
R6	20.1	20.0	2.87
R7	16.4	16.4	0.81
R8	12.8	12.7	0.65
R9	10.9	10.9	0.65
R10	9.1	9.1	0.64
R11	28.3	0.0	0.63

heat flux gauge	x (m)	y (m)	z (m)
R12	23.2	0.0	0.58
R13	18.1	0.0	0.58
R14	15.5	0.0	0.55
R15	12.9	0.0	0.52
R16	20.1	-20.1	0.35
R17	16.4	-16.4	0.36
R18	12.8	-12.8	0.40
R19	10.9	-10.9	0.36
R20	9.1	-9.1	0.33
R21	0.0	-28.3	-0.13
R22	0.0	-23.2	0.03
R23	0.1	-15.5	0.26
R24	0.0	-12.9	0.27
R25	0.0	-18.1	0.25
R26	-20.0	-20.0	-0.29
R27	-16.4	-16.4	-0.22
R28	-12.8	-12.8	0.05
R29	-11.2	-11.2	0.17
R30	-9.1	-9.1	0.29
R31	-28.3	0.0	-0.08
R32	-23.2	0.0	0.00
R33	-18.1	0.0	0.07
R34	-15.5	0.0	0.10
R35	-12.9	0.0	0.12
R36	-20.1	20.1	0.56
R37	-16.4	16.4	0.52
R38	-12.8	12.8	0.46
R39	-10.7	11.1	0.42
R40	-9.0	9.3	0.39

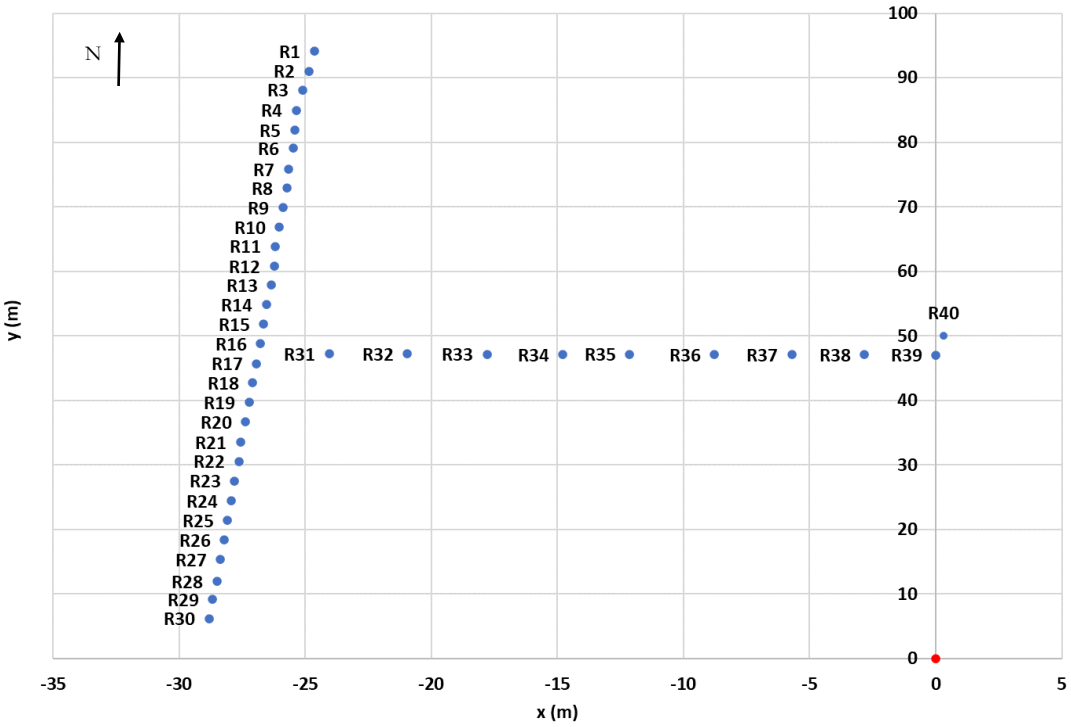

Figure 2-11: Layout of heat flux gauges for the fireball experiments.

Table 2-7: Fireball experiments: locations of heat flux gauges relative to fuel release location

heat flux gauge	x (m)	y (m)	z (m)
R1	-24.6	94.1	4.5
R2	-24.8	91.0	4.3
R3	-25.1	88.1	4.2
R4	-25.3	85.0	4.1
R5	-25.4	81.9	3.8
R6	-25.5	79.1	3.6
R7	-25.7	75.8	3.4
R8	-25.7	72.9	3.0
R9	-25.9	69.9	2.6
R10	-26.0	66.8	2.4
R11	-26.2	63.9	2.2
R12	-26.2	60.8	2.0
R13	-26.4	57.9	1.9

heat flux gauge	x (m)	y (m)	z (m)
R14	-26.5	54.9	1.8
R15	-26.6	51.8	1.7
R16	-26.8	48.8	1.6
R17	-26.9	45.7	1.5
R18	-27.1	42.7	1.5
R19	-27.2	39.7	1.4
R20	-27.4	36.6	1.3
R21	-27.6	33.5	1.2
R22	-27.6	30.5	1.2
R23	-27.8	27.5	1.1
R24	-27.9	24.5	1.0
R25	-28.1	21.4	0.9
R26	-28.2	18.4	0.9
R27	-28.4	15.3	0.8
R28	-28.5	12.0	0.7
R29	-28.7	9.2	0.7
R30	-28.8	6.2	0.6
R31	-24.1	47.2	1.6
R32	-20.9	47.2	1.8
R33	-17.8	47.1	1.8
R34	-14.8	47.1	1.8
R35	-12.1	47.1	1.9
R36	-8.8	47.1	1.9
R37	-5.7	47.1	2.1
R38	-2.8	47.1	2.2
R39	0.0	47.0	2.3
R40	0.3	50.1	2.6

2.2.3. Photometric

For the jet fire experiments, cameras are located at stations in the east, south, and west cardinal directions as shown in Figure 2-12. Three cameras, one infrared (IR) and two non-IR, are located at the east station, 58 m from the fuel release point and denoted as station 1. The IR camera, FLIR X6901sc, is a mid-wave infrared (MWIR) camera and is used to obtain surface emissive power. The two non-IR cameras, Phantom VEO4k 990 and Blackmagic 4k, are used to obtain fire dimensions. The Phantom VEO4k 990 is synchronized at 15 fps using the MWIR camera to provide non-IR imagery. The Blackmagic 4k camera provides a wider view and serves as a backup for measurement of fire dimensions.

A second Blackmagic is placed at the south station approximately 32 m from the fuel release point and monitors the on-axis/off-axis behavior of the jet fire. During the isopentane jet fire, the flame shifted out of the field of view due to the wind. Thus, the zoom setting was adjusted for the subsequent ethane and ethylene experiments. A 6k Z-camera is placed at the west station approximately 34 m from the release point to provide a real-time monitoring of the west side of the jet fire. Note that when wind conditions cause the flame to angle from its horizontal axis, this camera complements the camera set at the east station. The specification for all cameras is provided in Table 2-8.

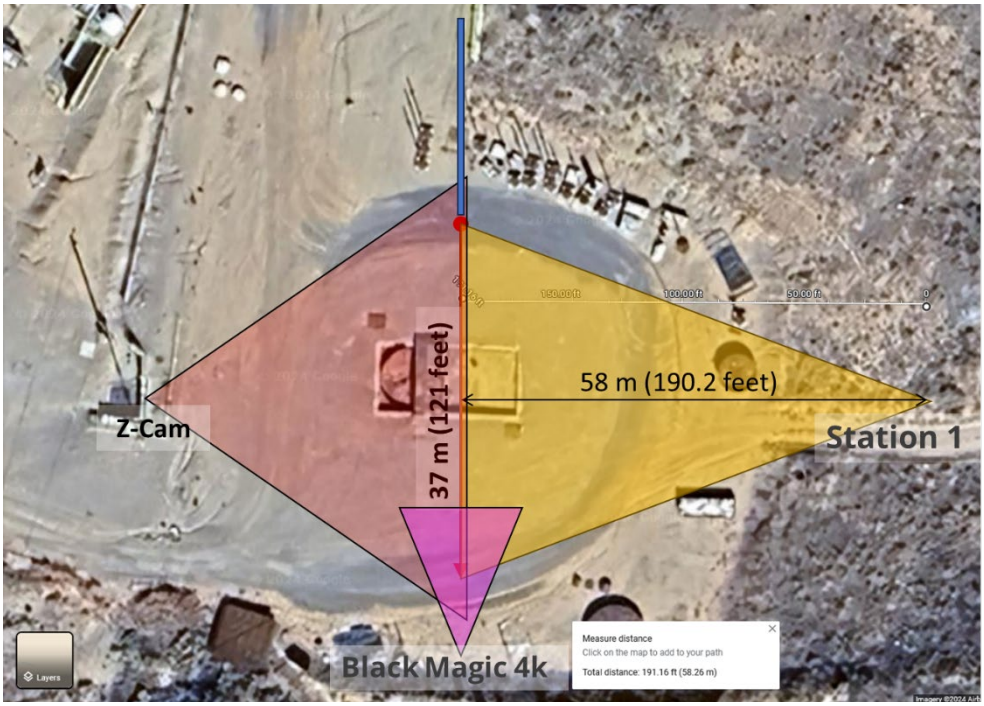

Figure 2-12: Camera layout for jet fire experiments.

Table 2-8: Basic parameters for cameras used in the jet fire tests.

	East station			South station	West station
Camera	X6901	VEO4k 990c	4k Blackmagic G2	4k Blackmagic G2	6k Z-Cam
Distance	58 m			30 m	34 m
Lens Focal Length	25mm	43mm	Zoom (26 mm)	Zoom (80 mm Isopentane) Zoom (50 mm Ethane & Ethylene)	Zoom (15mm)
Frame Rate	15 fps	15 fps	30 fps	30 fps	30 fps
Temperature Range / Exposure	850°C to 2000°C	250 µs	Auto	Auto	2 msec
Resolution	640x480	4096x2304	3840x2160	3840x2160	5760x3240

For the pool fire experiments three cameras are located at station 1 and three at station 2 shown in Figure 2-13. These two stations are located approximately 30 m from the center of the pool. Station 1 is angled counterclockwise by 15 degrees from the north cardinal direction and station 2 by 8 degrees from the west cardinal direction to avoid interfering with heat flux gauges aligned to cardinal axis centered at the pool. A 6k Z-camera is also placed approximately 50 m northwest from the pool center to provide real time imaging. The Phantom VEO 1310c is synchronized at 10 fps using the MWIR camera to provide non-IR imagery of the distribution of the flame and smoke. The type of camera used at each station and their specifications are provided in Table 2-9.

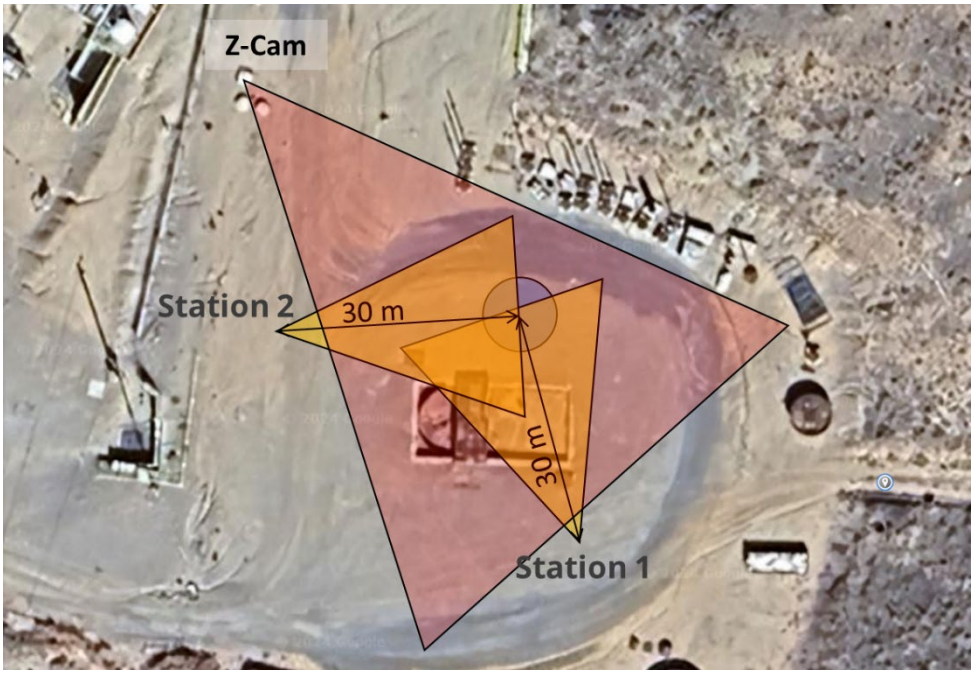

Figure 2-13: Camera layout for pool fire experiments.

Table 2-9: Basic parameters for cameras used in the pool fire tests.

Location	Station 1 (south)			Station 2 (west)			Northwest
Camera	X6901	VEO 1310c	4k Blackmagic G2	X6901	VEO 1310c	4k Blackmagic G2	6k Z-Cam
Distance	30 meters			30 meters			50 meters
Lens Focal Length	25mm	20 mm	Zoom (22.5 mm)	25 mm	20 mm	Zoom (22.5 mm)	15 mm
Frame Rate	10 fps	10 fps	30 fps	10 fps	10fps	30 fps	30 fps
Temperature Range / Exposure	850°C to 2000°C	40 µs	Auto	850°C to 2000°C	40 µs	Auto	2 msec
Resolution	640x480	1280x960	3840x2160	640x480	1280x960	3840x2160	5760x3240

For the fireball experiments there are five camera stations as shown in Figure 2-14. Station 1, 2 and 3 are approximately 352 m, 337 m and 284 m, respectively, from the test tank. Station 1 includes a FLIR X6901sc MWIR camera, a Phantom V1212c camera, and a high-speed, black & white, Phantom T3610 camera. The Phantom V1212c camera, set at 1000 fps, is synchronized to the X6900sc MWIR camera which allows frames to be matched. The matched images are used to compare flame and smoke in the visible cameras to hot and cold areas in the IR cameras. The Phantom T3610 camera is used to capture the opening of the tank and ignition of the fuel from the explosive charges which are described in section 2.3. The field of view of the T3610 camera is reduced to 384x640 binned pixels to run at 100,000 fps and increase sensitivity.

Station 2 includes a X6900sc MWIR and a Phantom V1212c camera, while station 3 includes a 4k Blackmagic G2 and Phantom T3610 camera. The 4k Blackmagic G2 provides an overall view of the fireball. The two other stations, north and northwest, are located approximately 137 m and 273 m from the test tank, respectively. The north station has Z-cam camera and the northeast station a 4k Blackmagic G2 camera. Both cameras provide real-time imagery of a fireball. The type of camera used at each station and their specifications are provided in Table 2-10 and Table 2-11..

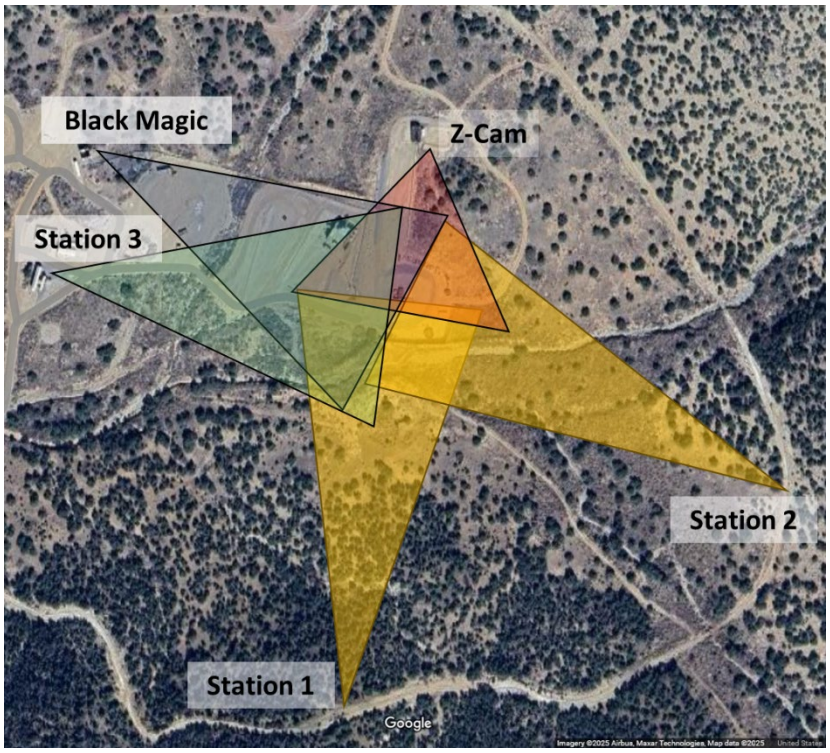

Figure 2-14: Camera layout for fireball experiments.

Table 2-10: Basic parameters for cameras used in the fireball experiments for stations 1, 2, and 3.

Location	Station 1 - South			Station 2 - East		Station 3 – West	
Camera	X6901	V1212c	T3610	X6901	V1212c	4k Blackmagic G2	T3610
Distance	352 m			337 m		284 m	
Lens Focal Length	25 mm	55 mm	1000 mm	25 mm	55 mm	Zoom (25.4 mm)	1000 mm
Frame Rate	1k fps	1k fps	100k fps	1k fps	1kfps	30 fps	100k fps
Temperature Range / Exposure	850°C to 2000°C	40, 20 µs	5, 3, 1 µs	850°C to 2000°C	40, 20 µs	Auto	5, 3, 1 µs
Resolution	640x480	1280x800	384x640 Binned	640x480	1280x80	3840x2160	384x640 Binned

Table 2-11: Basic parameters for cameras used in the fireball experiments for north and northeast stations.

Location	North	Northwest
Camera	Z-Cam	4 Blackmagic G2
Distance	137 m	273 m
Lens Focal Length	17 mm	Zoom (24 mm)
Frame Rate	30 fps	30 fps
Temperature Range / Exposure	2 msec	Auto
Resolution	5760x3240	3840x2160

The uncertainty for surface emissive power based on measurements from the FLIR X6901sc camera is ±6.3%. The uncertainty for the non-IR cameras is assumed to be ±10% based on recommendations by subject matter experts at Sandia. For each test, cameras were spatially calibrated by using flames from three propane torches.

The surface emissive power (SEP) is determined by using the IR camera temperature measurements and the equation $SEP=\varepsilon\tau\sigma T^4$, where ε is the flame's emissivity, τ is transmissivity, $\sigma=5.6696\text{x}10^{-8}$ $W/(m^2K^4)$ is the Stefan-Boltzmann constant, and T is temperature in Kelvin. Using a gray assumption for the flame, an emissivity of 1 is used to determine the SEP for all experiments. The transmissivity is the degree of atmospheric attenuation due principally to H_2O and CO_2 in the atmosphere and ranges in value from 0 to 1. The internal software of the camera calculates a transmissivity based on user entered values for distance, the ambient temperature and relative humidity. Results from the software are compared to the atmospheric absorption software, Hitran-PC, for verification. See section 5.2 on further discussion of the SEP.

2.2.4. Flow rate

The flow rate for the jet and pool fire experiments is measured by two methods, namely, using an orifice plate and a vortex meter. With the first method, the differential pressure across a 2" diameter orifice plate is measured using a differential pressure transmitter by Rosemount with a span uncertainty of ±0.035% and orifice plate uncertainty of ±1.4%. The second method uses a Rosemount (8800DR) vortex meter which has a mass flow uncertainty of ±2%. These values assume that a single phase is maintained. Based on measurements and Unisim Design® calculations, all jet and pool fire experiments indicate single phase flow, except for the ethane and ethylene jet fire experiments which indicates gaseous mass fractions of about 20% and 25% for ethylene and ethane, respectively. However, the orifice plate and vortex meter were both in agreement and pressure measurements were steady which indicates that ethane and ethylene jet fires were in liquid form. The development of vapor would cause significant oscillations in the pressure measurements. Nonetheless, without further verification, an uncertainty of ±10% is assumed for the flow rate measurements. This is based on analysis and experiments involving orifice plate measurements by Campos, et al. [5] where the uncertainty of assuming single phase flow for multiphase flow is assessed.

2.2.5. Pipeline pressure and temperature

Pressure is measured at four locations and temperature at two locations along the pipeline (see Figure A-1 in Appendix A). The Rosemount 3051S in-line pressure transmitter with an uncertainty of ±0.035% is used for pressure measurements, while the Rosemount 3144P temperature transmitter with an uncertainty of ±0.02% is used to for temperature measurements.

2.2.6. Weather

Four weather towers were placed at north, east, south, and west cardinal directions. Since they remained in the same location for the jet and pool fire tests the distances of these towers from the release point vary. For the jet fires and pool fires the range of distances are approximately 15-100 m and 45-50 m, respectively. Each tower has instruments placed at the height of 2 m, 5 m, and 7.62 m, measuring wind speed, wind direction, temperature, as well as relative humidity and atmospheric pressure. The height of the available towers limited the upper location to 7.62 m. For the fireball tests, the north, south, and east towers were removed to prevent damage to the instruments. The east tower was moved approximately 30 m further west. Table 2-12 provided information on the instruments used to obtain weather data and their uncertainty.

Table 2-12: Instruments and uncertainty of instruments used to obtain weather data

Measurement	Stations, Heights (m)	Manufacturer, Model	Uncertainty
Wind speed	All, 2, 5, 7.62	Met One Instruments, 010C	± 1% or 0.07 m/s, whichever is greater
Wind direction	All, 2, 5, 7.62	Met One Instruments, 020D	± 3°
Temperature	All, 2	Vaisala, HMP155A	± (0.226 - 0.0028T)°C at -80 to 20°C ± (0.055 + 0.0057T)°C at 20 to 60°C
Temperature	All, 5, 7.62	Campbell Scientific, CS107	± 0.4 °C (Note: a 1-point calibration by Sandia indicates an accuracy of ± 0.1°C or better).
Relative humidity	All, 2	Vaisala, HMP155A	± 1.4%
Pressure	East/South, 2	Setra, 278	± 200 Pa at -40 to 60°C
Pressure	North/West, 2	Vaisala, PTB101B	± 600 Pa at -40 to 60°C

2.3. Testing procedure

For the jet and pool fire experiments the ISO container for the respective fuel is first connected to the piping system. Then the fuel piping system is purged of oxygen using N_2 provided from the LN_2 tank via the vaporizer. The pipeline system is purged with several cycles until the O_2 concentration is below 2 vol%. Once the purge is completed the N_2 system is isolated from the fuel piping system.

For ethylene and ethane jet and pool fire tests, pre-chilling of the pipeline is performed using LN_2 to minimize the vaporization of the cryogens during the initial fuel fill. Pre-chilling of the 5-m diameter

concrete pool for the pool fire tests is also performed for both these fuels. The LN_2 is slowly introduced to the fuel pipeline for the pre-chilling process to avoid large pressure increases due to vaporization. Once the pre-chilling is complete, the LN_2 system is isolated from the pipeline and the vaporizer is activated to supply N_2 to the ISO container to drive fuel out of the container to the pipeline. The pressure of the ISO container is increased to 20 psi above the current storage pressure using the N_2. This pressure differential is required to provide adequate driving pressure to prevent flashing due to pressure losses while achieving the desired flow rates. The pressure of the ISO container is maintained at a lower pressure than the pressure rating of the storage container throughout a test.

Once the ISO container is pressurized three propane torches placed at 1' increments from the end of the pipeline are ignited and the spark generating heads are energized (Figure 2-15). Once ignitors are operational the flow control valve, FV-01 (Figure A-1) is utilized to initiate fuel flow. Upon verification of ignition the fuel flow is ramped up to target flow rates.

Figure 2-15: Three propane gas burners used for ignition

For the iso-pentane the same general procedure is utilized for jet and pool fire testing, though for the iso-pentane jet fire, fuel is transferred from the T-11 ISO container to the 1150-gallon vertical propane tank as mentioned in section 2.1. The propane tank is first purged with N_2 gas to reduce the concentration of O_2 to less than 2 vol.% prior to filling. For the transfer, the T-11 ISO container is positioned and connected to the propane tank via a hose 30' in length and 1.5" in diameter, rated for hydrocarbon fuel service up to 250 psig.

Once propane tank is purged, a connection is made from the N_2 vapor line to the tank vapor vent valve on the T-11 ISO container utilizing a 1" braided stainless-steel hose rated for 680 psig. The T-11 ISO container is pressurized to a maximum pressure of 35 psig to push approximately 500 gallons of iso-pentane into the propane tank. Once the propane is transferred the hose is disconnected from the T-11 container and connected to the 3" pipeline inlet via a 3" ANSI 300 flange. The 1" N_2 hose is disconnected from the T-11 ISO container and then connected to the propane tank to drive fuel out of the tank and into the pipeline for testing.

For the fireballs experiments, linear shaped charges (LSC) are used to open the tanks to release fuel and a 1-lb C-4 explosive charge is used to ignite the fuel. For the cryogenic tanks, the LSC design requires information on the inner and outer tank thicknesses and the distance between the inner and outer tank. Since this information was not provided by the supplier, it was obtained by using x-ray imaging and taking ultrasound measurements. In addition to providing information for the design of the LSC, the imaging provides the location of the inner tank. Based on this information the LSC is placed 1' below the tank's circumferential top seam to breach the inner tank. The thickness of the propane tank used for the iso-pentane fireball is provided by the supplier, thus diagnostics are not required. The same LSC placement on this tank is used for consistency. The LSC and C-4 charge are simultaneously ignited for each test. Once ignited, fragments from the copper lining of the LSC are thrown to potentially far distances, thereby causing damage to infrastructure. Thus, as mentioned previously, concrete blocks and steel barricades surround the test tank to reduce the distance of thrown fragments.

The isopentane fireball test requires that the tank is heated to a temperature and pressure that will cause most of the liquid to flash when released to the atmosphere. Radiant ceramic heaters are used to heat the tank. These same heaters are used to heat the concrete walls for the experiments described in section 4. Each ceramic heater is shaped in the form of a quarter circle with an inner diameter of 74", outer diameter of 80", and height of 1'. There are 12 heaters surrounding the tank stacked in three layers with 4 heaters per layer to form a complete circle. The heaters have a combined maximum power output of 96 kW. The time required to heat the tank to a temperature of 114°C and pressure of 164 psi is about 10 hrs. This time could greatly be reduced but the temperature on the outside of the tank is limited by temperature thresholds of a gasket installed on the tank. Thus, the tanks are heated overnight and monitored by personnel to perform the test in morning hours. The tank and heaters are covered with insulation to reduce heat loss as shown in Figure 2-16a. To prevent reaching critical temperatures that could jeopardize the operation of the LSC, additional insulation and aluminum foil to reduce radiation are applied to provide thermal protection as shown in Figure 2-16b. Since ethane and ethylene flash upon release without heating, preparation was much simpler than for the isopentane test.

Figure 2-16: Propane tank containing isopentane for fireball experiment: (a) insulated tank and heaters, (b) additional thermal protection at LSC location.

This page left blank

3. RESULTS

3.1. Jet Fires

Sections 3.1.1 through 3.1.3 provide measurements of release conditions, heat flux, surface emissive power, flame length, and weather conditions for the ethane, ethylene, and isopentane jet fires. For all jet fire experiments, the dimensions and surface emissive power are based on temperatures above 1123 K as measured from the IR camera. This temperature corresponds to an SEP value of 90 kW/m^2 assuming blackbody radiation. Inspection of real-time video also provided confirmation that this temperature threshold is indicative of the visible flame. Since the flame angled horizontally from the release direction for all tests, the reported flame dimensions are distances projected onto the north-south axis or aligned with the release direction as viewed from the east cameras. For all tests the mass flow rate has been corrected for losses using a discharge coefficient of 0.6 for the sharp-edged orifice at the exit. Some heat flux gauges failed due to their cabling overheating and are marked 'NA'.

3.1.1. Ethane

The following results are measurements averaged over a period from 2 to 3 minutes after ignition. The period is selected based on heat flux gauge measurements indicating a steady state. The test duration is 4 minutes and 26 seconds. As shown in Figure 3-1 the wind came from the southeast direction to cause the flame to angle laterally towards the northwest direction relative to the release direction. The average wind speed and direction are provided in Table 3-1. The average wind speed of about 2 m/s is relatively low but has a significant effect on angling the flame.

Table 3-2 and Table 3-3 provide the atmospheric and release conditions, respectively. Table 3-4 provides average incident heat flux measurements from the total heat flux gauges placed at locations shown in Figure 2-9. The spatially and temporally averaged surface emissive power (SEP) is provided in Table 3-5. The SEP is corrected for atmospheric attenuation using a transmissivity of 0.865. The average flame dimensions are provided in Table 3-6.

(a) (b)

Figure 3-1: Ethane jet fire as viewed from the (a) east, and (b) north.

Table 3-1: Ethane jet fire: Average wind speed and direction during test.

Height (m)	Average wind speed (m/s)
2	1.9 ± 0.2
5	2.2 ± 0.3
7.6	2.3 ± 0.2
Height (m)	**Average wind direction (deg)**
2	107.1 ± 3.7
5	108.7 ± 3.8
7.6	111.1 ± 4.2
Average among heights	109.0 ± 3.9

Table 3-2: Ethane jet fire: Atmospheric conditions

Condition	Value
Atmospheric pressure (Pa)	81,317 ± 0.2
Atmospheric temperature (°C)	3.3 ± 0.4
Relative humidity (%)	33.4 ± 1.0

Table 3-3: Ethane jet fire: Fuel release conditions

Release Condition	Averages
Height of release (m)	1.0
Pressure (psig)	104.8 ± 0.3
Temperature (°C)	-45.7 ± 3.5
Mass flow rate (kg/s)	3.1 ± 0.09
Mass flow rate at exit (kg/s)	1.8 ± 0.1

Table 3-4: Ethane jet fire: Time-averaged heat flux from heat flux gauges

Heat flux gauge	Average heat flux (kW/m^2)
R1	NA
R2	NA
R3	17.1 ± 2
R4	20.6 ± 1.8

Heat flux gauge	Average heat flux (kW/m^2)
R5	26.4 ± 2
R6	2.6 ± 0.4
R7	4.3 ± 0.5
R8	7.0 ± 0.7
R9	14.3 ± 1.4
R10	NA
R11	2.8 ± 0.3
R12	3.8 ± 0.4
R13	5.5 ± 0.7
R14	7.7 ± 1
R15	NA
R16	1.2 ± 0.4
R17	1.6 ± 0.3
R18	2.6 ± 0.5
R19	3.3 ± 0.5
R20	3.1 ± 0.6
R21	1.3 ± 0.3
R22	1.7 ± 0.2
R23	1.4 ± 0.2
R24	1.9 ± 0.3
R25	2.5 ± 0.3
R26*	1.0 ± 0.3
R27*	1.2 ± 0.3
R28	NA
R29	NA
R30	NA
R31	3.9 ± 0.6
R32	4.8 ± 0.8
R33	3.0 ± 0.5
R34*	1.1 ± 0.1
R35*	0.9 ± 0.1
R36	7.3 ± 1.3
R37	11.9 ± 1.8
R38	19.4 ± 3.4

Heat flux gauge	Average heat flux (kW/m^2)
R39**	28.7 ± 5.1
R40***	14.6 ± 4

*Consistent reading though suspect based on measurements from other gauges
**Potential for soot deposition.
***Engulfed in the fire for the first 30 seconds of the experiment

Table 3-5: Ethane jet fire: Temporal and spatially averaged SEP

Measurement	Average
Average SEP*† (kW/m^2)	155.0 ± 12.5
Maximum SEP**† (kW/m^2)	289.1 ± 29.0

*Spatially averaged
**Local maximum
†Corrected for atmospheric attenuation using a calculated transmissivity of 0.865

Table 3-6: Ethane jet fire: Average projected flame dimensions

Measurement	Average
Projected horizontal length* (m)	12.5 ± 1.3
Projected vertical height*‡ (m)	7.7 ± 2.0

*Projected onto north-south axis.
‡From ground.

3.1.2. Ethylene

The following are measurements averaged from 2 to 4 minutes, the period in which heat flux gauge measurements are steady. The duration of this test is 4 minutes and 5 seconds, similar to the ethane jet fire. As shown in Figure 3-2 the wind came from the southeast direction to cause the flame to angle laterally towards the northwest direction relative to the release direction. The average wind speed and direction are provided in Table 3-7. The average wind speed of about 2.5 m/s is slightly higher than for the ethane jet fire and the wind direction is similar for both tests. The relatively low wind speed has a significant effect on angling the flame. Table 3-8 and Table 3-9 provide the atmospheric and release conditions, respectively.

Table 3-10 provides average heat flux measurements from the total heat flux gauges placed at locations shown in Figure 2-9. The spatially and temporally averaged surface emissive power (SEP) is provided in Table 3-11. The SEP is corrected for atmospheric attenuation using a transmissivity of 0.867. The average flame dimensions are provided in Table 3-12.

(a) (b)

Figure 3-2: Ethylene jet fire as viewed from the (a) east, and (b) north.

Table 3-7: Ethylene jet fire: Average wind speed and direction during test.

Height (m)	Average wind speed (m/s)
2	2.2 ± 0.3
5	2.7 ± 0.4
7.6	3.1 ± 0.5
Height (m)	**Average wind direction (deg)**
2	106.3 ± 6.3
5	110.2 ± 3.6
7.6	115.2 ± 3.8
Average among heights	110.6 ± 4.5

Table 3-8: Ethylene jet fire: atmospheric conditions

Condition	Value
Atmospheric pressure (Pa)	81,030 ± 0.2
Atmospheric temperature (°C)	-1.0 ± 0.3
Relative humidity (%)	39.4 ± 0.7

Table 3-9: Ethylene jet fire: Fuel release conditions

Release Condition	Averages
Height of release (m)	1.0
Pressure (psig)	79.6 ± 0.2
Temperature (°C)	-71.3 ± 2.6
Mass flow rate (kg/s)	2.9 ± 0.1
Mass flow rate at exit (kg/s)	1.7 ± 0.1

Table 3-10: Ethylene jet fire: Time-averaged heat flux from heat flux gauges

Heat flux gauge	Average heat flux (kW/m^2)
R1	NA
R2	4.6 ± 1.0
R3	8.6 ± 1.0
R4	13.4 ± 1.4
R5	NA
R6	3.3 ± 0.5
R7	5.4 ± 0.6
R8	14.2 ± 1.4
R9	NA
R10	NA
R11	2.8 ± 0.3
R12	5.6 ± 0.5
R13	6.0 ± 0.7
R14	NA
R15	NA
R16	1.4 ± 0.3
R17	2.5 ± 0.4
R18	3.2 ± 0.4
R19	4.2 ± 0.5
R20	NA
R21	1.6 ± 0.2
R22	1.5 ± 0.2
R23	2.0 ± 0.2

Heat flux gauge	Average heat flux (kW/m^2)
R24	2.6 ± 0.3
R25	NA
R26	NA
R27	NA
R28	NA
R29	NA
R30	4.0 ± 0.8
R31	5.1 ± 0.8
R32*	3.1 ± 0.5
R33	NA
R34	NA
R35	7.8 ± 1.5
R36	15.8 ± 3.0
R37	25.9 ± 4.1
R38**	46.6 ± 7.7
R39**	46.6 ± 8.3
R40	NA

*Consistent reading though suspect based on measurements from other gauges
**Potential for soot deposition.

Table 3-11: Ethylene jet fire: Temporal and spatially averaged SEP

Measurement	Average
Average SEP*† (kW/m^2)	190.5 ± 9.0
Maximum SEP**† (kW/m^2)	435.8 ± 43.7

*Spatially averaged
**Local maximum
†Corrected for atmospheric attenuation using a calculated transmissivity of 0.867

Table 3-12: Ethylene jet fire: Flame length

Measurement	Average
Projected horizontal length* (m)	13.8 ± 2.1
Projected vertical height*‡ (m)	7.5 ± 1.8

*Projected onto north-south axis.
‡From ground.

3.1.3. Isopentane

The following are measurements averaged from 1 to 3 minutes, the period in which heat flux gauge measurements are steady. The test duration is 4 minutes and 17 seconds. As shown in Figure 3-3 the wind came from the southwest direction to cause the flame to angle laterally towards the northeast direction relative to the release direction. The average wind speed and direction are provided in Table 3-13. The atmospheric and release conditions are provided in Table 3-14 and Table 3-15, respectively.

Table 3-16 provides average heat flux measurements from the total heat flux gauges placed at locations shown in Figure 2-9. The spatially and temporally averaged surface emissive power (SEP) is provided inTable 3-17. The SEP is corrected for atmospheric attenuation using a transmissivity of 0.870. The average flame dimensions are provided in Table 3-18.

Figure 3-3: Isopentane jet fire as viewed from the (a) east, and (b) north.

Table 3-13: Isopentane jet fire: Average wind speed and direction during test.

Height (m)	Average wind speed (m/s)
2	2.9 ± 0.6
5	3.5 ± 0.7
7.6	3.8 ± 0.7
Height (m)	**Average wind direction (deg)**
2	227.0 ± 9.4
5	226.0 ± 6.2
7.6	228.0 ± 7.0
Average among heights	227.2 ± 7.5

Table 3-14: Isopentane jet fire: atmospheric conditions

Condition	Value
Atmospheric pressure (Pa)	81,520 ± 0.2
Atmospheric temperature (°C)	0.5 ± 0.4
Relative humidity (%)	28.0 ± 0.5

Table 3-15: Isopentane jet fire: Fuel release conditions

Release Condition	Averages
Height of release (m)	1.0
Pressure (psig)	107.6 ± 3.0
Temperature (°C)	-2.7 ± 0.4
Mass flow rate (kg/s)	3.9 ± 0.1
Mass flow rate at exit (kg/s)	2.3 ± 0.1

Table 3-16: Isopentane jet fire: Time-averaged heat flux from heat flux gauges

Heat flux gauge	Average heat flux (kW/m^2)
R1	5.7 ± 0.9
R2	7.0 ± 0.9
R3	10 ± 1.2
R4	12.6 ± 1.4
R5	18.4 ± 1.9
R6	NA
R7	NA
R8	NA
R9	NA
R10	NA
R11	9.0 ± 1.9
R12	16.6 ± 2.8
R13	36.8 ± 5.1
R14	50.2 ± 13.6
R15	NA
R16	4.6 ± 0.9

Heat flux gauge	Average heat flux (kW/m^2)
R17	5.1 ± 1.0
R18	3.8 ± 1.3
R19	3.0 ± 1.0
R20	NA
R21	1.6 ± 0.3
R22	2.8 ± 0.3
R23	1.9 ± 0.2
R24	2.5 ± 0.3
R25	3.4 ± 0.4
R26*	0.7 ± 0.5
R27	1.6 ± 0.3
R28	2.4 ± 0.3
R29	3.1 ± 0.4
R30	2.7 ± 0.3
R31	1.9 ± 0.3
R32	3.1 ± 0.4
R33	4.4 ± 0.6
R34	7.3 ± 1.0
R35	8.6 ± 1.5
R36	2.2 ± 0.5
R37	3.6 ± 0.7
R38	6.3 ± 0.8
R39	11.7 ± 1.4
R40	17.6 ± 2.3

*Consistent reading though suspect based on measurements from other gauges

Table 3-17: Isopentane jet fire: Temporal and spatially averaged SEP

Measurement	Average
Average SEP*† (kW/m^2)	166.8 ± 11.9
Maximum SEP**† (kW/m^2)	330 ± 36.8

*Spatially averaged
**Local maximum
†Corrected for atmospheric attenuation using a calculated transmissivity of 0.870

Table 3-18: Isopentane jet fire: Flame length and height

Measurement	Average
Projected horizontal length* (m)	17.3 ± 1.4
Projected vertical height*‡ (m)	9.8 ± 2.6

*Projected onto north-south axis.
‡From ground.

3.2. Pool Fires

Sections 3.2.1 through 3.2.4 provide measurements of release conditions, heat flux, surface emissive power, flame length, and weather conditions for the ethane, ethylene, propane, and isopentane pool fires, respectively. For all pool fire experiments the dimensions and surface emissive power are based on temperatures above 1123 K as measured from the IR camera. This temperature corresponds to an SEP value of 90 kW/m^2 assuming blackbody radiation.

For the ethane, ethylene, and propane pool fires the diptube instruments indicated that a liquid layer of at least ½" did not form within the pool for the given flow rates. The elevation of the diptubes is ½" from the bottom of the pool and can measure liquid depths greater than this distance. However, for each test the flame fully spread across the surface of the pool which indicated that a thin liquid layer did form. As the flow rate was increased the flame height increased which indicates that the burn rate was controlled by the fuel supply rate. For liquid pool fires heat transferred from the flame to the surface of the pool controls the burn rate. Since the burn rate was controlled by the fuel supply rate as evident from the flame height increasing with increasing mass flow rates, the configuration acted similar to a gas burner. Experimentally, gas burners have been shown to preserve the gas phase dynamics of a liquid pool fire [6]. This has also been confirmed through model validation in which the liquid pool is not modeled, and the gaseous fuel is supplied uniformly at the boundary of the pool's surface [7]. Herein, the mass flow rate is considered to be the burn rate of the fire. Note that due to the MAWP of the ISO containers, the fuel supply rate is limited. The depth of fuel forming in the pool would increase with higher mass flow rates. Thus, given the limitations of the fuel delivery system a liquid layer of significant depth could not form.

Based on the results of the isopentane pool fire, the orifice plate measurements are multiplied by a discharge coefficient of 0.35 due to losses incurred principally by the diffuser. The method to determine the discharge coefficient is provided in 3.2.4.

The flame length is measured from the center of the pool to the tip of the flame going through its middle and the tilt angle is with respect to the vertical axis. The flame length and tilt for all pool fires

are determined from the visible cameras by masking the image to a black and white scheme where white indicates the luminous portion of the flame and black indicates either smoke or the surroundings.

3.2.1. Ethane

The 5-m diameter ethane pool fire is shown in Figure 3-4. The test duration is about 11 minutes. Measurements are averaged over periods in which the wind speed is steady, and the wind direction has the least variance over the test duration. Table 3-19 provides time averaged wind speed and direction over two periods identified. The test was performed under nearly quiescent conditions with wind speeds around 1 m/s. The vertical orientation of the flame in Figure 3-4 reflects the quiescent conditions. Thus, the variance of the wind direction mostly influences the identification of the averaging periods. The atmospheric and release conditions are provided in

Table 3-20 and Table 3-21, respectively. The average mass flow rate provided in Table 3-21 is from the orifice plate flow measurements. The vortex meter after reaching about 4 kg/s abruptly decreased to values on the order of 0.1 kg/s, the cause of which is uncertain.

Figure 3-4: Ethane pool fire

Table 3-19: Ethane pool fire: Wind conditions during periods of steady wind speed and direction

	Period 72-100 s	Period 129-156 s
Height (m)	Average wind speed (m/s)	
2	1.0 ± 0.04	1.2 ± 0.04
5	0.9 ± 0.03	1.3 ± 0.03
7.6	1.0 ± 0.04	1.2 ± 0.04
	Average wind direction (deg)	
2	255.0 ± 5.0	268.9 ± 8.6
5	283.7 ± 5.8	285.7 ± 13.6
7.6	291.4 ± 8.0	288.4 ± 8.5
Average among heights	276.7 ± 19.8	281.0 ± 13.3

Table 3-20: Ethane pool fire: Atmospheric conditions

Condition	Period 72-100 s	Period 129-156 s
Atmospheric pressure (Pa)	80,390 ± 0.2	
Atmospheric temperature (°C)	-0.32 ± 0.13	0.58 ± 0.14
Relative humidity (%)	46.7 ± 0.2	46.4 ± 0.06

Table 3-21: Ethane pool fire: Fuel release conditions during steady-state wind conditions

Condition	Period 72-100 s	Period 129-156 s
Mass flow rate* (kg/s)	3.2 ± 0.08	3.0 ± 0.07
Temperature (°C)	-64.5 ± 0.1	-65.2 ± 0.1

* By orifice plate

Table 3-22 provides the time-averaged heat flux measurements from the heat flux gauges over periods of steady wind conditions. The spatially and temporally averaged surface emissive power (SEP) is provided in Table 3-23. The SEP is corrected for atmospheric attenuation using a transmissivity of 0.892. The average flame length and tilt for the two periods is provided in Table 3-24 with results indicating a flame height of about 5 pool diameters. Typically for liquid pool fires of this diameter, the flame height is about 2-3 pool diameters. This difference is due to the fuel supply rate which is reflective of the burn rate. As long as the flame is buoyancy controlled the flame height will increase as the burn rate is increased. Thus, as the fuel supply rate is increased, the flame height will increase.

Table 3-22: Ethane pool fire: Time-averaged heat flux from heat flux gauges during steady wind conditions

Heat flux gauge	Average heat flux (kW/m^2)	
	72-100 s	129-156 s
R1	6.5 ± 0.7	5.1 ± 0.7
R2	8.4 ± 0.9	6.8 ± 0.9
R3	12.7 ± 1.5	9.8 ± 1.2
R4	17.6 ± 1.9	14 ± 1.7
R5	NA	NA
R6	4.3 ± 0.4	3.1 ± 0.4
R7	NA	NA
R8	13.5 ± 1.6	10.1 ± 1
R9	NA	NA
R10	NA	NA
R11	8.5 ± 0.9	6.4 ± 0.9
R12	12 ± 1.3	8.9 ± 1.4
R13	16.6 ± 2	12 ± 2
R14	28.9 ± 3.8	20 ± 3.5
R15	NA	NA
R16	7.4 ± 0.8	6.4 ± 1
R17	10.7 ± 1.3	9.3 ± 1.5
R18	NA	NA
R19	21 ± 2.5	18.1 ± 3.2
R20	NA	NA
R21	6.3 ± 0.6	6.0 ± 0.7
R22	7.3 ± 0.6	7.3 ± 0.9
R23	13.7 ± 1	13.2 ± 1.7
R24	NA	NA
R25	10.5 ± 0.8	10.7 ± 1.2
R26	5.4 ± 0.5	5.3 ± 0.6
R27	8.1 ± 0.7	7.8 ± 0.8
R28	11.3 ± 1	11.1 ± 1.1

Heat flux gauge	Average heat flux (kW/m^2)	
R29	12.3 ± 1.1	12.1 ± 1.2
R30	16.7 ± 1.5	16.8 ± 1.7
R31	5.7 ± 0.5	5.5 ± 0.6
R32	8.2 ± 0.7	8.3 ± 0.9
R33	10.2 ± 0.8	10.3 ± 0.9
R34	15.4 ± 1.3	16 ± 1.6
R35	17.3 ± 1.4	17.9 ± 1.6
R36	6.7 ± 0.7	6.3 ± 0.8
R37	8.5 ± 0.9	7.9 ± 1
R38	11 ± 1.1	10.4 ± 1.3
R39	15.8 ± 1.5	14.8 ± 1.7
R40	23.3 ± 2	21.9 ± 2.4

Table 3-23: Ethane pool fire: Temporal and spatially averaged SEP during steady wind conditions

	Period 72-100 s			Period 129-156 s		
	Average	Min	Max	Average	Min	Max
	Station 1 (south)					
SEP* (kW/m^2)	167.3 ± 13.1	136.1	212.9	170.7 ± 13.5	142.2	212.7
Maximum SEP**† (kW/m^2)	321.2 ± 27.5	241.9	413.9	324.3 ± 26.3	252.5	384.5
	Station 2 (west)					
SEP* (kW/m^2)	175.2 ± 13.2	143.6	226.7	182.2 ± 14.6	146.9	221.6
Maximum SEP** † (kW/m^2)	358.5 ± 35.7	288.9	494.5	370.8 ± 33.9	274.5	461.2

*Spatially averaged
**Local maximum
†Corrected for atmospheric attenuation using a calculated transmissivity of 0.892

Table 3-24: Ethane pool fire: Flame length and tilt angle during steady wind conditions

	Period 72-100 s			Period 129-156 s		
	Average	Min	Max	Average	Min	Max
	Station 1 (south)					
Length (m)	25.3 ± 2.8	17.3	29.8	25.7 ± 3.0	17.6	29.3
Tilt Angle (deg)	12.4 ± 2.6	7.8	20.8	0.7 ± 7.8	-12.1	15.6
	Station 2 (west)					
Length (m)	20.9 ± 2.9	14.5	29.1	23.2 ± 3.6	15.0	29.1
Tilt Angle (deg)	10.4 ± 2.7	-9.6	15.9	10.7 ± 4.4	-5.0	25.7

3.2.2. Ethylene

The 5-m diameter ethylene pool fire is shown in Figure 3-5. The test duration is about 10 minutes. Measurements are averaged over periods in which the wind speed is steady, and the wind direction has the least variance over the test duration. There are two periods identified in which provides the average wind speed and direction over these periods. Table 3-25 provides wind speed and direction time averaged over the two periods identified. The average wind speed is much higher compared to the ethane pool fire test which is evident in Figure 3-5 by the degree of flame tilt. The flame is tilted towards the northeast direction due to the southeastern wind. The atmospheric and release conditions are provided in Table 3-26Table 3-27, respectively. The average mass flow rate provided in Table 3-27is from the orifice plate flow measurements. The vortex meter after reaching about 5 kg/s abruptly decreased to values on the order of 0.1 kg/s, the cause of which is uncertain.

Figure 3-5: Ethylene pool fire

Table 3-25: Ethylene pool fire: Periods of steady wind conditions based on wind speed

	Period 320-346 s	Period 433-462 s
Height (m)	Average wind speed (m/s)	
2	3.37 ± 0.13	4.16 ± 0.14
5	3.80 ± 0.15	4.88 ± 0.13
7.6	3.96 ± 0.15	5.11 ± 0.15
	Average wind direction (deg)	
2	225.9 ± 7.3	239.0 ± 5.5
5	222.6 ± 6.1	239.3 ± 4.8
7.6	221.2 ± 5.0	241.7 ± 6.5
Average among heights	223.2 ± 4.3	240.0 ± 4.4

Table 3-26: Ethylene pool fire: Atmospheric conditions

Condition	Period 320-346 s	Period 433-462 s
Atmospheric pressure (Pa)	81,250 ± 0.2	
Atmospheric temperature (°C)	5.5 ± 0.02	5.8 ± 0.02
Relative humidity (%)	32.7 ± 0.1	33.3 ± 0.1

Table 3-27: Ethylene pool fire: Fuel release conditions during steady wind conditions

Condition	Period 320-346 s	Period 433-462 s
Mass flow rate* (kg/s)	2.4 ± 0.1	2.3 ± 0.2
Temperature (°C)	-84.0 ± 0.01	-84.2 ± 0.03

* By orifice plate

Table 3-28 provides the time-averaged heat flux measurements from the heat flux gauges over periods of steady wind conditions. The spatially and temporally averaged SEP is provided in Table 3-29. The SEP is corrected for atmospheric attenuation using a transmissivity of 0.867. The average flame length and tilt for the two periods is provided in Table 3-30. The flame height is about 3 pool diameters over both periods.

Table 3-28: Ethylene pool fire: Time-averaged heat flux from heat flux gauges during steady wind conditions

Heat flux gauge	Average heat flux (kW/m^2)	
	320-346 s	433-462 s
R1	7.1 ± 0.8	6.2 ± 1.1
R2	8.9 ± 0.9	7.9 ± 1.1

Heat flux gauge	Average heat flux (kW/m^2)	
R3	15.5 ± 1.6	14.4 ± 1.9
R4	20.4 ± 1.8	19.8 ± 2.1
R5	NA	NA
R6	8.8 ± 2.2	8.0 ± 1.9
R7	15.9 ± 4.	14.3 ± 3.2
R8	23.7 ± 5.1	22.1 ± 5
R9	NA	NA
R10	NA	NA
R11	5.8 ± 1.6	7.0 ± 1.9
R12	10.2 ± 2.1	11.8 ± 2.8
R13	20.2 ± 3.7	21.8 ± 4.4
R14	42.6 ± 6.3	41.9 ± 6.3
R15*	1.3 ± 0.2	1.4 ± 0.2
R16	6.1 ± 1.2	6.7 ± 1.1
R17	8.0 ± 1.4	8.4 ± 1.4
R18	NA	NA
R19	16.6 ± 1.9	17.4 ± 1.8
R20	NA	NA
R21	4.5 ± 0.6	4.8 ± 0.5
R22	5.8 ± 0.7	6.2 ± 0.7
R23	8.7 ± 1	9.2 ± 0.9
R24	NA	NA
R25	7.2 ± 0.8	7.6 ± 0.7
R26	1.6 ± 0.3	2.2 ± 0.4
R27	2.2 ± 0.4	3.0 ± 0.5
R28	4.1 ± 0.6	4.9 ± 0.8
R29	4.5 ± 0.6	5.4 ± 0.8
R30	6.7 ± 0.7	7.9 ± 1.0
R31	2.2 ± 0.2	2.6 ± 0.3
R32	3.4 ± 0.2	3.9 ± 0.4
R33	4.5 ± 0.3	5.2 ± 0.5

Heat flux gauge	Average heat flux (kW/m^2)	
R34	6.1 ± 0.4	6.9 ± 0.7
R35	6.9 ± 0.4	7.8 ± 0.8
R36	4.3 ± 0.3	4.3 ± 0.3
R37	5.7 ± 0.4	5.7 ± 0.4
R38	7.7 ± 0.5	7.7 ± 0.5
R39	10.7 ± 0.7	10.9 ± 0.7
R40	12.4 ± 0.7	13.2 ± 0.9

*Consistent reading though suspect based on measurements from other gauges

Table 3-29: Ethylene pool fire: Temporal and spatially averaged flame temperature and SEP during steady wind conditions

	Period 320-346 s			Period 433-462 s		
	Average	Min	Max	Average	Min	Max
	Station 1 (south)					
SEP* (kW/m^2)	188.4 ± 11.4	165.3	226.6	188.3 ± 10.0	159.1	209.7
Maximum SEP** † (kW/m^2)	424.1 ± 52.6	312.9	631.8	418.9 ± 48.1	303.5	617.5
	Station 2 (west)					
SEP* (kW/m^2)	185.6 ± 9.0	160.1	212.9	185.9 ± 9.2	163.5	225.2
Maximum SEP** † (kW/m^2)	420.1 ± 41.5	333.8	602.4	410.9 ± 37.5	318.8	517.9

*Spatially averaged
**Local maximum
†Corrected for atmospheric attenuation using a calculated transmissivity of 0.867

Table 3-30: Ethylene pool fire: Flame length and tilt angle during steady wind conditions

	Period 320-346 s			Period 433-462 s		
	Average	Min	Max	Average	Min	Max
	South 1 (south)					
Length (m)	16.3 ± 2.3	11.5	22.7	17.3 ± 3.2	10.3	27.5
Angle (deg)	58.0 ± 6.2	41.5	70.8	53.0 ± 6.3	37.6	68.4
	Station 2 (west)					
Length (m)	6.0 ± 1.3	3.9	11.1	6.5 ± 1.4	4.2	11.6
Angle (deg)	-19.9 ± 11.3	-44.0	25.5	-19.4 ± 12.7	-41.8	27.5

3.2.3. Propane

The 5-m diameter propane pool fire is shown in Figure 3-6. The test duration is about 12 minutes. Measurements are averaged over periods in which the wind speed is steady, and the wind direction has the least variance over the test duration. Table 3-31 provides time averaged wind speed and direction over the one period identified. The flame is tilted towards the east direction due to the westerly wind. The atmospheric and release conditions are provided in Table 3-32 and Table 3-33, respectively. The average mass flow rate provided in Table 3-33 is from the orifice plate flow measurements. The vortex meter after reaching about 4 kg/s abruptly decreased to values on the order of 0.1 kg/s, the cause of which is uncertain.

Figure 3-6: Propane pool fire

Table 3-31: Propane pool fire: Period of steady-state wind conditions based on wind speed

	Period 328-378 s
Height (m)	Average wind speed (m/s)
2	2.57 ± 0.10
5	2.81 ± 0.09
7.6	2.91 ± 0.08
	Average wind direction (deg)
2	278.0 ± 8.2
5	277.4 ± 12.3
7.6	280.5 ± 6.8
Average among heights	278.6 ± 6.5

Table 3-32: Propane pool fire: atmospheric conditions

Condition	Value
Atmospheric pressure (Pa)	81,186 ± 0.2
Atmospheric temperature (°C)	0.84 ± 0.07
Relative humidity (%)	19.1 ± 0.6

Table 3-33: Propane pool fire: Fuel release conditions during steady-state wind conditions

Condition	Period 328-378 s
Mass flow rate* (kg/s)	2.2 ± 0.1
Temperature (°C)	-18.2 ± 0.01

* By orifice plate

Table 3-34 provides the time-averaged heat flux measurements from the heat flux gauges over the period of steady wind conditions. The spatially and temporally averaged SEP is provided in Table 3-25. The SEP is corrected for atmospheric attenuation using a transmissivity of 0.90. The average flame length and tilt is provided in Table 3-36. The flame height is about 4 pool diameters.

Table 3-34: Propane pool fire: Time-averaged heat flux from heat flux gauges during steady-state wind conditions

Heat flux gauge	Average heat flux (kW/m^2)
	328-378 s
R1	6.5 ± 0.6
R2	8.8 ± 0.8

Heat flux gauge	Average heat flux (kW/m^2)
R3	14.4 ± 1.4
R4	18.2 ± 1.6
R5	NA
R6	6 ± 0.5
R7	14.3 ± 2.1
R8	20.9 ± 3.3
R9	NA
R10	NA
R11	13.5 ± 1.4
R12	22.9 ± 2.2
R13	37.3 ± 3.8
R14*	72.2 ± 7
R15**	6.1 ± 0.6
R16	9.5 ± 1.7
R17	14.9 ± 2.5
R18	NA
R19	33.9 ± 6
R20	NA
R21	7.1 ± 0.8
R22	8.9 ± 1.1
R23	17.1 ± 1.6
R24	NA
R25	13.2 ± 1.3
R26	4.6 ± 0.5
R27	6.5 ± 0.6
R28	9.8 ± 1
R29	10.4 ± 1
R30	14.8 ± 1.5
R31	4.2 ± 0.5
R32	5.5 ± 0.6
R33	7.7 ± 0.9

Heat flux gauge	Average heat flux (kW/m^2)
R34	12.0 ± 1.6
R35	11.9 ± 1.4
R36	5.8 ± 0.4
R37	6.8 ± 0.5
R38	9.3 ± 0.7
R39	12.4 ± 0.9
R40	17.9 ± 1.4

*Consistent reading though suspect since beyond range of gauge
**Consistent reading though suspect based on measurements from other gauges

Table 3-35: Propane pool fire: Temporal and spatially averaged SEP during steady-state wind conditions

	Period 328-378 s		
	Average	Min	Max
	Station 1 (south)		
SEP* (kW/m^2)	186.0 ± 13.4	141.9	218.3
Maximum SEP** † (kW/m^2)	362.2 ± 33.3	264.4	468.5
	Station 2 (west)		
SEP* (kW/m^2)	200.1 ± 13.0	163.7	232.9
Maximum SEP** † (kW/m^2)	420.8 ± 37.3	336.0	572.6

*Spatially averaged
**Local maximum
†Corrected for atmospheric attenuation using a calculated transmissivity of 0.90

Table 3-36: Propane pool fire: Flame length and tilt angle during steady-state wind conditions

	Period 328-378 s		
	Average	Min	Max
	South Station		
Length (m)	21.0 ± 3.6	12.5	31.9
Angle (deg)	40.9 ± 6.9	20.0	58.5
	West Station		
Length (m)	10.1 ± 1.4	6.3	15.0
Angle (deg)	23.9 ± 7.9	-13.6	48.2

3.2.4. Isopentane

The 5-m diameter isopentane pool fire is shown in Figure 3-7. The test duration is about 25 minutes. The fuel was supplied for 10 minutes after which the fire continued to burn for another 15 minutes. Measurements are averaged over periods in which the wind speed is steady, and the wind direction has the least variance over the test duration. Table 3-37 provides time averaged wind speed and direction over the one period identified. The flame is tilted towards the lightly towards the west direction due to the easterly wind.

The atmospheric and release conditions are provided in Table 3-38 and Table 3-39, respectively. The diptube instruments indicated that a liquid layer formed within the pool. Since the boiling point of isopentane is much higher than the other fuels, it did not rapidly vaporize upon contact with the concrete pool, thereby allowing for liquid accumulation. The fuel regression rate is equivalent to a steady fuel supply rate when the liquid fuel height is steady. Under steady conditions the liquid height is about 3".

The loss due to the diffuser is determined by comparing the flow rate measurements from the orifice plate to the three diptube measurements. Although the vortex meter provided measurements, the orifice plate is used for comparison since the vortex meter did not function during the entirety of the other pool fire tests. At the end of the isopentane test, the fuel supply was turned off and the fuel burned down at a constant rate. Thus, during this time a fuel regression rate can be calculated by fitting a line to a plot of height versus time from the diptube measurements. The slope of that curve is the fuel regression rate which is converted to a mass flow rate by using a density of 640 kg/m^3. The ratio of the orifice plate flow rate measurement to the measurements by the diptubes is the loss coefficient. The mass flow rate accounting for a loss coefficient of 0.352 is provided in Table 3-38.

Figure 3-7: Isopentane pool fire.

Figure 3-8: Isopentane pool fire: Period of steady wind conditions based on wind speed and direction.

	Period 356-383 s
Height (m)	Average wind speed (m/s)
2	1.40 ± 0.08
5	1.46 ± 0.03
7.6	1.44 ± 0.05
	Average wind direction (deg)
2	99.9 ± 3.6
5	95.8 ± 2.8
7.6	100.8 ± 5.7
Average among heights	98.8 ± 4.2

Table 3-37: Isopentane pool fire: atmospheric conditions

Condition	Value
Atmospheric pressure (Pa)	81,020 ± 0.2
Atmospheric temperature (°C)	-1.1 ± 0.04
Relative humidity (%)	57.6 ± 0.1

Table 3-38: Isopentane pool fire: Fuel release conditions during steady wind conditions

Condition	Period 356-383 s
Mass flow rate* (kg/s)	0.87 ± 0.02
Temperature (°C)	0.1 ± 0.01

* By orifice plate and vortex meter

Table 3-39 provides the time-averaged heat flux measurements from the heat flux gauges over the period of steady wind conditions. The spatially and temporally averaged temperature and surface emissive power (SEP), as well as their maximum values, are provided in Table 3-40. The SEP is corrected for atmospheric attenuation using a transmissivity of 0.891. The average flame length and tilt is provided in Table 3-41. The flame height is about 2 pool diameters.

Table 3-39: Isopentane pool fire: Time-averaged heat flux from heat flux gauges during steady wind conditions

Heat flux gauge	Average heat flux (kW/m^2)
	356-383 s
R1	2.8 ± 0.3

Heat flux gauge	Average heat flux (kW/m^2)
R2	3.6 ± 0.5
R3	4.0 ± 0.6
R4	9.6 ± 0.9
R5	NA
R6	2.5 ± 0.3
R7	3.5 ± 0.5
R8	4.8 ± 0.6
R9	NA
R10	NA
R11	2.1 ± 0.2
R12	3.0 ± 0.2
R13	4.6 ± 0.4
R14	7.9 ± 0.6
R15	NA
R16	2.3 ± 0.3
R17	3.0 ± 0.4
R18	NA
R19	6.2 ± 0.9
R20	NA
R21	1.4 ± 0.2
R22	3.0 ± 0.4
R23	5.3 ± 0.8
R24	NA
R25	4.2 ± 0.7
R26	1.3 ± 0.2
R27	3.1 ± 0.3
R28	5.1 ± 0.5
R29	5.9 ± 0.5
R30	9.3 ± 0.7
R31	2.5 ± 0.5
R32	4.5 ± 0.8

Heat flux gauge	Average heat flux (kW/m^2)
R33	7.4 ± 1.0
R34	11.6 ± 1.5
R35	13.3 ± 1.6
R36	3.2 ± 0.5
R37	5.2 ± 0.6
R38	8.7 ± 0.8
R39	14.2 ± 1.6
R40	15.4 ± 1.3

Table 3-40: Isopentane pool fire: Temporal and spatially averaged flame temperature and SEP during steady-state wind conditions

	Period 356-383 s		
	Average	Min	Max
	Station 1 (south)		
SEP* (kW/m^2)	154.4 ± 9.4	91.8	176.6
Maximum SEP**† (kW/m^2)	290.1 ± 29.1	102.1	379.1
	Station 2 (west)		
SEP* (kW/m^2)	162.7 ± 12.7	132.1	190.1
Maximum SEP**† (kW/m^2)	331.2 ± 36.1	238.1	451.0

*Spatially averaged
**Local maximum
†Corrected for atmospheric attenuation using a calculated transmissivity of 0.891

Table 3-41: Isopentane pool fire: Flame length and tilt angle during steady-state wind conditions

	Period 328-378 s		
	Average	Min	Max
	Station 1 (west)		
Length (m)	10.3 ± 1.6	6.4	15.9
Angle (deg)	-18.3 ± 5.3	-31.9	-8.0
	Station 2 (west)		
Length (m)	11.6 ± 2.2	5.7	17.7
Angle (deg)	-13.7 ± 6.2	-27.9	9.0

3.3. Fireballs

Sections 3.3.1 through 3.3.3 provide measurements of release conditions, heat flux, surface emissive power, diameter, rise height, and weather conditions for the ethane, ethylene, and isopentane fireballs, respectively. For all fireball experiments the dimensions and surface emissive power are based on temperatures above 1123 K as measured from the IR camera. This temperature corresponds to an SEP value of 90 kW/m^2 assuming blackbody radiation.

Since all heat flux measurements from the heat flux gauges vary over time during the entire test, the maximum heat flux and the thermal dose unit are provided. For events that have exposure to a high heat flux level over a short duration such as a fireball, a common measure for the effects from radiant heat exposure is thermal dose or also termed thermal dosage. It is determined by integrating the heat flux over time. A commonly used equation for thermal dose is the thermal dose unit (TDU), that is,

$$\text{thermal dose unit}(t) = \int_0^t q(t)^{\frac{4}{3}} dt \qquad \text{Eq. 3.3.1}$$

where q(t) is the time varying radiant flux (kW/m^2) and t is the duration of exposure (s). A constant heat flux level of 5 kW/m^2 over 30 seconds exposure, for example, corresponds to a TDU of 256 (kW/m^2)$^{4/3}$s.

Table 3-42 provides the mean and range of TDU values that result in different levels of injury [8]. A range is typically reported in the literature because various researchers have used different test methodologies, such as, type of test subject (animals versus human), clothed or bare skin, and different exposure sources. Thermal dose is utilized in probit equations for quantitative risk-analysis to estimate the probability of fatality. A 50% probability of fatality corresponds to TDU values ranging from about 1000 to 4000 (kW/m^2)$^{4/3}$s, with the existence of a range due to the reasons given above.

Measurements of surface emissive power, effective diameter, rise height, and duration from the infrared cameras are provided for the fireball experiments. Derived quantities such as power and energy are also provided. The total energy is derived by integrating the SEP over the duration of the fireball and the power is the product of the projected area and SEP. Since the radiant heat transferred to the heat flux gauges decreases over time due to the fireball moving further away as it evolves, lower heights will result in higher heat flux measurements compared to later times. To account for the movement away from the heat flux gauges, a fractional height is defined as the ratio of height to the maximum height over time where the height is from the center of the fireball to the ground. The fractional height is then substracted from a value of one and then multiplied by the power. Herein, this is referred to as the power-fractional height product. The time to maximum power, maximum average SEP, and the power-fractional height product are compared to the maximum heat flux measurements from the gauges to assess correspondance.

Table 3-42: Injury for different thermal dose levels

Injury	Thermal dose (kW/m^2)$^{4/3}$s	
	mean	range
pain	92	86-103
Threshold 1st degree burn	105	80-130
Threshold 2nd degree burn	290	240-350
Threshold 3rd degree burn	1000	870-2600

3.3.1. Ethane

The ethane fireball, shown in Figure 3-9, reached complete burn out approximately 8 seconds after release. The fuel is released vertically from the top of the cryogenic tank, where the diameter of release is that of the inner tank which is 48". Figure 3-10(a-d) shows the tank post-test, the perlite insulation, and the severed inner and outer lids. The average wind speed and direction during the test is provided in Table 3-43. The atmospheric conditions and release conditions are provided in Table 3-44 and Table 3-45, respectively. The maximum heat flux and thermal dose unit from the heat flux gauges are provided in Table 3-46,. Heat flux over time from the gauge measurements are provided in Figure 3-11 through Figure 3-14.

Figure 3-9: Ethane fireball.

(a) (b) (c) (d)

Figure 3-10: Ethane fireball: post-test (a) tank, (b) perlite insulation, (c) inner lid, and (d) outer lid.

Table 3-43: Ethane fireball: Average wind speed and direction during test.

Height (m)	Average wind speed (m/s)
2	3.8 ± 0.4
5	4.2 ± 0.5
7.6	4.5 ± 0.4
Height (m)	**Average wind direction (deg)**
2	229.5 ± 7.5
5	237.1 ± 21.4
7.6	231.8 ± 13.2
Average among heights	232.8 ± 15.0

Table 3-44: Ethane fireball: atmospheric conditions

Condition	Value
Atmospheric pressure (Pa)	80,188 ± 0.2
Atmospheric temperature (°C)	5.9 ± 0.02
Relative humidity (%)	36.5 ± 0.05

Table 3-45: Ethane fireball: release conditions

Condition	Values
Tank pressure (psig)	181
Temperature (°C)	-32.8
Amount of fuel (kg)(gallons)	1157 (656)
Density (kg/m3)	466

Table 3-46: Ethane fireball: Maximum heat flux and thermal dose unit from heat flux gauges

Heat flux gauge	Maximum heat flux (kW/m^2)	Thermal dose unit $(kW/m^2)^{4/3}s$
R1	20.6	189.1
R2	20.2	178.4
R3	22.1	205.2
R4	22.8	208.5
R5	NA	NA
R6	27.1	256.3
R7	26.7	246.9
R8	27.1	246.9
R9	33.2	325.7
R10	NA	NA
R11	35.0	347.5
R12	35.2	347.7
R13	32.1	313.4
R14	38.1	395.8
R15	43.2	453.2
R16	41.2	429.2
R17	42.1	435.8
R18	NA	NA
R19	43.8	441.6
R20	42.2	415.4
R21	53.0	539.5
R22	54.9	545.1
R23	59.5	629.1
R24	69.9	670.8
R25	65.0	682.0
R26	71.7	723.0
R27	68.5	742.5
R28	75.3	795.4
R29	77.1	819.6
R30	76.5	808.8
R31	42.0	441.6
R32	47.7	516.9
R33	48.2	511.9

Heat flux gauge	Maximum heat flux (kW/m^2)	Thermal dose unit $(kW/m^2)^{4/3}s$
R34	52.2	575.6
R35	51.1	537.1
R36	57.1	619.9
R37	58.7	633.1
R38	60.1	648.1
R39	68.8	773.8
R40	NA	NA

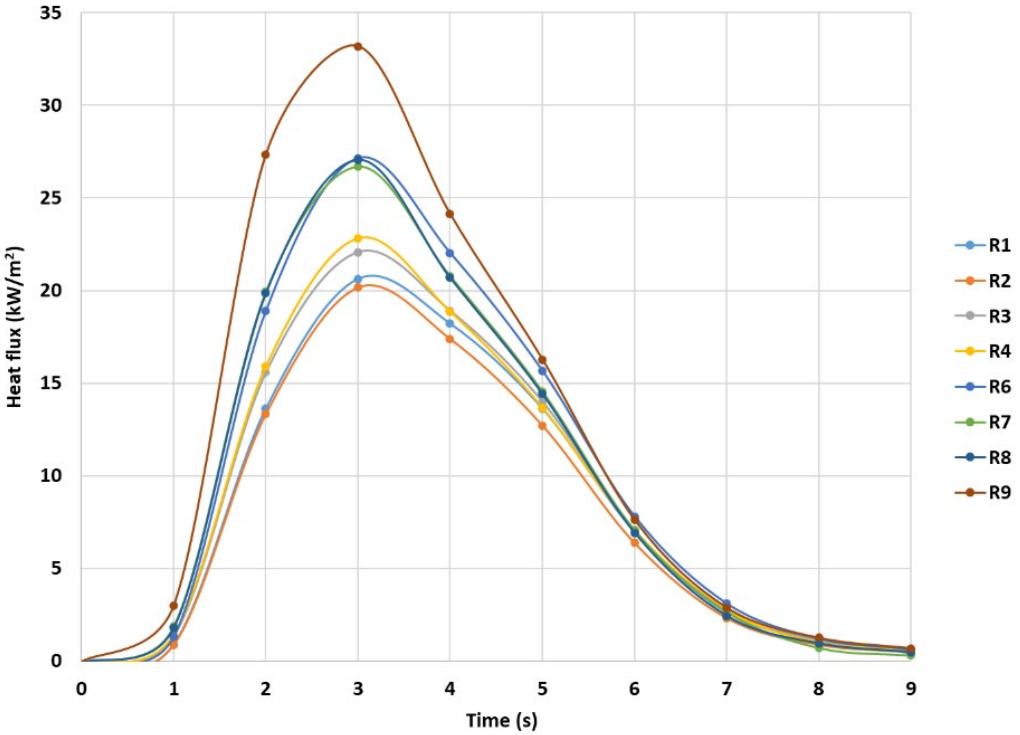

Figure 3-11: Ethane fireball: Heat flux measurements from gauges R1 through R9

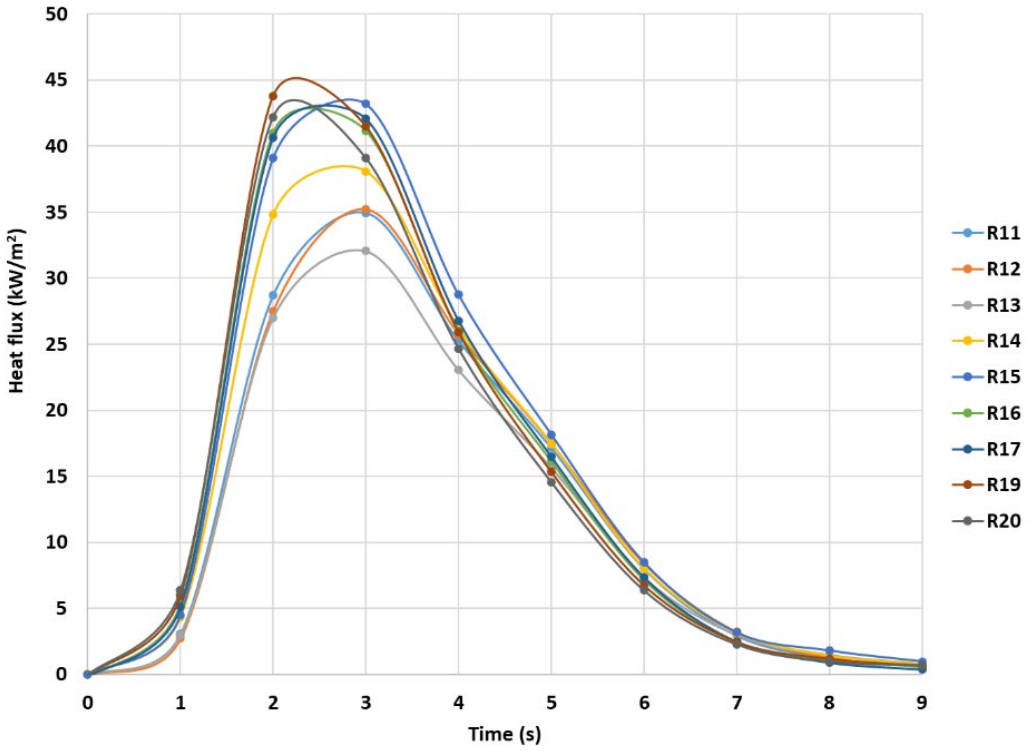

Figure 3-12: Ethane fireball: Heat flux measurements from gauges R11 through R20

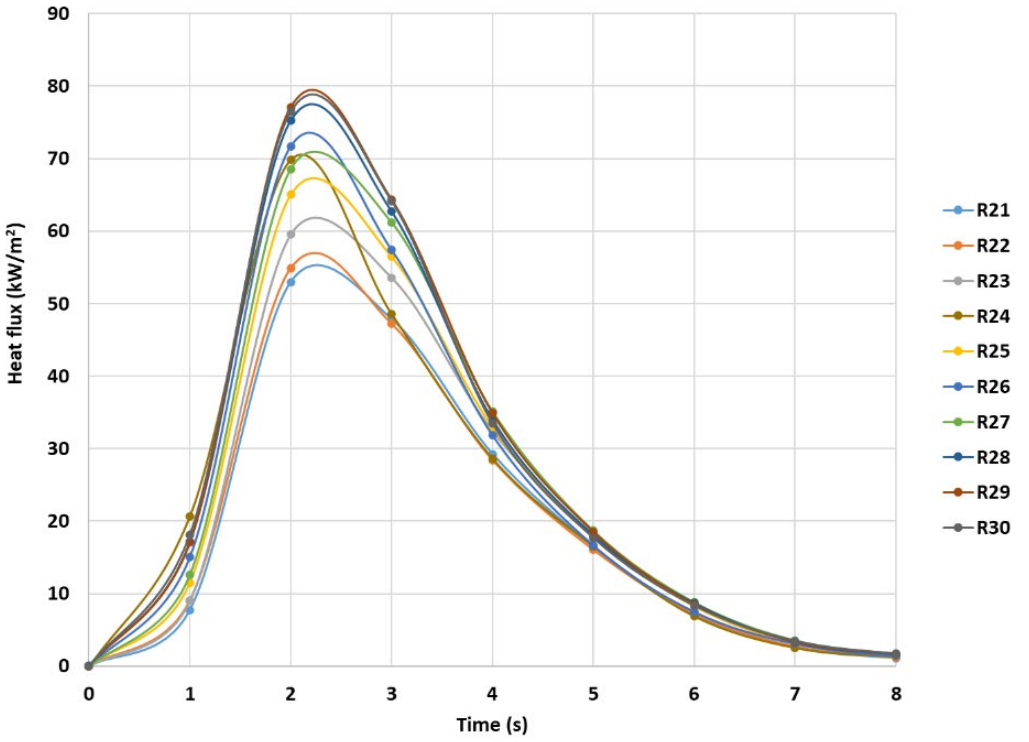

Figure 3-13: Ethane fireball: Heat flux measurements from gauges R21 through R30

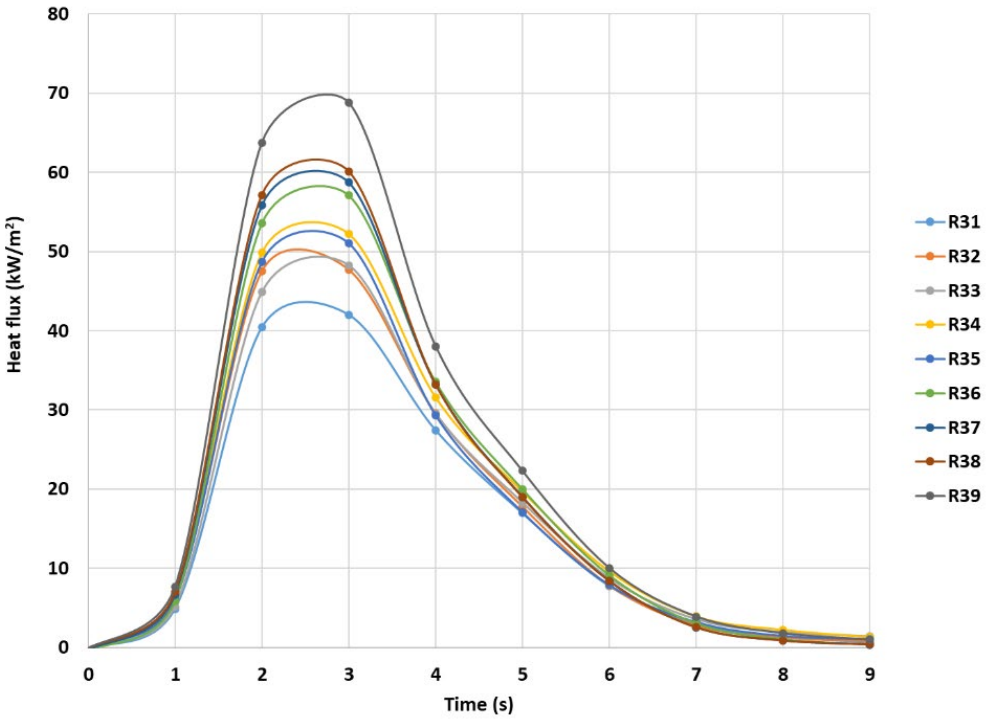

Figure 3-14: Ethane fireball: Heat flux measurements from gauges R31 through R40

Table 3-47 provides measurements of surface emissive power, effective diameter, rise height, duration, power, energy, and the power-fractional height product. The power-fractional height product over time is shown in Figure 3-15. The time to maximum power, maximum average SEP, and maximum power-fractional height product is 2.9, 3.3, and 2.2 seconds, respectively. This range of values agrees with times at which peak heat flux values from the gauge measurements occurred as show in Figure 3-11 through Figure 3-14.

Table 3-47: Ethane fireball: measurements from infrared cameras

Measurement	Station location	Value	Average between stations
Time at maximum power (s)	South	2.3	
	East	3.5	2.9
Maximum power (MW)	South	1194	
	East	1614	1404
Total energy (MJ)	South	4237	
	East	3355	3796
Average SEP at maximum power*† (kW/m^2)	South	341	
	East	341	341
Maximum average SEP*†	South	346	

Measurement	Station location	Value	Average between stations
	East	354	350
Time at maximum average SEP* (s)	South	3.7	
	East	2.8	3.3
Height at maximum average SEP (m)	South	68	
	East	56	62
Effective diameter at maximum average SEP (m)	South	70	
	East	77	74
Maximum SEP** † (kW/m^2)	South	717	
	East	617	667
Time to maximum SEP (s)	South	4.2	
	East	2.0	3.1
Effective diameter at maximum power (m)	South	71	
	East	81	76
Maximum effective diameter (m)	South	71	
	East	84	78
Maximum rise height (m)	South	126	
	East	152	139
Height at maximum power (m)	South	41	
	East	69	55
Maximum $P(1-h/h_{max})$ (MW)	South	813	
	East	1028	921
Time at maximum $P(1-h/h_{max})$ (s)	South	2.2	
	East	2.3	2.2
Height at maximum $P(1-h/h_{max})$ (m)	South	40	
	East	44	42
Effective diameter at maximum $P(1-h/h_{max})$ (m)	South	71	
	East	77	74
Time at total burnout (s)		8.0	

*Spatially averaged
**Local maximum
†Corrected for atmospheric attenuation using a calculated transmissivity of 0.761

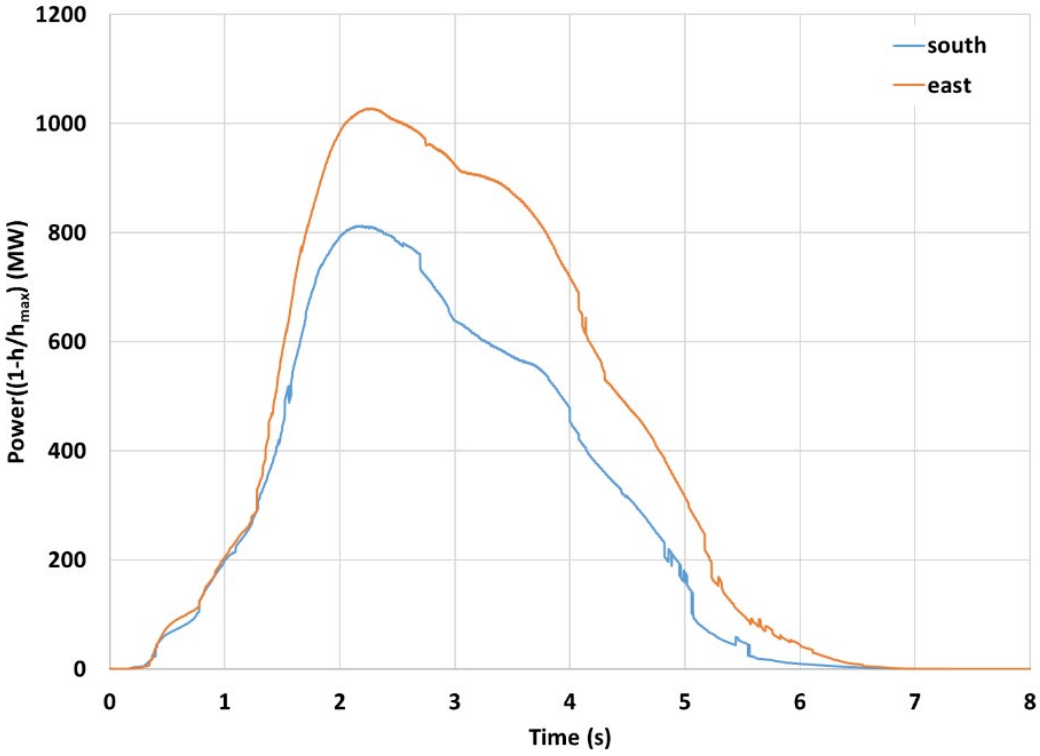

Figure 3-15: Ethane fireball: power-fractional height product over time

3.3.2. Ethylene

The ethylene fireball, shown in Figure 3-16, reached complete burn out approximately 13 seconds after release. The fuel is released vertically from the top of the cryogenic tank with a release diameter of 48". Figure 3-17(a-c) shows the tank post-test as well as the severed inner and outer lids. The blocks surrounding the tank became unstable upon release due to tension from the chain attached to the top lid. The tank however remained constrained by the other barricades. The chain caused the outer lid to fall near the tank, while the inner lid was thrown in a direction away from personnel and infrastructure about 250' from the tank.

This test was performed in quiescent conditions with wind speeds below 1 m/s. The average wind speed and direction during the test is provided in Table 3-48. The atmospheric conditions and release conditions are provided in Table 3-49 and Table 3-50, respectively. The maximum heat flux and the thermal dose unit are provided in Table 3-51. Heat flux over time from the gauge measurements are provided in Figure 3-18 through Figure 3-21. Note that the heat flux measurements do not drop steadily after reaching a maximum value as seen with the ethane and isopentane fireballs, but plateus for about 3 seconds before decreasing.

Figure 3-16: Ethylene fireball

(a) (b) (c)

Figure 3-17: Ethylene fireball: post-test (a) tank, (b) inner lid, and (c) outer lid.

Table 3-48: Ethylene fireball: Average wind speed and direction during test.

Height (m)	Average wind speed (m/s)
2	0.87 ± 0.01
5	0.80 ± 0.02
7.6	0.74 ± 0.01
Height (m)	**Average wind direction (deg)**
2	56.9 ± 10.3
5	47.7 ± 13.3
7.6	60.0 ± 9.0
Average among heights	54.9 ± 10.1

Table 3-49: Ethylene fireball: atmospheric conditions

Condition	Value
Atmospheric pressure (Pa)	80,547 ± 0.2
Atmospheric temperature (°C)	2.1 ± 0.03
Relative humidity (%)	41.3 ± 0.06

Table 3-50: Ethylene fireball: release conditions

Condition	Values
Tank pressure (psig)	175
Temperature (°C)	-59.4
Amount of fuel (kg)(gallons)	1153 (613)
Density (kg/m3)	497

Table 3-51: Ethylene fireball: Maximum heat flux from heat flux gauges

Heat flux gauge	Maximum heat flux (kW/m^2)	Thermal dosage unit $(kW/m^2)^{4/3}s$
R1	8.1	123.8
R2	7.7	115.4
R3	8.3	128.8
R4	8.3	129.2
R5	NA	NA
R6	9.8	152.3
R7	9.6	146.2
R8	9.8	147.1

Heat flux gauge	Maximum heat flux (kW/m^2)	Thermal dosage unit $(kW/m^2)^{4/3}s$
R9	11.5	174.8
R10	NA	NA
R11	12.6	197.0
R12	12.6	195.4
R13	12.0	182.5
R14	14.2	220.9
R15	16.0	219.6
R16	16.4	223.2
R17	17.3	237.0
R18	NA	NA
R19	20.3	251.1
R20	19.0	230.5
R21	25.7	294.4
R22	27.9	313.6
R23	30.2	328.4
R24	32.7	397.2
R25	35.8	368.8
R26	41.3	386.9
R27	42.4	400.9
R28	46.6	443.0
R29	48.6	458.1
R30	49.6	468.3
R31	17.5	247.0
R32	18.6	245.0
R33	18.0	243.1
R34	18.1	251.3
R35	18.3	233.5
R36	19.0	260.9
R37	19.7	255.3
R38	19.5	257.8
R39	21.4	295.0
R40	NA	NA

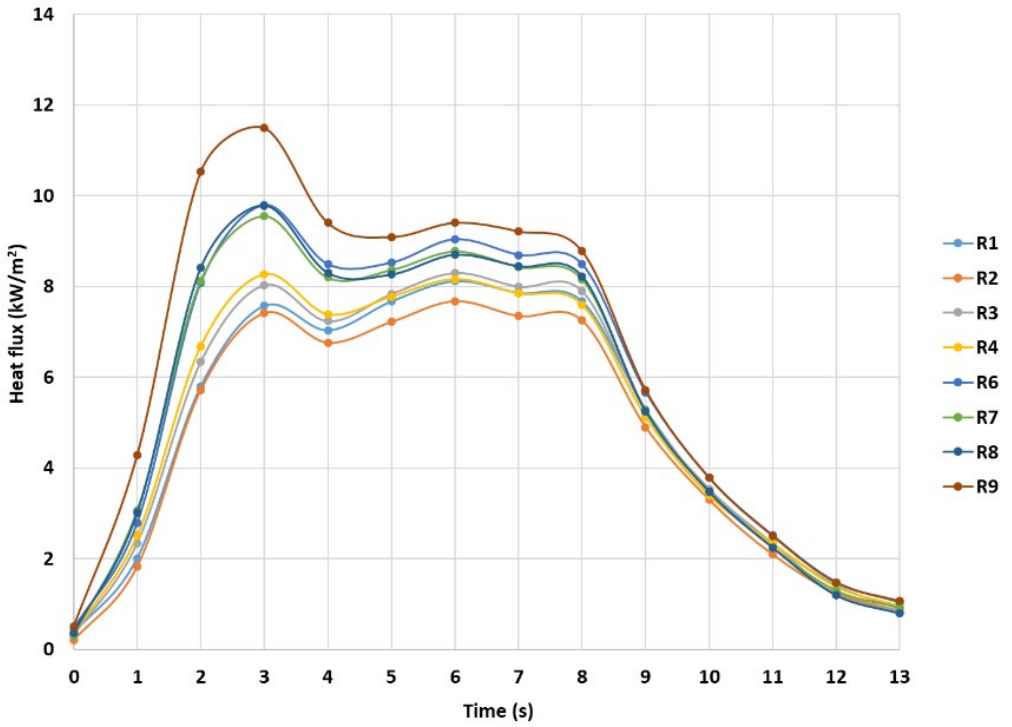

Figure 3-18: Ethylene fireball: Heat flux measurements from gauges R1 through R9

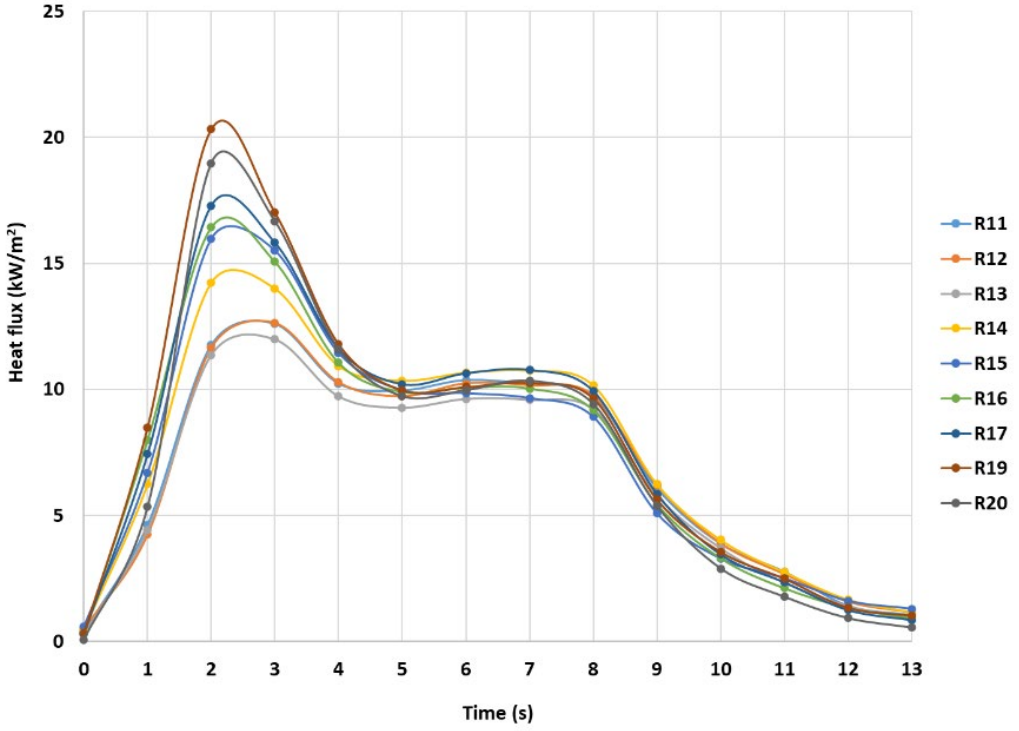

Figure 3-19: Ethylene fireball: Heat flux measurements from gauges R11 through R20

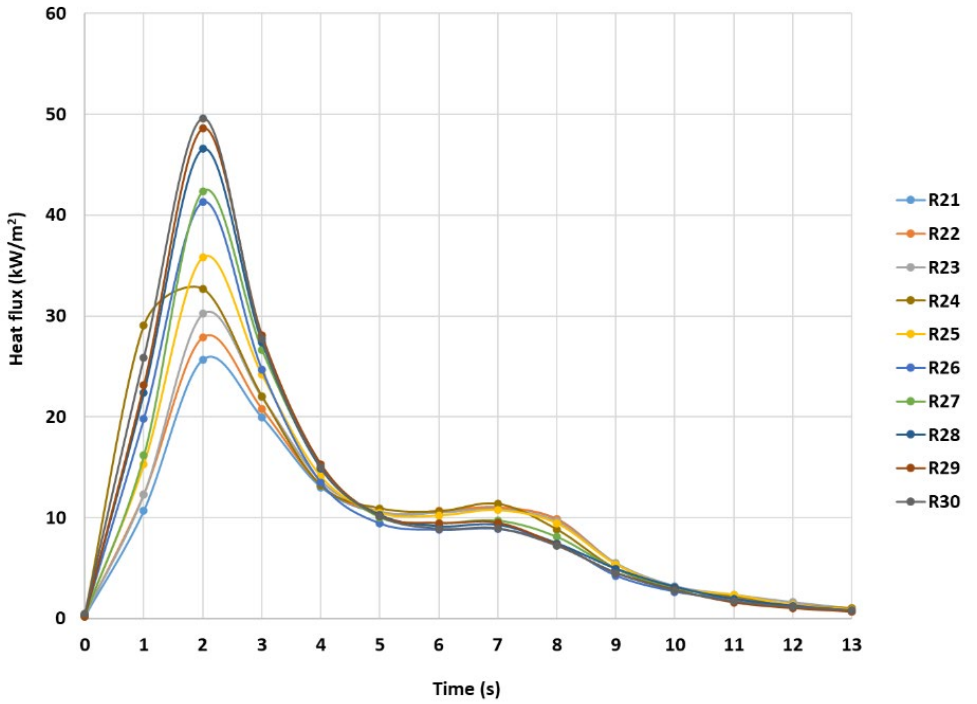

Figure 3-20: Ethylene fireball: Heat flux measurements from gauges R21 through R30

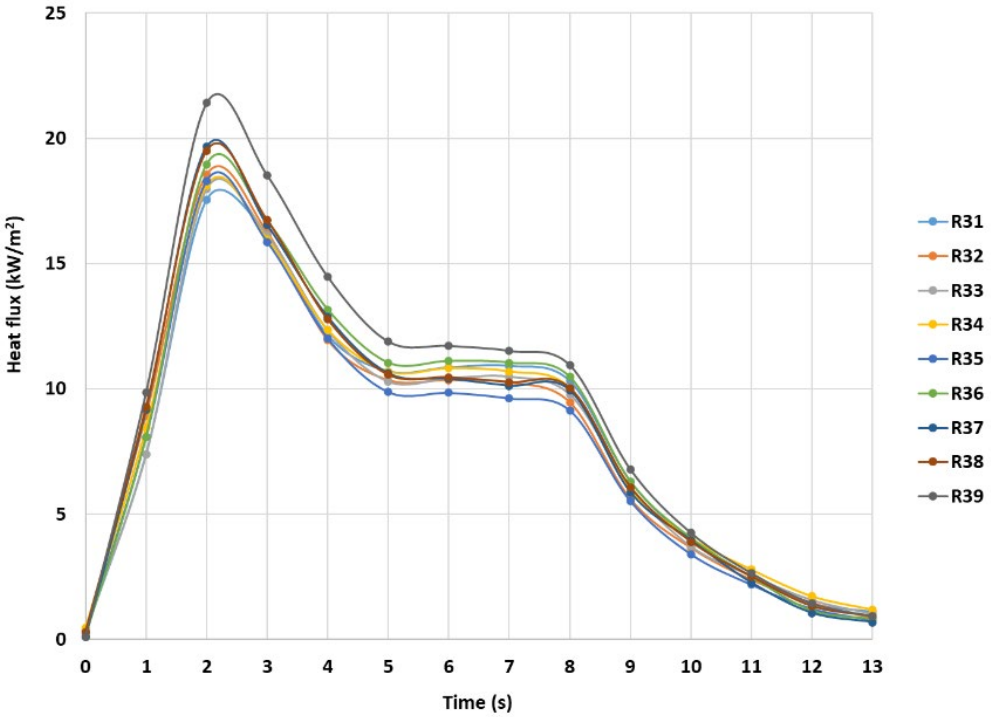

Figure 3-21: Ethylene fireball: Heat flux measurements from gauges R11 through R39

Table 3-52 provides measurements of surface emissive power, effective diameter, rise height, duration, power, energy, and the power-fractional height product. The power-fractional height product over time is shown in Figure 3-22. The time to maximum power, maximum average SEP, and maxium power-fractional height product is 6.3, 0.9, and 2.2 seconds, respectively. In comparing to times at which peak heat flux values occur from the gauge measurements as show in Figure 3-18 through Figure 3-21, the maximum power-fractional height product provides the best agreement. In contrast to the other fireball experiments, this fireball lasted longer and at its later stages formed an expanding toroidal shape which was maintained beyond complete burn out resulting in a smoke ring. The formation and expansion of the toroidal shape is the cause of an increase in area which thus results in the peak power occurring at a much later time than the other experiments.

Table 3-52: Ethylene fireball: measurements from infrared cameras

Measurement	Station location	Value	Average between stations
Time at maximum power (s)	South	5.2	
	East	7.5	6.3
Maximum power (MW)	South	660	
	East	724	692
Total energy (MJ)	South	4344	
	East	4867	4806
Average SEP at maximum power* (kW/m^2)	South	283	
	East	237	260
Maximum average SEP*	South	340	
	East	258	299
Time at maximum average SEP (s)	South	0.7	
	East	1.2	0.9
Height at maximum average SEP (m)	South	8.3	
	East	20.9	15
Effective diameter at maximum average SEP (m)	South	30	
	East	37	34
Maximum SEP** (kW/m^2)	South	849	
	East	652	751
Time to maximum SEP** (s)	South	3.6	
	East	4.5	4.1

Measurement	Station location	Value	Average between stations
Effective diameter at maximum power (m)	South	56	
	East	71	64
Maximum effective diameter (m)	South	72	
	East	84	78
Maximum rise height (m)	South	172	
	East	175	173
Height at maximum power (m)	South	93	
	East	124	109
Maximum P(1-h/hmax) (MW)	South	370	
	East	403	387
Time at maximum P(1-h/hmax) (s)	South	2.1	
	East	2.2	2.2
Height at maximum P(1-h/h_{max}) (m)	South	36	
	East	38	37
Effective diameter at maximum P*(1-h/h_{max}) (m)	South	50	
	East	55	53
Time at total burnout (s)		13	

*Spatially averaged
**Local maximum
†Corrected for atmospheric attenuation using a calculated transmissivity of 0.766

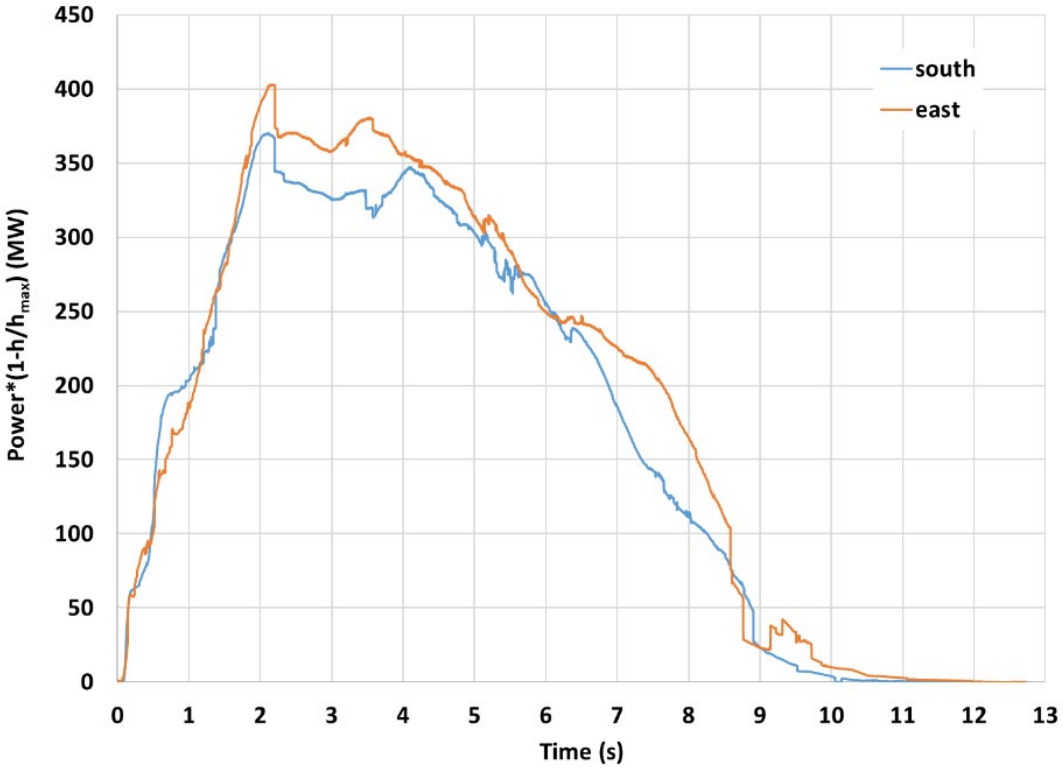

Figure 3-22: Ethylene fireball: power-fractional height product over time

3.3.3. Isopentane

The isopentane fireball, shown in Figure 3-23, reached complete burn out approximately 10 seconds after release. The fuel is released vertically from the top of the tank, where the diameter of release is 48". Figure 3-24(a-b) shows the tank post-test as well as the severed lid. The blocks surrounding the tank remained stable during release due to adjustment of the chain attached to the top lid. The lid was thrown in a direction away from personnel and infrastructure about 250' from the tank.

The average wind speed and direction during the test is provided in Table 3-53. The atmospheric conditions and release conditions are provided in Table 3-54 and Table 3-55, respectively. This test was performed in nearly quiescent conditions with wind speeds around 1 m/s. The maximum heat flux and the thermal dose unit are provided in Table 3-56. Heat flux over time from the gauge measurements are provided in Figure 3-25 through Figure 3-28.

Figure 3-23: Isopentane fireball.

(a) (b)

Figure 3-24: Isopentane fireball: post-test (a) tank, and (b) lid.

Table 3-53: Isopentane fireball: Average wind speed and direction during test.

Height (m)	Average wind speed (m/s)
2	1.11 ± 0.1
5	0.81 ± 0.06
7.6	0.94 ± 0.1
Height (m)	**Average wind direction (deg)**
2	101.2 ± 11.2
5	107.8 ± 15.3
7.6	126.1 ± 17.1
Average among heights	111.8 ± 16.7

Table 3-54: Isopentane fireball: atmospheric conditions

Condition	Value
Atmospheric pressure (Pa)	81,260 ± 0.2
Atmospheric temperature (°C)	11.5 ± 0.05
Relative humidity (%)	26.4 ± 0.05

Table 3-55: Isopentane fireball: release conditions

Condition	Values
Tank pressure (psig)	164
Temperature (°C)	114
Amount of fuel (kg)(gallons)	1150 (481)
Density (kg/m3)	509

Table 3-56: Isopentane fireball: Maximum heat flux from heat flux gauges

Heat flux gauge	Maximum heat flux (kW/m^2)	Thermal dose unit $(kW/m^2)^{4/3}s$
R1	20.0	184.9
R2	22.2	211.7
R3	21.4	194.5
R4	NA	NA
R5	25.2	230.6
R6	26.2	242.0
R7	25.1	223.8

Heat flux gauge	Maximum heat flux (kW/m^2)	Thermal dose unit $(kW/m^2)^{4/3}s$
R8	35.5	348.2
R9	NA	NA
R10	37.6	378.6
R11*	29.6	269.9
R12	38.6	393.2
R13	34.5	335.1
R14	40.2	397.1
R15	46.4	483.5
R16	44.6	450.8
R17	NA	NA
R18	46.3	464.8
R19	44.6	446.4
R20	55.3	568.0
R21	53.1	566.7
R22	55.3	570.7
R23	NA	NA
R24	NA	NA
R25	66.7	686.9
R26	64.5	704.2
R27	65.5	672.8
R28	71.1	767.7
R29	77.8	782.0
R30*	46.8	484.3
R31	42.5	420.0
R32	43.8	436.5
R33	43.1	421.0
R34	45.7	451.9
R35	43.8	428.8
R36	50.0	513.0
R37*	42.0	406.9
R38	57.0	610.1
R39	NA	NA
R40	NA	NA

*Consistent reading though suspect based on measurements from other gauges

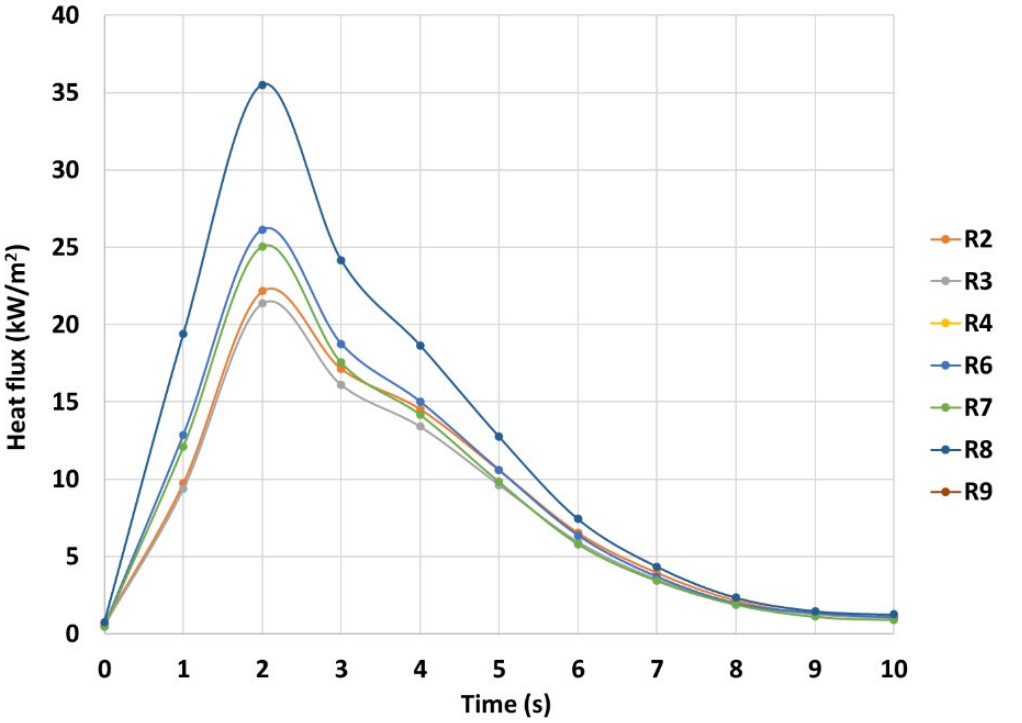

Figure 3-25: Isopentane fireball: Heat flux measurements from gauges R2 through R9

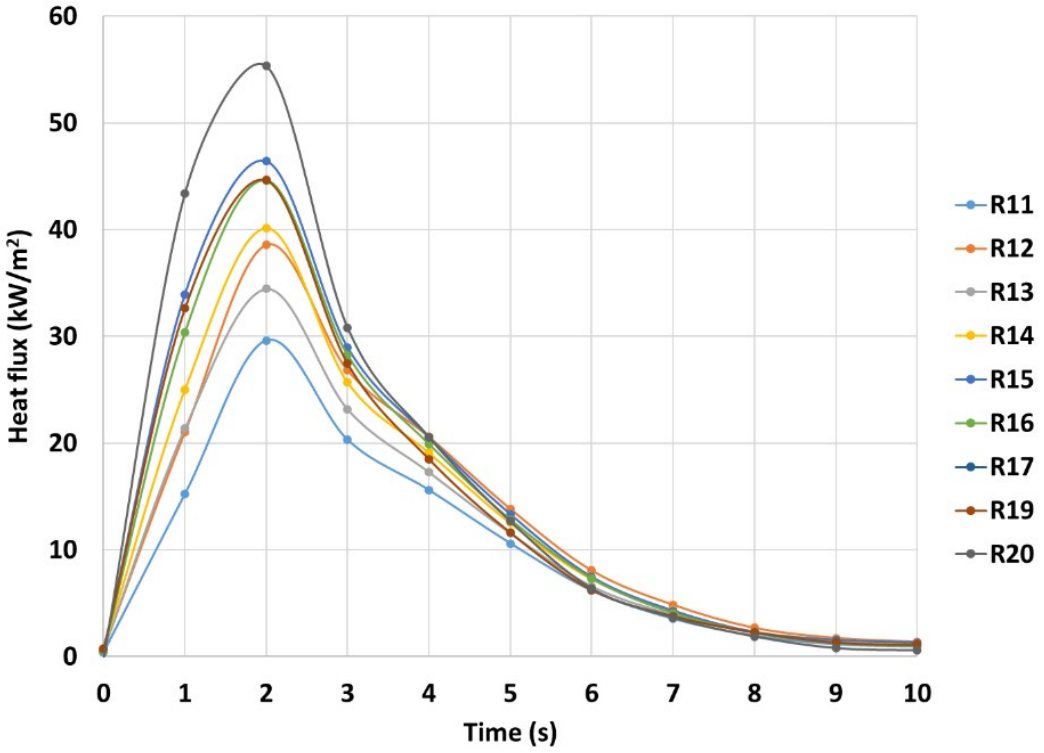

Figure 3-26: Isopentane fireball: Heat flux measurements from gauges R11 through R20

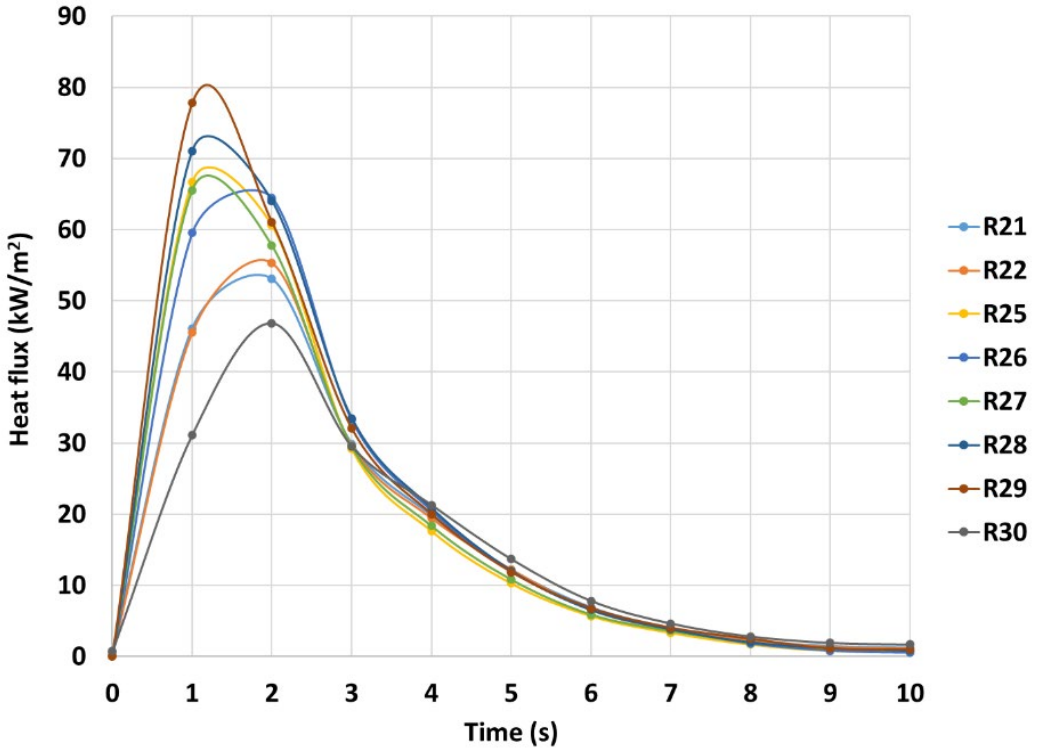

Figure 3-27: Isopentane fireball: Heat flux measurements from gauges R21 through R30

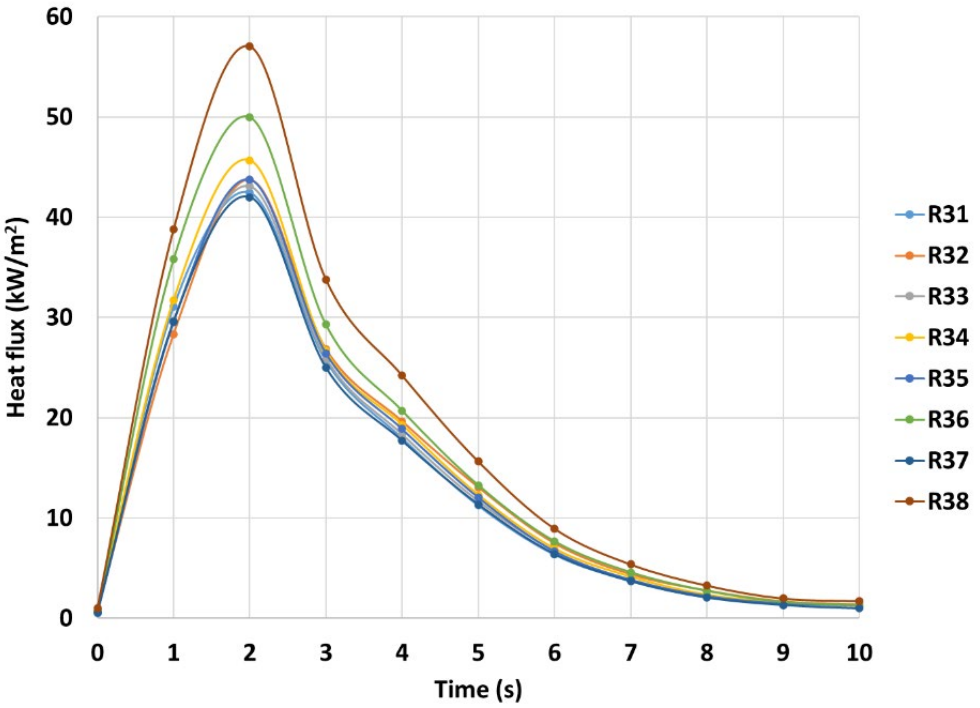

Figure 3-28: Isopentane fireball: Heat flux measurements from gauges R11 through R30

Table 3-57 provides measurements of surface emissive power, effective diameter, rise height, duration, power, energy, and the power-fractional height product. The power-fractional height product over time is shown in Figure 3-29. The time to maximum power, maximum average SEP, and maxium power-fractional height product is 1.7, 2.3, and 1.7 seconds, respectively. This range of values agrees with times at which peak heat flux values from the gauge measurements occurred as shown in Figure 3-25 through Figure 3-28.

Table 3-57: Isopentane fireball: measurements from infrared cameras

Measurement	Station location	Value	Average between stations
Time at maximum power (s)	South	1.8	
	East	1.7	1.7
Maximum power (MW)	South	1061	
	East	1280	1171
Total energy (MJ)	South	4479	
	East	5258	4869
Average SEP at maximum power* (kW/m^2)	South	385	
	East	362	373

Measurement	Station location	Value	Average between stations
Maximum average SEP*	South	395	
	East	368	381
Time at maximum average SEP* (s)	South	1.4	
	East	3.1	2.3
Height at maximum average SEP (m)	South	39	
	East	82	61
Effective diameter at maximum average SEP (m)	South	57	
	East	67	62
Maximum SEP** (kW/m^2)	South	779	
	East	733	756
Time to maximum SEP** (s)	South	1.8	
	East	2.8	2.3
Effective diameter at maximum power (m)	South	63	
	East	71	67
Maximum effective diameter (m)	South	63	
	East	72	67
Maximum rise height (m)	South	176	
	East	152	164
Height at maximum power (m)	South	45	
	East	43	44
Maximum P(1-h/h_{max}) (MW)	South	792	
	East	919	855
Time at maximum P(1-h/h_{max}) (s)	South	1.8	
	East	1.7	1.7
Height at maximum P(1-h/h_{max}) (m)	South	45	
	East	43	44
Effective diameter at maximum P(1-h/h_{max}) (m)	South	63	
	East	71	67
Time at total burnout		10.0	

*Spatially averaged
**Local maximum
†Corrected for atmospheric attenuation using a calculated transmissivity of 0.759

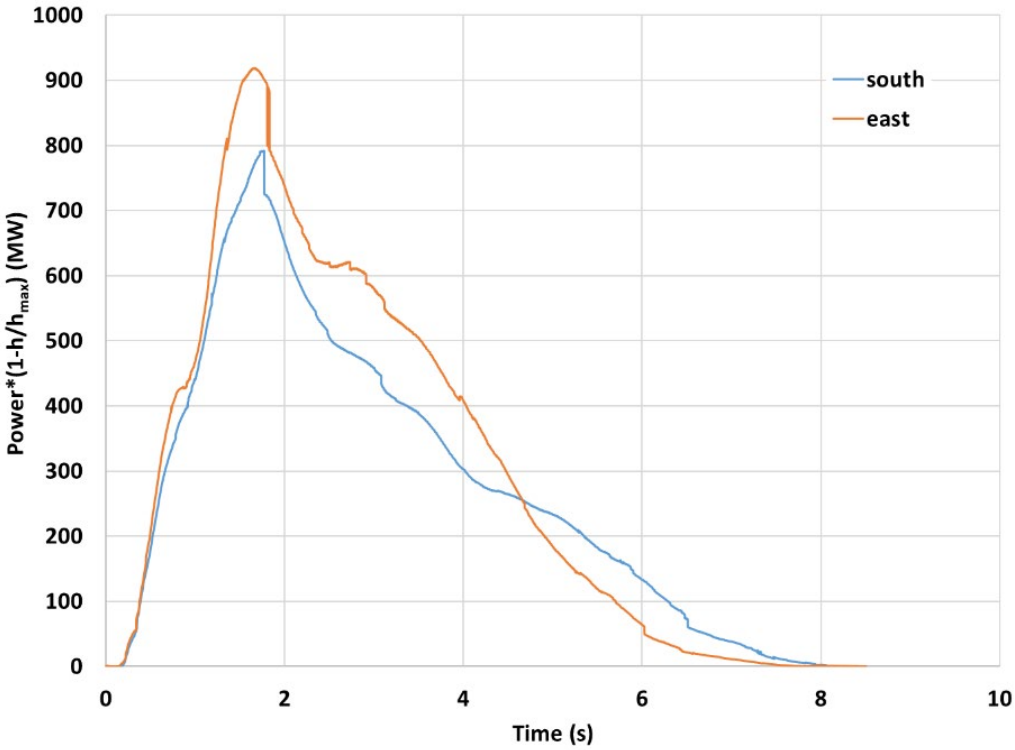

Figure 3-29: Isopentane fireball: power-fractional height product over time

4. EXPERIMENTAL DESCRIPTION OF WALL EXPERIMENTS

The objective of these experiments is to obtain data for model validation, specifically for models used to assess the performance of concrete walls that serve as thermal barriers to reduce the hazards associated with potential accidents at LNG facilities. To carry out this objective, the experiments involve measuring the thermal response of two types of concrete walls when exposed to a radiant ceramic heater. The experimental arrangement, instrumentation, thermal properties, testing procedures, and results are provided in the following sections.

4.1. Experimental Arrangement

Two types of walls are tested which include a formed insulated concrete wall and an insulated concrete masonry wall. The walls are heated using the same ceramic heaters used for the isopentane fireball experiment as previously mentioned. The heaters are arranged in a half circle which is built up from twelve quarter-round ceramic heaters (Figure 4-1). Combined the heaters have a maximum power output of 96 kW. The heaters heat a 1/8" thick stainless-steel shroud (5'4" x 5'4") placed 2" from the walls (Figure 4-2). The purpose of the shroud is to provide a more uniform temperature and a well-characterized boundary condition for model validation. The formed wall is tested at targeted shroud temperatures of 272°C, 375°C, and 444°C which corresponds to blackbody heat flux levels 5 kW/m^2, 10 kW/m^2, and 15 kW/m^2, while the masonry wall is tested at 470°C which corresponds to a blackbody heat flux of 17.3 kW/m^2.

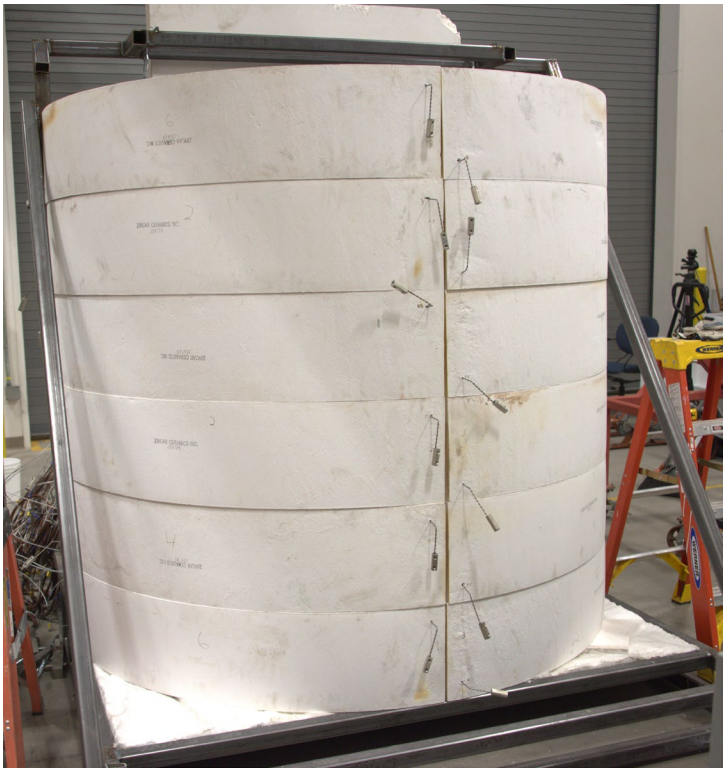

Figure 4-1: Ceramic heaters to heat walls

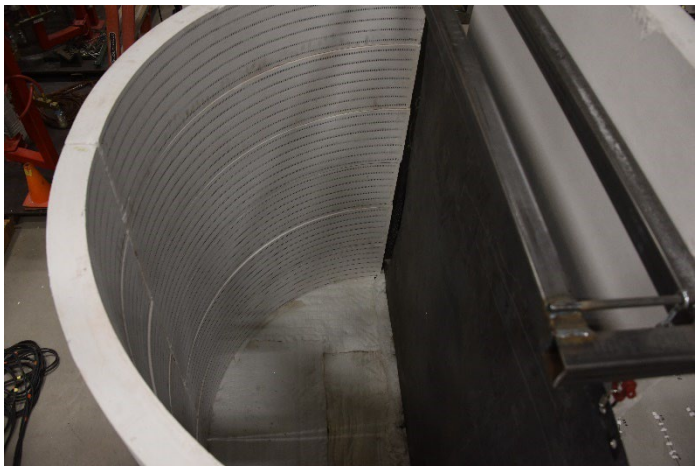

Figure 4-2: Top view of wall arrangement showing stainless steel shroud on the right.

The formed wall has two layers of 3" thick standard concrete (3/8" aggregate) with 2" thick insulation board between them fitted with ties which provide shear strength and allows the insulation to anchor to the concrete. The concrete layers also have wire meshing reinforcement to prevent cracking. The insulation board is comprised of bonded mineral wool and can be used for continuous service up to 649°C and is noncorrosive, noncombustible, and is dimensionally stable at elevated temperatures. Its compressive strength is 270 lbs/ft^2 which is below the pressure of 40 lb/ft^2 resulting from the weight of the 3" layer of concrete during the horizontal build and thus will not compress. The preformed wall is constructed horizontally using a wooden form. Figure 4-3 shows an exploded view of the assembly of the formed wall with the heater while Figure 4-4 provides dimensions. This heater arrangement and placement are used for both walls.

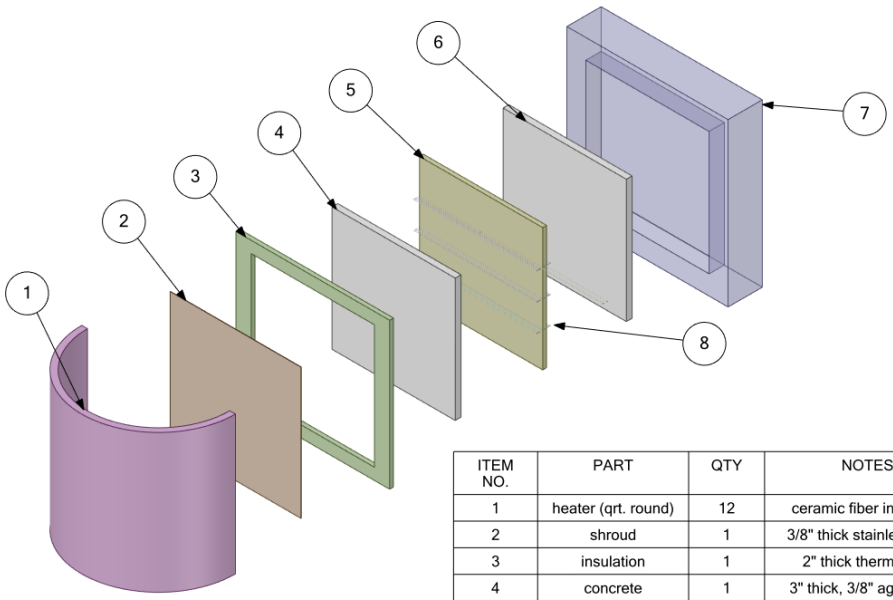

ITEM NO.	PART	QTY	NOTES
1	heater (qrt. round)	12	ceramic fiber insulated
2	shroud	1	3/8" thick stainless steel
3	insulation	1	2" thick thermafiber
4	concrete	1	3" thick, 3/8" aggregate
5	insulation	1	2" thick thermafiber
6	concrete	1	3" thick, 3/8" aggregate
7	insulation	1	5 x 2" thick thermagiver
8	wires	18	Wire supports for embeded TCs. Wire mesh within concrete provides support at midplane

Figure 4-3: Exploded view of wall assembly with heater.

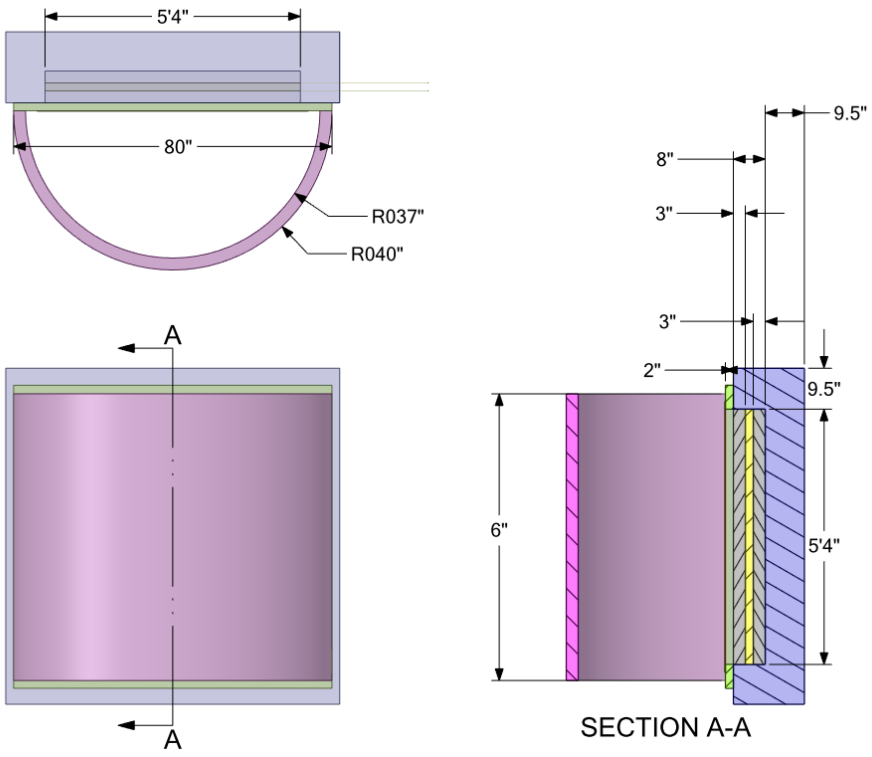

Figure 4-4: Dimensions of heater and wall assembly.

The concrete masonry wall, 4 blocks wide and 8 blocks high (5'4" x 5'4"), is comprised of hollow blocks (16" x 8" x 8") filled with loose-fill perlite. The perlite, made from naturally occurring siliceous rock, can be used for continuous service up to 649°C and is noncombustible, nonflammable, and noncorrosive.

For both walls, insulation extends from the shroud to the front face of the wall to prevent any gaps. All sides of the wall except for the face exposed to the shroud are surrounded with 10" thick mineral-wool based insulation.

Both walls are tested on a support frame to allow insulation to be placed on all sides of the wall except for the front face (Figure 4-5). The frame also allows the formed wall to be rotated into place, negating the need to embed supports for lifting hoists which would complicate thermal analyses for model validation. After the formed wall is constructed on top of the tilt-up or rotatable frame, the frame is rotated into place using swivel hoist connections at the top of the frame. The set of top stop plates nearest the wall at the top of the main frame are removed when rotating the wall into place. A removable large stop plate is in place during rotation to prevent the wall from falling forwards. Once the wall is in place the top plates are installed and the large stop plate removed. The four stop plates at the top of the main frame prevent the wall from falling forwards or backwards during testing. Pins holding the rotatable frame in place are then removed to allow the tilt-up frame to be removed. Note that the tilt-up frame is not required for the masonry wall since it can be built in place vertically on the main frame. Figure 4-6 shows the wall assembly with the heater during testing. The shroud is suspended from the top bar of the main frame.

Structural simulations were performed using ANSYS Mechanical to ensure the frame could support the wall without failure and without excessive deflection. The results of these simulations indicate that the frame will have minimal deflection and sufficient safety factors. The simulations are conservative in that the filleted edges of the tubular bars and welds are not included. The fillet welds using a E7018 electrode on standard structural steel (A36 or 530) have a strength of 1400 lbs per inch of weld [8]. Each bar having 8" of weld all around can support 11,200 lbs. The wall weighs about 2,200 lbs with its load distributed over several weld connections. The construction sequence of the formed wall is shown in Figure 4-7.

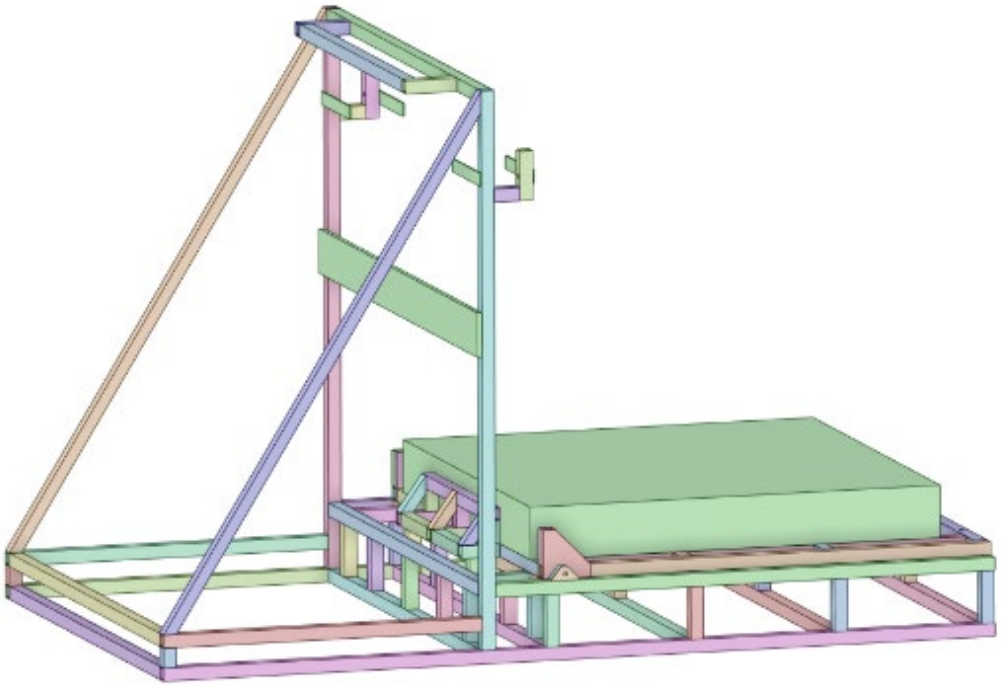

Figure 4-5: Frame supports walls during testing and to place preformed wall.

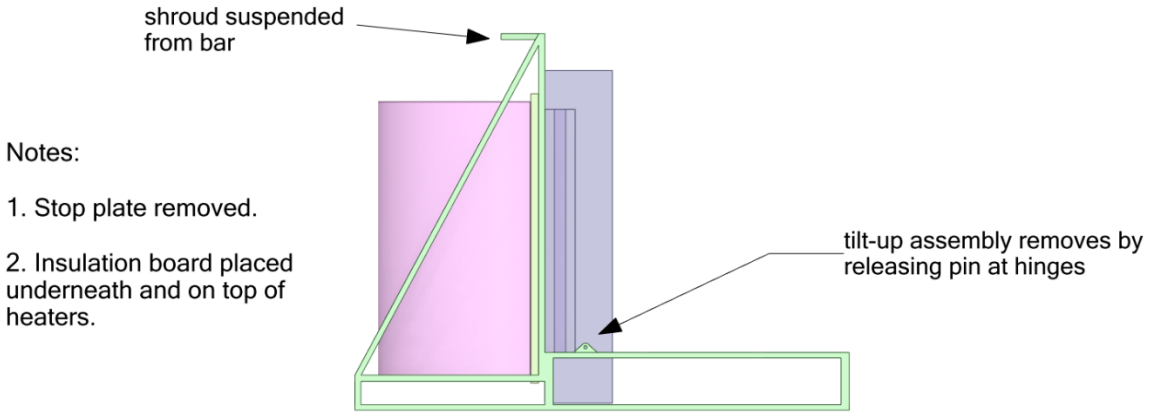

Figure 4-6: Wall assembly with frame during testing.

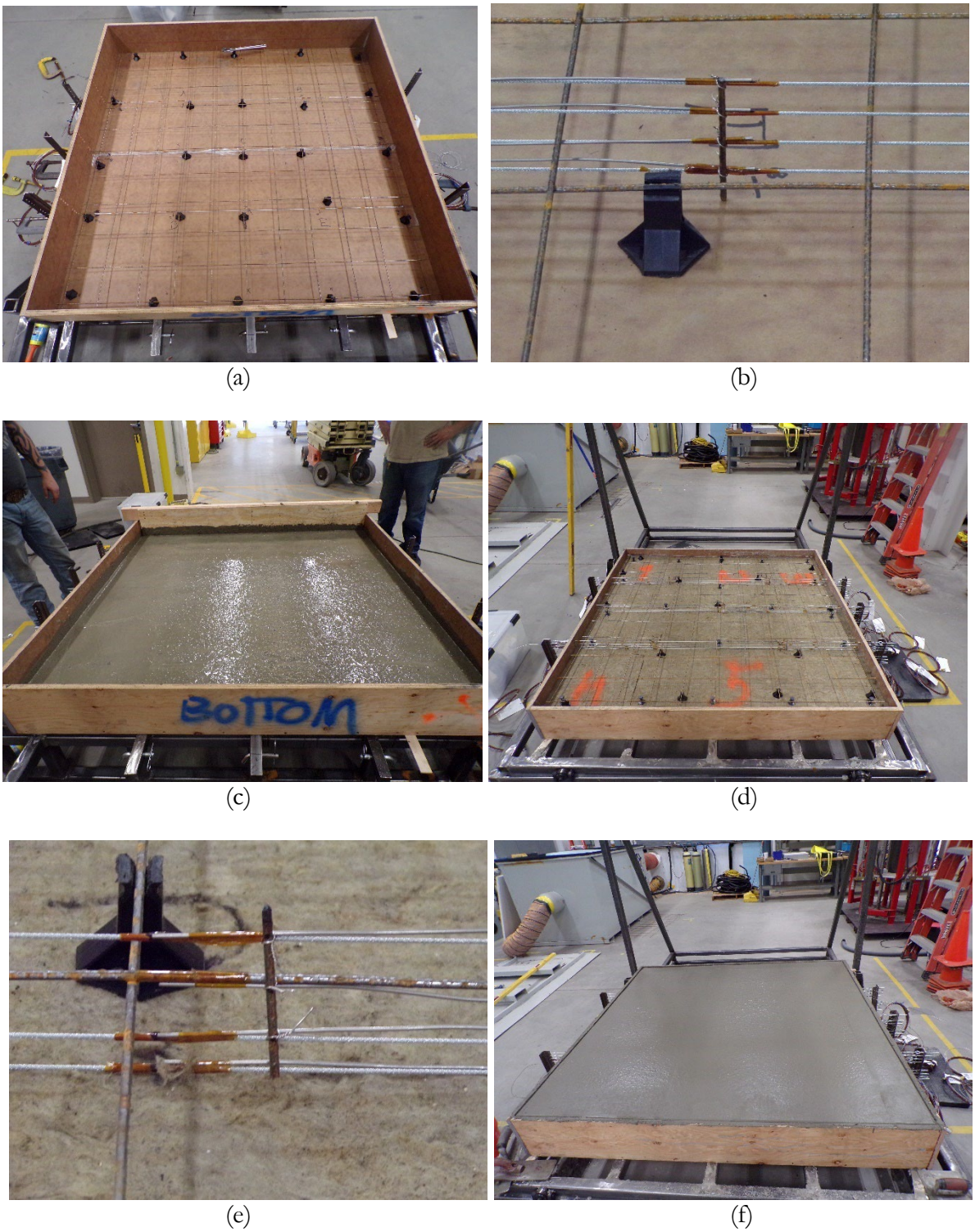

(a) (b)

(c) (d)

(e) (f)

Figure 4-7: Construction sequence of formed wall: (a) wooden form assembled (b) thermocouples attached to support wires; also shown is cradle to support wire mesh (c) first concrete layer poured, (d) mineral wool insulation installed, (e) thermocouples attached to next set of support wires, and (f) final layer of concrete poured.

4.2. Instrumentation

The walls are instrumented with 0.062 gauge (1/16" dia.) ungrounded junction, mineral insulated metal sheathed, type K thermocouples (TCs) attached to the front and back faces as well as embedded. Figure 4-8 and Figure 4-9 shows the placement of 33 TCs on the front face and 5 TCs on the back face of the formed wall, respectively. Based on calibration results following the International Temperature Scale of 1990 (ITS-90) and using the standard reference function for a Type K thermocouple as defined in NIST Monograph 175 the measurement uncertainty is ±1.1 °C or 0.4% of the reading, whichever is greater for a 95% confidence interval. In addition to this calibration resistance checks are performed to verify TC functionality in both cold and hot condition. At 0°C and 100°C, the average temperature reading among all thermocouples with the standard deviation is 99.4 ± 1.1°C and 0.6 ± 1.3°C, respectively. Values as provided in reference [9] are used to account for other sources of uncertainty such as TC attachment to a solid surface. By calculating the square root of the sum of the squares of the uncertainties, the combined uncertainty is 1.1%.

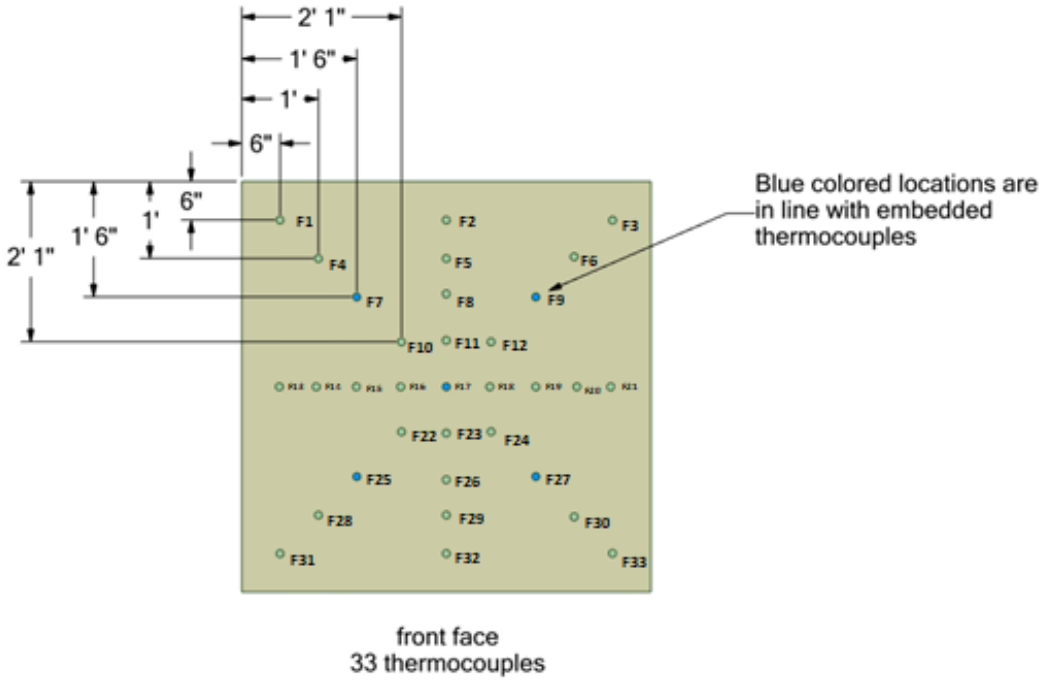

Figure 4-8: Thermocouple placement on surface of formed wall facing heaters.

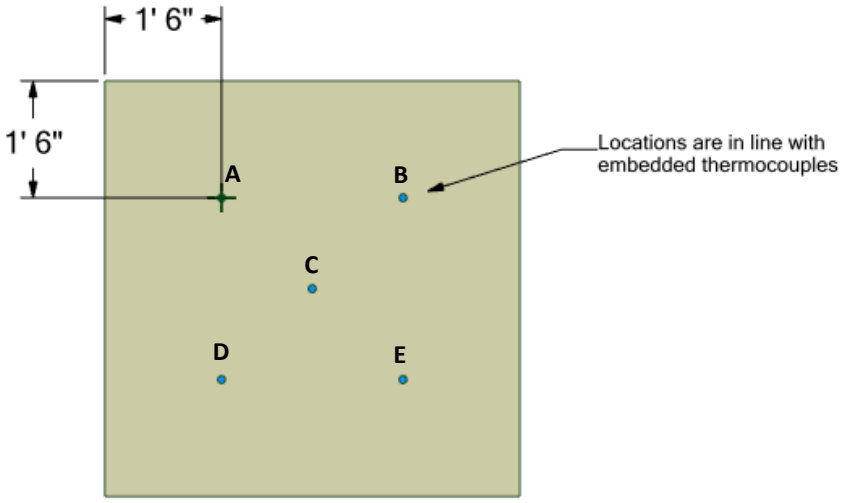

Figure 4-9: Frontal view of thermocouple placement on back face of formed wall in line with embedded thermocouples.

Figure 4-10 shows the embedded TCs in the formed wall which are placed at heights of 1'6", 2'8", and 3'10". The middle height has only one station of embedded TCs while the other heights have two. At each height 3 TCs are placed ¾" apart in the concrete layers and one TC attached to each face of the insulation board. The TC wires extend parallel to the front face and are attached to embedded wires that are parallel to the front face. During the building process the wires are placed and held secure to the wood frame that forms the wall. Holes (3/16" dia.) are drilled in the side panels of the wooden frame to allow the support wires to be secured on the outside of the frame and to allow passage of the TC wires. The midplane TCs are supported by the wire mesh in each concrete layer. There is a total of 78 TCs for this wall, that is, 40 embedded, 33 on the front face, and 5 on the back face.

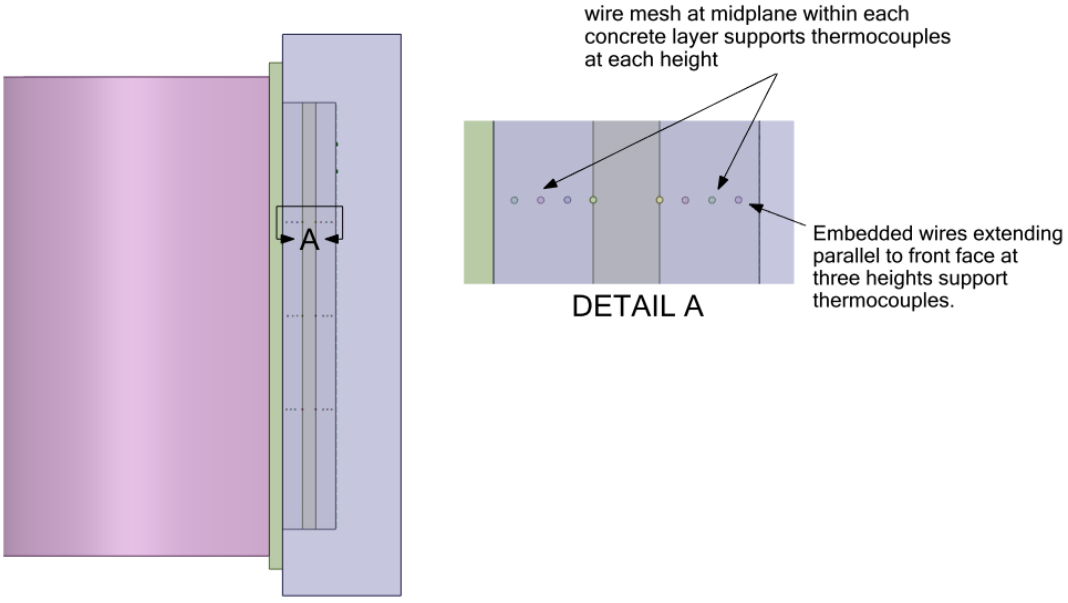

Figure 4-10: Placement of embedded thermocouples for formed wall.

Figure 4-11 shows the blocks instrumented with TCs for the masonry wall which are highlighted in blue. Figure 4-12 shows the placement of the TCs within these blocks. The TCs are placed in 1" deep drilled holes within the block and their wires parallel to the front face of the wall. The TCs on the front and back faces of the wall are 1" from the top of a respective block and centered, the same depth as the embedded TCs. The wires run between bricks within the mortar layer. Each of the five blocks have 13 embedded thermocouples providing a total of 65 thermocouples. The front and back faces of the masonry wall are instrumented with 5 TCs each. Thus, a total of 75 TCs is used for masonry wall. The identification of the TCs is provided in Figure 4-13 where first letter in the identification refers to level, that is, 'L' refers to the lower level, 'M' the mid-level, and 'U' the upper level for blocks instrumented with TCs. The label 'through' in Figure 4-13 pertains to the sequential numbering of the thermocouples on the front and rear locations. For instance, in Figure 4-13 the thermocouple to the right of the thermocouple labeled 'U-F1' is U-F2, with the incremental numbering continuing up to U-F10.

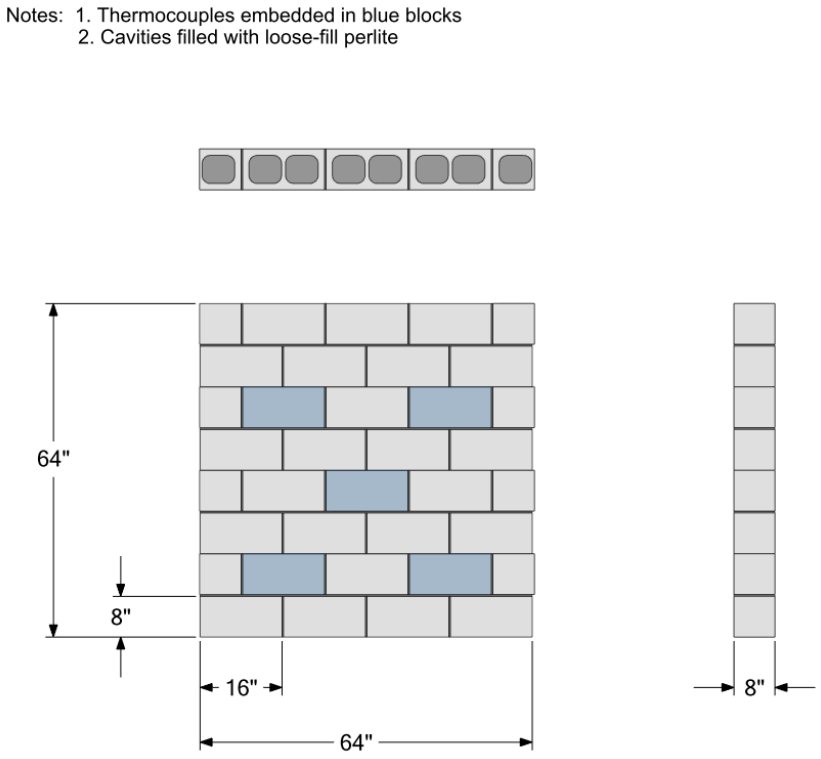

Figure 4-11: Blocks with surface and embedded thermocouples for the masonry wall.

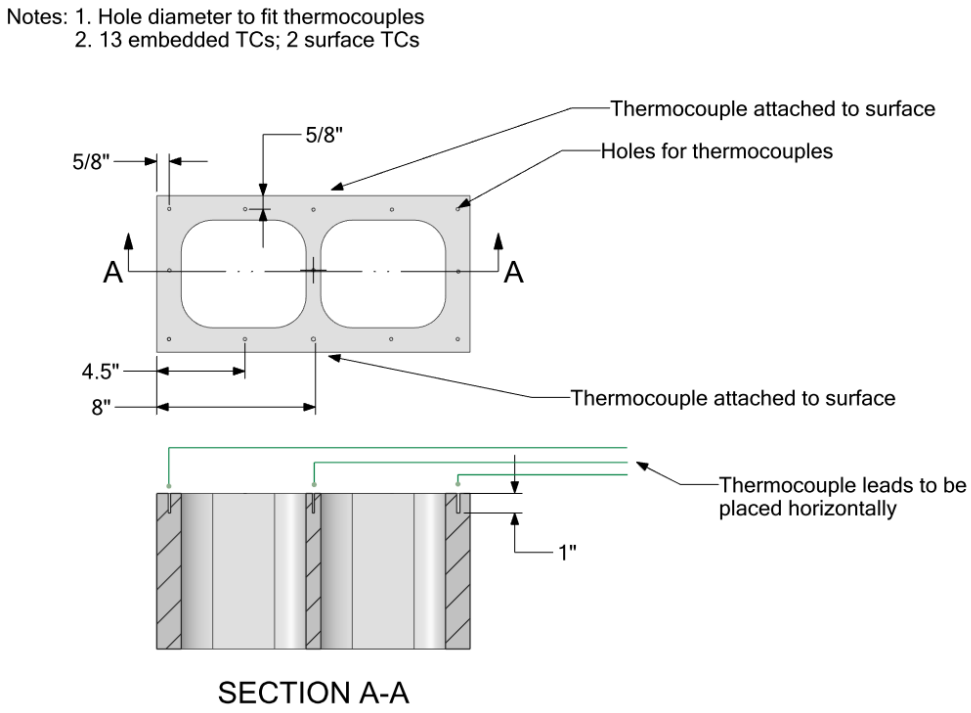

Figure 4-12: Location of thermocouples for instrumented blocks for masonry wall.

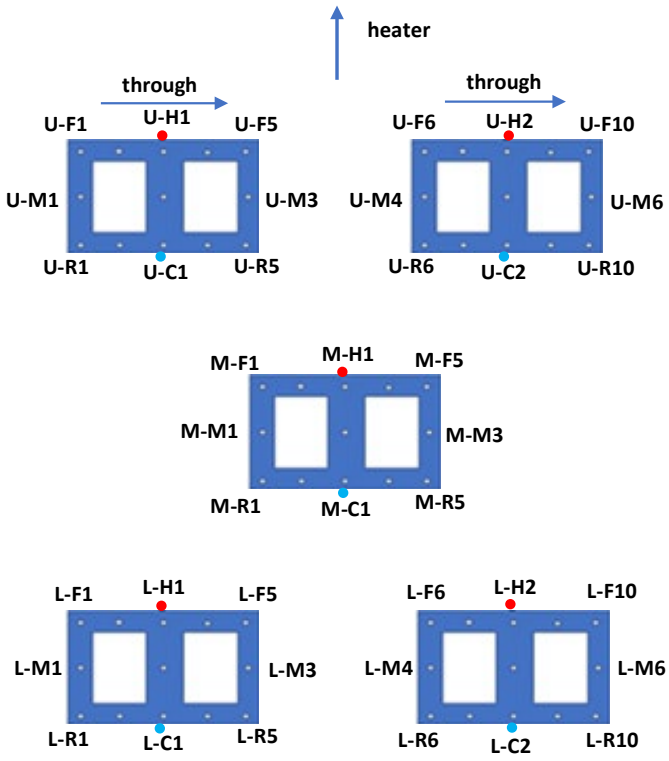

Figure 4-13: Masonry wall: Naming correspondence for thermocouples locations. 'L', 'M', and 'U' denote lower, middle, and upper level.

Figure 4-14: Thermocouples inserted into holes drilled in masonry block filled with perlite

The shroud is instrumented with centered 3x3 array of 9 thermocouples spaced equally apart (16") for both walls. The number designation for each thermocouple attached to the shroud surface facing the wall is provided in Figure 4-15.

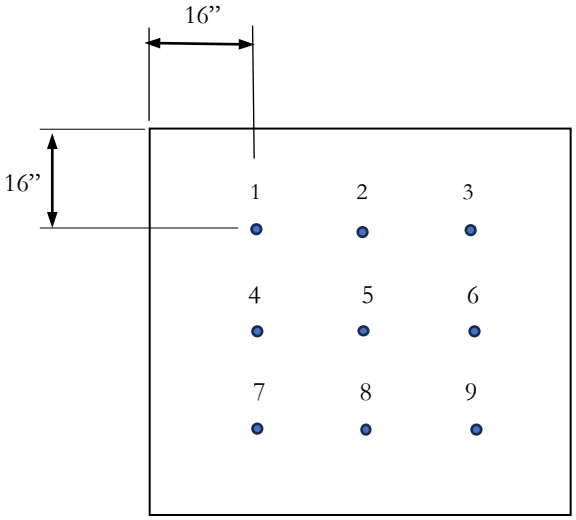

Figure 4-15: Number designation of the thermocouples attached to the shroud surface facing wall.

To determine the corresponding heat flux of the targeted temperatures for the experiments, five wide-angle heat flux (180°) water-cooled gauges (Hukseflux, SBG01) are used before the walls are put in place. Note that the heat flux gauges measure total heat flux which included radiative and convective heat transfer. The gauges are embedded in a 5'4" x 5'4" insulation board and positioned flush with its surface and placed at the same locations, A to E, as shown in Figure 4-9. The gauges embedded in the insulation board are placed the same distance as the wall in place, that is, 2" from the shroud to measure heat flux at representative test temperatures. Thermocouple measurements on the shroud for are shown in Figure 4-16 and the corresponding heat flux measurements is shown in Figure 4-17.

Table 4-1 provides thermocouple and gauge measurements averaged at times in which temperatures are steady. The results indicate that temperatures among the locations are not completely uniform and

have a standard deviation of approximately 5°C. The corresponding heat flux measurements are within 10% of each other and have a standard deviation of approximately 1 kW/m^2.

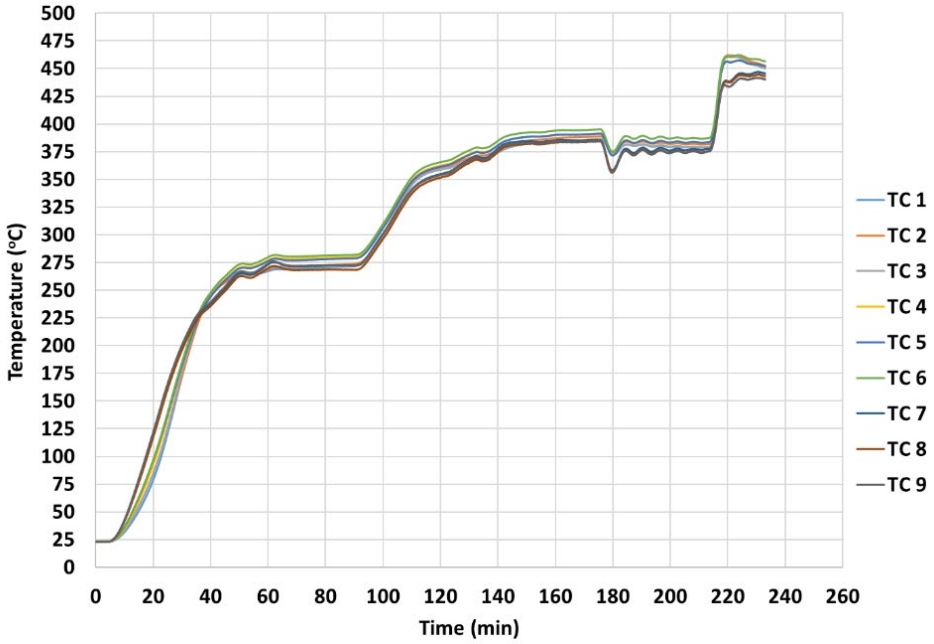

Figure 4-16: Shroud thermocouple measurements with heat flux gauges 2" from shroud.

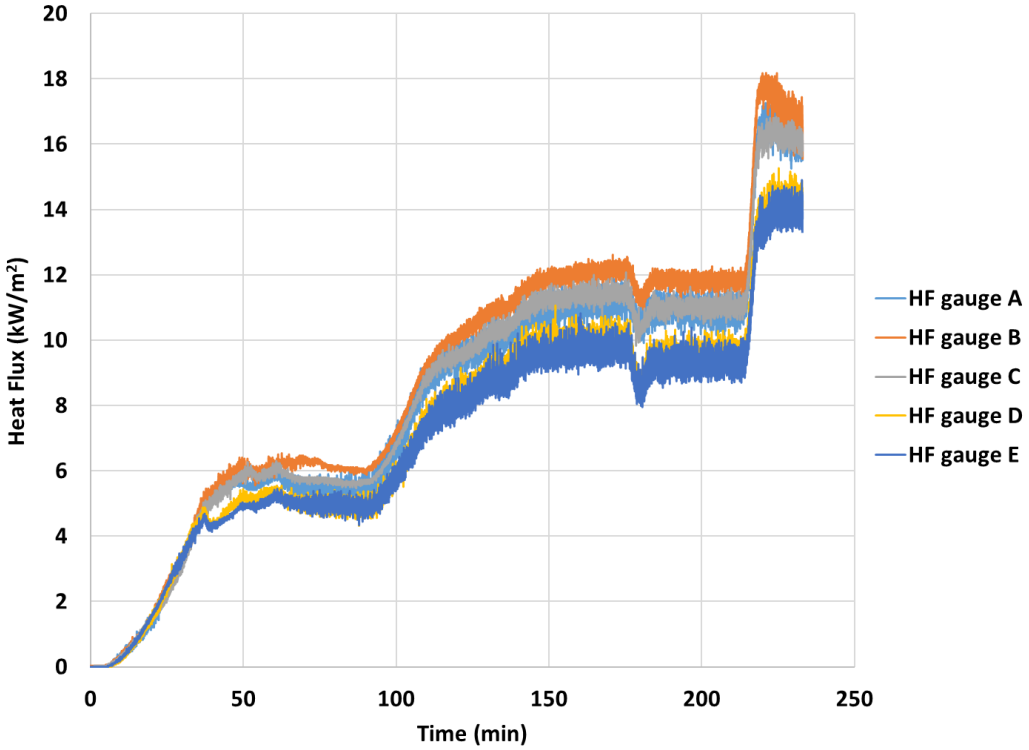

Figure 4-17: Heat flux gauge measurements 2" from shroud.

Table 4-1: Average temperature among thermocouples on shroud and average heat flux among gauges

Time (min)	Average temperature among TCs (°C)	Average heat flux (kW/m^2)
75	273.6 ± 4.3	5.5 ± 0.6
170	387.5 ± 3.6	11.0 ± 1.0
210	379.9 ± 4.2	10.4 ± 1.0
233	449.1 ± 5.2	15.1 ± 1.0

4.3. Thermal Properties

Since temperature varies over time during all experiments, the thermal diffusivity is pertinent. The thermal diffusivity of both types of concrete used for the walls is determined by using the one-dimensional heat conduction equation,

$$\frac{dT}{dt} = \alpha \frac{d^2T}{dx^2} \tag{4.3.1}$$

where $\alpha = k/\rho c_p$, is the thermal diffusivity (m^2/s) which is the ratio of the thermal conductivity, k, to the product of density, ρ, and specific heat, c_p.

The thermal diffusivity is determined by evaluating the temporal derivative and spatial second derivative of temperature in equation (1) using temperature measurements. The temporal derivative of temperature is determined by curve fitting a linear function to temperature measurements over time using the first embedded thermocouple. The linear function is fit to a range of $\pm$10 seconds at each time evaluated. The derivative of the linear function with respect to time is then evaluated.

To evaluate the second derivative of temperature with respect to distance, a double exponential function is fit to temperature measurements as a function of distance. This is done for embedded thermocouples in the first layer of concrete for the formed wall experiments and at a block's web for the masonry wall experiment. Measurements at the middle location for both walls are considered to more closely satisfy the one-dimensional assumption of eq. (1) than other locations which are more impacted by lateral heat transfer despite the surrounding insulation. Thus, results from this analysis are provided at the center location of the wall of embedded thermocouples.

Table 4-2 provides the thermal diffusivity using the above method for the concrete used in the wall experiments in tabular form while Figure 4-18 provides these results in graphical form. The results indicates that the thermal diffusivity is higher for the formed wall experiments at shroud temperatures of 375°C and 444°C than the 272°C experiment which was performed first. The masonry wall experiment did not have a prior test, and the results are closer to the formed wall test at shroud temperature of 272°C than the other formed wall tests. This indicates that the first test altered the thermal properties, most likely through water loss and chemical reaction of Portland cement.

Table 4-2: Thermal diffusivity as a function of temperature for concrete used in wall experiments

	Formed wall (272°C)		Formed wall (375°C)		Formed wall (444°C)		masonry (472°C)
Temp. (°C)	α (m^2/s)	Temp. (°C)	α (m^2/s)	Temp. (°C)	α (m^2/s)	Temp. (°C)	α (m^2/s)
24	4.02E-07	33	4.54E-07	25	4.47E-07	26	1.68E-07
30	2.46E-07	40	2.76E-07	31	3.07E-07	41	1.59E-07
40	1.87E-07	50	2.34E-07	41	2.61E-07	66	1.67E-07
50	1.74E-07	60	2.23E-07	51	2.48E-07	96	1.92E-07
60	1.73E-07	70	2.28E-07	61	2.45E-07	120	2.14E-07
70	1.82E-07	80	2.42E-07	72	2.62E-07	143	2.45E-07
79	1.97E-07	89	2.65E-07	82	2.75E-07	164	2.59E-07
89	2.01E-07	99	2.91E-07	92	2.9E-07	185	2.72E-07
100	2.10E-07	109	3.13E-07	102	3.01E-07	204	2.86E-07
110	2.07E-07	119	3.33E-07	112	3.11E-07	221	2.93E-07
121	2.03E-07	130	3.42E-07	122	3.24E-07	237	3.12E-07
131	2.02E-07	140	3.46E-07	132	3.41E-07	252	3.32E-07
140	2.08E-07	151	3.36E-07	142	3.48E-07	265	3.64E-07
-	-	162	3.24E-07	152	3.51E-07	-	-
-	-	172	3.22E-07	162	3.54E-07	-	-
-	-	183	3.23E-07	172	3.52E-07	-	-
-	-	193	3.27E-07	183	3.6E-07	-	-
-	-	203	3.44E-07	193	3.65E-07	-	-
-	-	-	-	203	3.78E-07	-	-
-	-	-	-	212	3.83E-07	-	-
-	-	-	-	222	3.89E-07	-	-
-	-	-	-	232	3.88E-07	-	-
-	-	-	-	241	4.04E-07	-	-

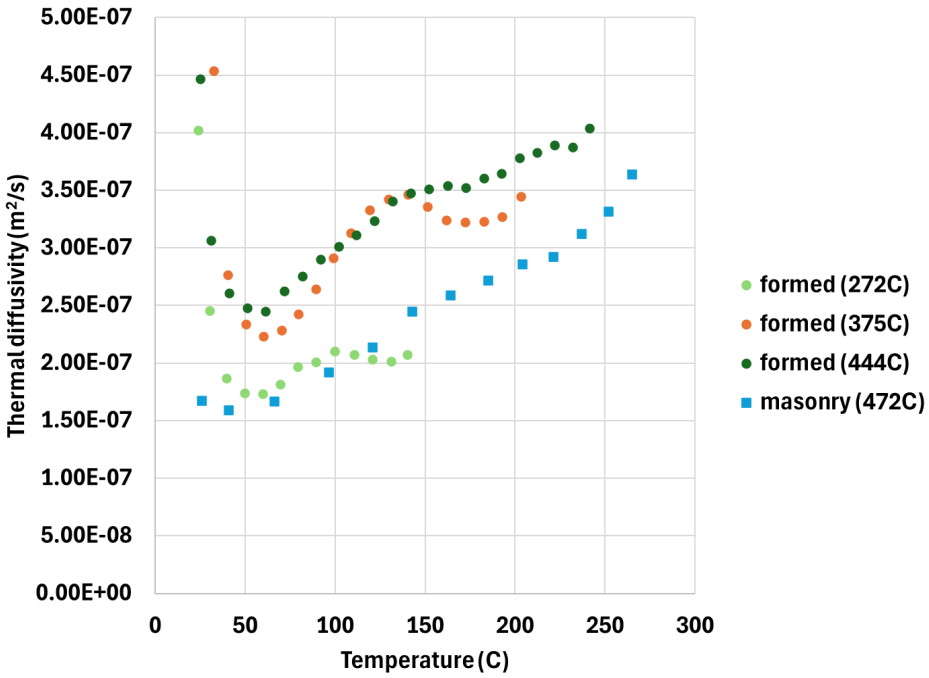

Figure 4-18: Thermal diffusivity as a function of temperature for both walls based on measurements at middle location

The density of the concrete based on post-test measurements from several samples is 2133 kg/m^3 and 1616 kg/m^3 for the formed wall and masonry wall, respectively. For the mineral wool insulation, the thermal properties as provided by the manufacturer are listed in Table 4-3. The density of the insulation also provided by the manufacturer is 93 kg/m^3.

Table 4-4 provides the thermal properties of loose fill perlite [10] [11]. The density of the loose fill perlite based on post-test measurement from several samples is 93 kg/m^3. Measurement of emissivity on the surface of the shroud facing the wall is provided in Table 4-5.

Table 4-3: Thermal properties of mineral wool insulation

temperature (°C)	k (W/mK)	C_p (J/kgK)
20	0.0368	996.1
100	0.0462	1008.6
200	0.0612	1024.3
300	0.0807	1040
400	0.1058	1055.7
500	0.1375	1071.5

Table 4-4: Thermal conductivity and specific heat of loose fill perlite.

temperature (°C)	k (W/mK) [10]	temperature (°C)	C_p (J/kgK) [11]
0	0.043	2	761.0
93	0.059	25	802.0
149	0.076	127	919.5
204	0.090	177	965.6
260	0.105	227	1001.3
316	0.126	277	1030.3
371	0.141	327	1054.7
427	0.163	377	1075.8
538	0.214		

Table 4-5: Shroud emissivity measurements.

Location*	emissivity
1	0.758 ± 0.002
2	0.748 ± 0.002
3	0.735 ± 0.007
4	0.747 ± 0.005
5	0.738 ± 0.0003
6	0.747 ± 0.004
7	0.763 ± 0.008
8	0.764 ± 0.001
9	0.739 ± 0.004
average	0.749 ± 0.004

*Locations correspond to those shown in Figure 4-15

4.4. Testing Procedure

The duration of the tests is based on the time required for the thermocouples on the back face of the wall to increase in temperature above ambient. When a temperature rise is indicated the heater is shut off. This criterion is chosen since the length of time to reach a steady state would require overnight monitoring by personnel. The formed wall was allowed to cool down for a week or more before the next test was performed.

4.5. Results

The following sections, 4.5.1 and 4.5.2, provide the results for temperature from thermocouple measurements for the formed wall and masonry wall, respectively.

4.5.1. Formed wall

The formed wall is tested at three shroud temperatures, namely, 272°C, 375°C, and 444°C. Note that the temperature varies across the shroud for each test by up to about 10°C, most likely due to nonuniform heat transfer at the boundaries.

4.5.1.1. Shroud temperature 272°C

Figure 4-19 provides temperature measurements at the surface of the shroud facing the wall from nine thermocouples at locations shown in Figure 4-15. Figure 4-20 provides temperature measurements on the surface of the wall facing the shroud from thermocouples at locations shown in Figure 4-8. The measurements shown in these figures are provided in tabular form at discrete times in Table 4-6 for the shroud and in Table 4-7 through Table 4-9 for the front face of the wall. Note that there is a much greater spread in temperature over the wall than the shroud. Temperatures in tabular form at discrete times for embedded thermocouples is provided in Table 4-10 through Table 4-14 at locations A, B, C, D, and E as shown in Figure 4-9 and Figure 4-10, respectively.

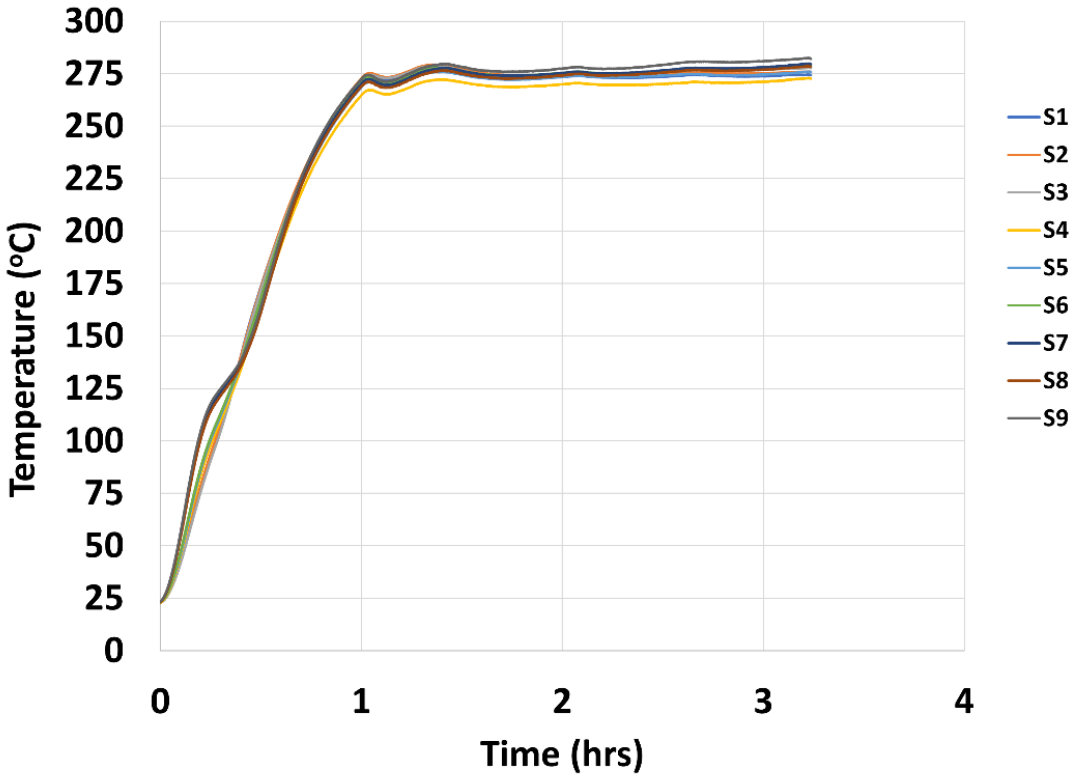

Figure 4-19: Formed wall shroud temperature 272°C: Temperature on surface of shroud at nine locations.

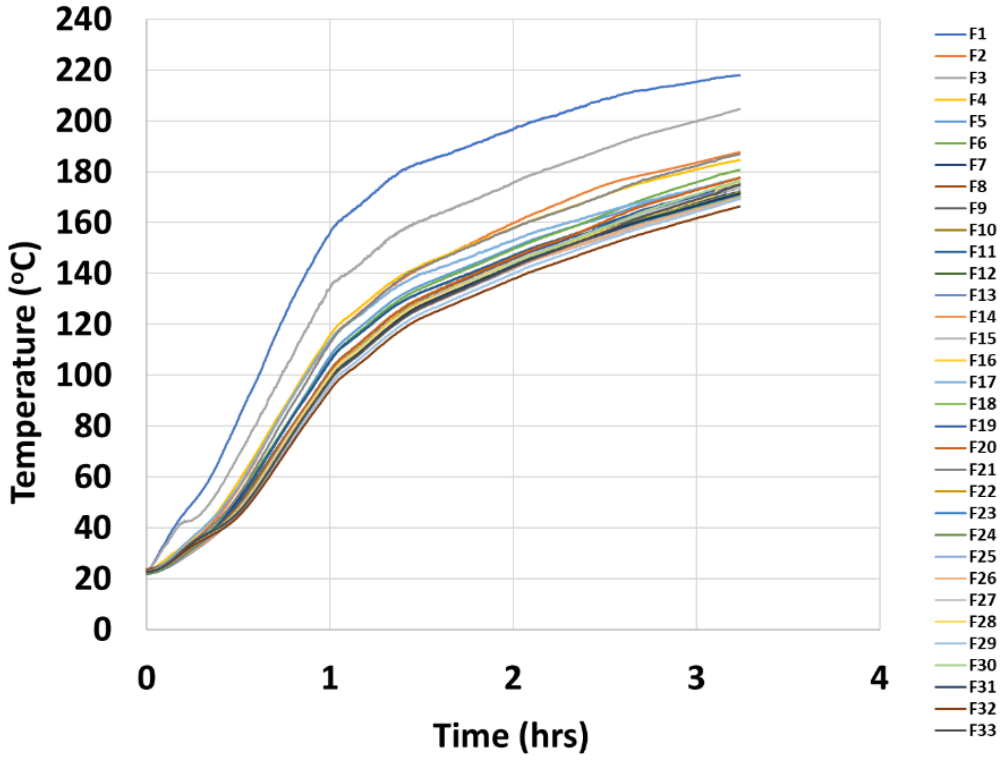

Figure 4-20: Formed wall shroud temperature 272°C: Temperature on wall surface facing shroud.

Table 4-6: Formed wall shroud temperature 272°C: Temperature on surface of shroud at nine locations

	Temperature (°C)								
	location								
Time (s)	S1	S2	S3	S4	S5	S6	S7	S8	S9
0	23.0	23.0	22.8	22.8	23.1	23.1	23.3	23.1	23.4
300	38.0	37.4	36.6	39.1	40.0	40.9	46.7	45.8	47.9
600	66.9	66.5	64.1	71.1	73.1	74.6	88.5	86.8	90.9
900	92.7	93.8	90.5	97.8	100.4	101.7	115.6	113.7	117.7
1200	117.2	117.8	115.1	117.3	119.7	121.0	127.4	125.8	129.0
1500	146.4	145.9	144.2	138.4	140.9	142.5	140.2	138.8	141.6
1800	173.5	173.0	171.8	162.7	165.6	167.8	162.1	160.9	163.7
2100	197.0	197.2	195.9	187.9	191.1	193.8	189.9	188.5	191.8
2400	217.6	218.4	217.0	210.2	213.5	216.4	214.4	212.9	216.6
2700	235.0	236.2	234.8	228.3	232.0	234.8	233.5	232.1	236.1
3000	249.4	250.8	249.5	243.0	246.6	249.3	248.7	247.2	251.2
3300	261.5	262.8	261.7	254.8	258.7	261.2	260.5	259.0	262.8
3600	271.4	272.7	271.7	264.7	268.5	270.8	270.2	268.8	272.4
3900	272.9	274.2	273.6	266.0	269.7	271.7	270.6	269.4	272.2
4200	272.6	273.9	273.5	266.0	269.5	271.4	270.2	269.0	272.1
4500	275.5	276.8	276.2	268.8	272.5	274.6	273.7	272.4	275.6
4800	277.8	279.1	278.5	271.4	275.3	277.2	276.5	275.2	278.6
5100	277.6	279.0	278.4	272.1	275.7	277.8	277.8	276.5	279.7
5400	275.8	277.3	276.5	271.0	274.5	276.4	276.4	274.9	278.3
5700	274.1	275.7	274.9	269.7	273.1	275.0	274.9	273.6	276.8
6000	273.1	274.7	274.0	269.0	272.4	274.3	274.2	272.9	276.2
6300	272.6	274.3	273.6	268.6	272.1	274.1	274.0	272.7	276.0
6600	272.7	274.2	273.5	269.1	272.3	274.2	274.3	273.0	276.2
6900	272.9	274.6	274.0	269.0	272.8	274.8	274.7	273.5	276.6
7200	273.4	275.1	274.5	269.9	273.4	275.4	275.3	274.1	277.3
7500	273.9	275.6	275.0	270.5	274.1	276.1	275.9	274.9	278.1
7800	273.4	274.9	274.5	269.8	273.5	275.3	275.2	274.2	277.4

	Temperature (°C)								
8100	273.0	274.7	274.3	269.6	273.1	275.2	275.2	274.3	277.3
8400	273.0	274.8	274.5	269.6	273.4	275.4	275.4	274.5	277.5
8700	273.2	275.0	274.9	269.8	273.9	275.6	275.9	274.9	278.2
9000	273.5	275.3	275.6	270.1	274.0	276.1	276.6	275.6	279.2
9300	274.0	275.7	276.2	270.4	274.5	276.7	277.3	276.2	280.2
9600	274.4	275.8	276.7	271.1	274.8	277.4	277.9	276.8	280.7
9900	274.1	275.4	276.6	270.8	274.4	277.2	277.7	276.6	280.6
10200	273.8	275.1	276.5	270.5	274.3	277.0	277.6	276.5	280.4
10500	273.6	275.0	276.6	271.0	274.3	277.2	277.7	276.6	280.6
10800	273.8	275.2	276.8	271.2	274.6	277.4	278.1	276.9	281.0
11100	274.1	275.5	277.2	271.7	275.0	277.9	278.6	277.5	281.5
11400	274.4	275.8	277.5	272.6	275.5	278.4	279.2	278.1	281.9

Table 4-7: Formed wall shroud temperature 272°C: temperatures at wall surface facing heaters, F1 to F11

	Temperature (°C)										
	location										
Time (s)	F1	F2	F3	F4	F5	F6	F7	F8	F9	F10	F11
0	22.7	22.6	22.8	23.0	22.7	22.8	23.1	23.7	22.9	22.5	22.2
300	22.7	22.6	22.8	23.0	22.7	22.8	23.1	23.7	22.9	22.5	22.2
600	22.7	22.6	22.8	23.0	22.7	22.8	23.0	23.7	22.9	22.4	22.1
900	22.8	22.6	22.8	23.0	22.7	22.8	23.0	23.7	22.9	22.4	22.1
1200	22.8	22.6	22.8	23.0	22.7	22.8	23.1	23.7	22.9	22.4	22.1
1500	22.8	22.6	22.8	23.0	22.7	22.8	23.0	23.7	22.9	22.4	22.1
1800	22.8	22.6	22.8	23.0	22.7	22.8	23.0	23.7	22.9	22.4	22.1
2100	22.8	22.6	22.8	23.0	22.7	22.8	23.0	23.7	22.9	22.4	22.1
2400	22.8	22.6	22.8	23.0	22.7	22.8	23.0	23.7	22.9	22.4	22.1
2700	22.8	22.6	22.8	23.0	22.7	22.8	23.0	23.7	22.8	22.4	22.1
3000	28.4	23.9	27.8	24.9	24.0	23.8	24.2	24.6	23.8	23.2	23.0
3300	39.0	27.9	37.0	29.7	27.4	27.1	27.0	27.5	26.8	25.8	26.3
3600	47.5	32.8	42.6	34.2	31.6	31.5	30.4	31.3	31.0	29.6	30.7

	Temperature (°C)										
3900	55.0	38.0	46.4	39.5	36.0	35.9	35.1	35.5	35.3	33.7	35.2
4200	65.4	44.4	54.3	46.3	41.6	41.7	41.0	40.7	40.2	38.8	40.8
4500	78.3	52.4	64.6	55.0	48.9	49.2	48.5	47.3	47.0	45.4	47.5
4800	91.6	61.6	75.4	64.4	57.1	58.0	56.8	55.0	55.1	53.0	56.2
5100	104.7	71.9	86.5	74.2	66.2	66.9	65.8	63.4	63.8	61.4	65.7
5400	118.4	82.9	97.7	84.3	75.7	76.1	75.2	72.1	72.6	70.5	75.4
5700	131.0	92.7	109.2	93.8	85.3	85.0	84.7	80.9	81.3	79.2	84.8
6000	142.3	102.0	120.3	103.5	94.9	94.0	93.4	89.5	89.7	88.0	93.7
6300	152.8	110.4	130.6	112.5	104.5	103.0	102.3	98.1	98.0	96.6	102.6
6600	160.8	118.2	138.5	120.4	112.3	110.6	110.4	105.3	105.8	103.8	110.4
6900	165.4	123.2	142.4	125.1	117.5	115.9	115.2	110.3	111.0	108.8	115.0
7200	170.6	128.0	147.1	130.1	122.4	120.9	119.9	115.0	115.9	113.5	119.8
7500	175.9	133.4	152.9	135.1	127.3	125.9	124.8	119.9	120.7	118.6	124.5
7800	180.3	137.5	156.9	139.0	131.4	130.1	128.6	124.0	125.0	122.7	128.7
8100	183.0	141.3	159.8	142.2	134.5	133.4	131.6	127.0	128.3	125.9	131.6
8400	184.9	144.3	162.8	145.1	137.1	135.9	134.2	129.7	130.9	128.7	134.2
8700	186.8	147.1	164.6	147.4	139.5	138.4	136.5	132.0	133.4	131.2	136.4
9000	188.9	150.2	167.3	149.9	141.9	141.0	138.8	134.4	135.7	133.8	138.8
9300	191.4	152.9	169.5	152.3	144.4	143.4	141.2	136.9	138.2	136.4	141.3
9600	193.8	156.3	172.3	154.8	146.9	146.0	143.5	139.3	140.7	138.9	143.7
9900	195.9	158.9	174.6	157.2	149.4	148.7	145.9	141.8	143.3	141.4	146.3
10200	198.3	161.6	177.6	159.6	151.9	151.1	148.4	144.2	145.8	144.1	148.7
10500	200.4	164.2	179.8	161.8	154.1	153.5	150.5	146.4	148.1	146.4	151.0
10800	202.1	166.7	182.0	163.8	156.1	155.7	152.2	148.4	150.1	148.4	152.8
11100	203.9	169.3	184.0	165.9	158.0	157.8	153.9	150.4	152.2	150.6	154.8
11400	205.9	171.8	186.0	168.0	159.8	160.0	155.7	152.4	154.4	152.5	156.9
11700	207.8	174.1	188.5	170.1	161.6	162.4	157.4	154.3	156.8	154.4	158.9
12000	209.4	176.1	190.5	172.2	163.5	164.7	159.2	156.3	158.9	156.2	161.1
12300	211.2	177.7	192.6	174.3	165.6	167.3	161.2	158.3	161.2	158.2	163.0
12600	212.0	179.0	194.6	176.0	167.5	169.4	162.8	160.1	163.0	159.9	164.5

	Temperature (°C)										
12900	213.2	180.3	196.1	177.5	169.2	171.5	164.4	161.7	164.7	161.5	166.1
13200	214.1	181.7	197.7	178.9	170.9	173.4	165.9	163.4	166.5	163.1	167.7
13500	215.0	183.1	199.5	180.5	172.5	175.2	167.5	165.1	168.3	164.8	169.3
13800	216.1	184.5	200.9	181.9	174.2	177.1	169.0	166.7	170.1	166.3	170.8
14100	217.1	186.0	202.5	183.3	175.8	179.0	170.5	168.4	171.7	167.9	172.6
14400	217.9	187.4	204.3	184.4	177.3	180.5	171.9	170.0	173.5	169.4	174.2

Table 4-8: Formed wall shroud temperature 272°C: temperatures at wall surface facing heaters, F12 to F22

	Temperature (°C)										
	location										
Time (s)	F12	F13	F14	F15	F16	F17	F18	F19	F20	F21	F22
0	22.7	22.5	22.6	22.7	22.7	23.0	22.8	22.6	22.6	22.4	22.4
300	22.7	22.5	22.6	22.7	22.6	23.0	22.7	22.6	22.6	22.4	22.4
600	22.7	22.4	22.5	22.6	22.6	22.9	22.6	22.4	22.5	22.3	22.3
900	22.6	22.4	22.5	22.5	22.5	22.8	22.6	22.4	22.4	22.2	22.2
1200	22.6	22.4	22.5	22.6	22.5	22.8	22.6	22.4	22.4	22.2	22.2
1500	22.6	22.4	22.4	22.5	22.5	22.8	22.5	22.3	22.4	22.2	22.2
1800	22.6	22.4	22.5	22.5	22.5	22.8	22.6	22.4	22.4	22.2	22.2
2100	22.6	22.4	22.4	22.5	22.5	22.8	22.5	22.4	22.3	22.2	22.2
2400	22.6	22.4	22.4	22.5	22.5	22.8	22.5	22.3	22.4	22.2	22.2
2700	22.6	22.4	22.4	22.5	22.4	22.8	22.5	22.3	22.3	22.2	22.2
3000	23.4	22.9	23.0	23.2	23.2	24.2	23.2	23.1	23.1	23.4	22.8
3300	26.2	25.4	25.6	26.0	26.1	28.6	25.9	26.1	26.3	27.5	26.0
3600	30.2	29.1	29.6	30.4	30.3	34.5	30.1	30.7	30.5	32.2	30.6
3900	34.5	33.2	33.6	34.7	34.5	39.7	34.3	35.0	34.8	37.4	35.0
4200	39.8	38.0	38.3	39.5	39.5	45.7	39.2	40.2	39.9	42.9	39.6
4500	46.2	44.0	44.4	46.0	45.8	53.3	45.1	46.1	46.0	50.0	45.3
4800	53.6	51.4	51.7	53.4	53.6	62.5	52.6	53.5	53.5	58.9	52.6
5100	61.8	60.0	60.2	62.1	62.4	72.7	61.1	61.9	62.6	69.2	61.4
5400	70.7	69.0	69.2	71.2	71.7	82.8	70.1	70.9	71.9	79.7	70.5

	Temperature (°C)										
5700	79.6	78.1	78.1	80.3	80.9	92.9	79.1	80.8	81.1	89.6	79.7
6000	88.1	87.0	86.8	89.0	89.7	102.3	87.6	90.0	90.0	99.4	88.6
6300	96.6	95.4	94.8	97.1	98.5	110.8	96.2	99.0	98.6	109.5	97.3
6600	104.1	103.5	102.7	105.2	105.8	118.0	103.4	106.5	106.2	117.6	104.4
6900	108.8	108.7	107.5	109.8	110.9	122.4	108.5	111.2	111.1	122.8	109.5
7200	113.6	113.8	112.7	115.0	116.0	127.1	113.5	116.4	116.5	128.0	114.5
7500	118.6	119.2	117.6	119.8	121.0	131.6	118.5	121.5	121.6	133.2	119.5
7800	122.8	123.9	122.0	124.0	125.4	135.6	122.9	125.7	126.1	138.0	124.0
8100	126.2	127.6	125.7	127.6	128.7	138.7	126.5	129.4	129.6	141.4	127.5
8400	128.8	130.7	128.6	130.3	131.6	141.1	129.3	132.2	132.5	144.0	130.5
8700	131.4	133.4	131.0	132.8	134.2	143.1	131.8	134.7	135.2	146.6	132.9
9000	133.9	136.1	133.8	135.1	136.7	145.5	134.7	137.2	137.7	149.4	135.5
9300	136.5	138.9	136.2	137.6	139.3	147.9	137.2	139.7	140.3	151.9	138.1
9600	139.0	141.6	138.9	140.2	141.7	149.9	139.8	142.4	142.9	154.3	140.7
9900	141.7	144.2	141.3	142.5	144.1	152.4	142.4	144.9	145.4	156.8	143.2
10200	144.1	146.9	143.8	144.9	146.8	154.4	144.9	147.4	148.0	159.4	145.6
10500	146.6	149.2	146.0	147.1	148.7	156.9	147.2	149.6	150.4	161.5	147.9
10800	148.7	151.2	147.8	149.1	150.5	158.3	149.2	151.4	152.4	163.5	149.9
11100	150.9	153.2	149.7	150.7	152.6	160.1	151.4	153.4	154.8	165.7	151.9
11400	152.8	155.5	151.6	152.6	154.5	161.8	153.5	155.5	157.0	167.9	153.9
11700	154.7	157.5	153.6	154.4	156.3	163.7	155.5	157.8	159.6	170.2	155.9
12000	156.5	159.9	155.6	156.1	158.2	165.4	157.3	160.7	162.3	172.6	157.7
12300	158.4	161.9	157.6	158.0	159.8	166.9	159.2	163.1	164.7	174.8	159.6
12600	160.1	163.8	159.4	159.9	161.7	168.7	160.8	165.3	166.9	177.0	161.6
12900	161.7	165.5	161.4	161.5	163.3	169.8	162.4	167.2	168.8	178.7	163.0
13200	163.3	167.2	163.0	163.1	165.0	171.4	163.9	168.6	170.3	180.3	164.6
13500	164.9	169.1	164.8	164.6	166.5	172.7	165.6	170.1	172.2	181.8	166.3
13800	166.5	170.9	166.5	166.2	168.1	174.3	167.2	171.9	173.9	183.6	167.9
14100	168.2	172.6	168.3	167.9	169.9	175.8	168.9	173.4	175.6	185.4	169.7
14400	169.8	174.4	170.0	169.5	171.5	177.4	170.5	174.9	177.3	186.7	171.4

Table 4-9: Formed wall shroud temperature 272°C: temperatures at wall surface facing heaters, F23 to F33

	Temperature (°C)										
	location										
Time (s)	F23	F24	F25	F26	F27	F28	F29	F30	F31	F32	F33
0	22.7	22.5	22.6	22.7	22.7	23.0	22.8	22.6	22.6	22.4	22.4
300	22.7	22.5	22.6	22.7	22.6	23.0	22.7	22.6	22.6	22.4	22.4
600	22.7	22.4	22.5	22.6	22.6	22.9	22.6	22.4	22.5	22.3	22.3
900	22.6	22.4	22.5	22.5	22.5	22.8	22.6	22.4	22.4	22.2	22.2
1200	22.6	22.4	22.5	22.6	22.5	22.8	22.6	22.4	22.4	22.2	22.2
1500	22.6	22.4	22.4	22.5	22.5	22.8	22.5	22.3	22.4	22.2	22.2
1800	22.6	22.4	22.5	22.5	22.5	22.8	22.6	22.4	22.4	22.2	22.2
2100	22.6	22.4	22.4	22.5	22.5	22.8	22.5	22.4	22.3	22.2	22.2
2400	22.6	22.4	22.4	22.5	22.5	22.8	22.5	22.3	22.4	22.2	22.2
2700	22.6	22.4	22.4	22.5	22.4	22.8	22.5	22.3	22.3	22.2	22.2
3000	23.4	22.9	23.0	23.2	23.2	24.2	23.2	23.1	23.1	23.4	22.8
3300	26.2	25.4	25.6	26.0	26.1	28.6	25.9	26.1	26.3	27.5	26.0
3600	30.2	29.1	29.6	30.4	30.3	34.5	30.1	30.7	30.5	32.2	30.6
3900	34.5	33.2	33.6	34.7	34.5	39.7	34.3	35.0	34.8	37.4	35.0
4200	39.8	38.0	38.3	39.5	39.5	45.7	39.2	40.2	39.9	42.9	39.6
4500	46.2	44.0	44.4	46.0	45.8	53.3	45.1	46.1	46.0	50.0	45.3
4800	53.6	51.4	51.7	53.4	53.6	62.5	52.6	53.5	53.5	58.9	52.6
5100	61.8	60.0	60.2	62.1	62.4	72.7	61.1	61.9	62.6	69.2	61.4
5400	70.7	69.0	69.2	71.2	71.7	82.8	70.1	70.9	71.9	79.7	70.5
5700	79.6	78.1	78.1	80.3	80.9	92.9	79.1	80.8	81.1	89.6	79.7
6000	88.1	87.0	86.8	89.0	89.7	102.3	87.6	90.0	90.0	99.4	88.6
6300	96.6	95.4	94.8	97.1	98.5	110.8	96.2	99.0	98.6	109.5	97.3
6600	104.1	103.5	102.7	105.2	105.8	118.0	103.4	106.5	106.2	117.6	104.4
6900	108.8	108.7	107.5	109.8	110.9	122.4	108.5	111.2	111.1	122.8	109.5
7200	113.6	113.8	112.7	115.0	116.0	127.1	113.5	116.4	116.5	128.0	114.5
7500	118.6	119.2	117.6	119.8	121.0	131.6	118.5	121.5	121.6	133.2	119.5
7800	122.8	123.9	122.0	124.0	125.4	135.6	122.9	125.7	126.1	138.0	124.0

	Temperature (°C)										
8100	126.2	127.6	125.7	127.6	128.7	138.7	126.5	129.4	129.6	141.4	127.5
8400	128.8	130.7	128.6	130.3	131.6	141.1	129.3	132.2	132.5	144.0	130.5
8700	131.4	133.4	131.0	132.8	134.2	143.1	131.8	134.7	135.2	146.6	132.9
9000	133.9	136.1	133.8	135.1	136.7	145.5	134.7	137.2	137.7	149.4	135.5
9300	136.5	138.9	136.2	137.6	139.3	147.9	137.2	139.7	140.3	151.9	138.1
9600	139.0	141.6	138.9	140.2	141.7	149.9	139.8	142.4	142.9	154.3	140.7
9900	141.7	144.2	141.3	142.5	144.1	152.4	142.4	144.9	145.4	156.8	143.2
10200	144.1	146.9	143.8	144.9	146.8	154.4	144.9	147.4	148.0	159.4	145.6
10500	146.6	149.2	146.0	147.1	148.7	156.9	147.2	149.6	150.4	161.5	147.9
10800	148.7	151.2	147.8	149.1	150.5	158.3	149.2	151.4	152.4	163.5	149.9
11100	150.9	153.2	149.7	150.7	152.6	160.1	151.4	153.4	154.8	165.7	151.9
11400	152.8	155.5	151.6	152.6	154.5	161.8	153.5	155.5	157.0	167.9	153.9
11700	154.7	157.5	153.6	154.4	156.3	163.7	155.5	157.8	159.6	170.2	155.9
12000	156.5	159.9	155.6	156.1	158.2	165.4	157.3	160.7	162.3	172.6	157.7
12300	158.4	161.9	157.6	158.0	159.8	166.9	159.2	163.1	164.7	174.8	159.6
12600	160.1	163.8	159.4	159.9	161.7	168.7	160.8	165.3	166.9	177.0	161.6
12900	161.7	165.5	161.4	161.5	163.3	169.8	162.4	167.2	168.8	178.7	163.0
13200	163.3	167.2	163.0	163.1	165.0	171.4	163.9	168.6	170.3	180.3	164.6
13500	164.9	169.1	164.8	164.6	166.5	172.7	165.6	170.1	172.2	181.8	166.3
13800	166.5	170.9	166.5	166.2	168.1	174.3	167.2	171.9	173.9	183.6	167.9
14100	168.2	172.6	168.3	167.9	169.9	175.8	168.9	173.4	175.6	185.4	169.7
14400	169.8	174.4	170.0	169.5	171.5	177.4	170.5	174.9	177.3	186.7	171.4

Table 4-10: Formed wall shroud temperature 272°C: thermocouple measurements at discrete times at distances from front surface at location A

Location A	Time (hrs)						
Distance from front surface (m)	0	0.5	1	1.5	2	2.5	3
	Temperature (°C)						
0.0000	23.0	51.1	105.4	132.5	146.7	158.0	168.0
0.0191	22.4	33.3	65.1	92.0	108.2	121.7	133.9
0.0381	22.5	27.0	47.1	72.6	92.2	107.2	118.7
0.0572	22.5	24.9	39.8	63.3	83.8	101.1	113.3
0.0762	22.5	24.0	36.3	58.2	78.6	96.3	108.7
0.1270	22.0	22.0	22.3	23.9	26.7	30.3	36.8
0.1461	21.8	21.9	22.0	23.0	25.2	28.3	33.6
0.1651	21.8	21.8	21.9	22.5	24.1	26.7	30.9
0.1842	21.9	21.9	21.9	22.4	23.7	26.0	29.8
0.2033	21.7	21.6	21.7	22.0	23.3	25.5	28.8

Table 4-11: Formed wall shroud temperature 272°C: Thermocouples measurements at discrete times at distances from front surface at location B

Location B	Time (hrs)						
Distance from front surface (m)	0	0.5	1	1.5	2	2.5	3
	Temperature (°C)						
0.0000	22.9	49.6	101.0	129.2	144.2	157.5	168.9
0.0191	22.6	33.1	63.9	90.9	107.7	122.2	134.8
0.0381	22.4	26.9	46.8	72.6	92.7	108.1	118.9
0.0572	22.6	25.1	40.3	64.2	85.2	102.2	112.9
0.0762	22.6	24.4	38.0	60.9	81.5	98.5	109.6
0.1270	22.0	22.1	22.5	24.1	27.1	31.7	40.2
0.1461	21.9	21.9	22.1	23.2	25.5	29.2	36.1
0.1651	21.8	21.8	22.0	22.6	24.3	27.0	32.2
0.1842	21.8	21.8	21.9	22.4	23.8	26.2	30.5
0.2033	21.7	21.6	21.7	22.0	23.3	25.5	29.5

Table 4-12: Formed wall shroud temperature 272°C: Thermocouples measurements at discrete times at distances from front surface at location C

Location C	Time (hrs)						
Distance from front surface (m)	0	0.5	1	1.5	2	2.5	3
	Temperature (°C)						
0.0000	22.8	56.0	113.7	140.0	153.1	164.2	173.3
0.0191	22.6	33.4	64.7	91.3	108.5	122.6	134.9
0.0381	22.3	27.5	48.8	74.7	94.3	108.9	119.8
0.0572	22.5	25.4	41.6	65.9	86.6	103.3	115.0
0.0762	22.5	24.6	38.7	61.9	82.6	99.2	111.2
0.1270	21.8	21.8	22.0	23.1	25.2	28.1	33.0
0.1461	21.7	21.7	21.8	22.7	24.6	27.3	31.7
0.1651	21.7	21.7	21.8	22.4	23.9	26.3	30.0
0.1842	21.5	21.5	21.6	22.0	23.2	25.4	28.6
0.2033	21.6	21.5	21.6	22.0	23.1	25.1	28.2

Table 4-13: Formed wall shroud temperature 272°C: Thermocouples measurements at discrete times at distances from front surface at location D

Location D	Time (hrs)						
Distance from front surface (m)	0	0.5	1	1.5	2	2.5	3
	Temperature (°C)						
0.0000	22.4	46.7	97.6	126.3	141.8	154.4	165.0
0.0191	22.5	32.5	62.1	88.7	105.7	120.0	132.0
0.0381	22.4	27.5	47.7	73.2	92.9	107.1	117.5
0.0572	22.3	25.2	40.3	64.1	84.4	100.4	110.9
0.0762	22.4	24.5	37.3	59.5	79.5	96.1	106.8
0.1270	21.5	21.5	21.9	23.4	26.5	30.8	38.9
0.1461	21.6	21.5	21.7	22.6	24.7	27.9	33.9
0.1651	21.6	21.6	21.7	22.2	23.8	26.4	31.0
0.1842	21.7	21.7	21.7	22.1	23.3	25.6	29.5
0.2033	21.6	21.5	21.6	22.0	23.2	25.5	29.4

Table 4-14: Formed wall shroud temperature 272°C: Thermocouples measurements at discrete times at distances from front surface at location E

Location E	Time (hrs)						
Distance from front surface (m)	0	0.5	1	1.5	2	2.5	3
	Temperature (°C)						
0.0000	22.3	47.2	100.0	128.7	144.5	158.2	169.3
0.0191	22.3	34.2	67.3	94.8	112.7	127.8	140.7
0.0381	22.0	28.3	51.2	78.4	98.1	112.2	123.1
0.0572	22.6	26.6	44.5	70.3	91.5	107.3	117.4
0.0762	21.7	24.5	39.6	64.1	85.3	101.9	112.2
0.1270	21.6	21.7	22.0	23.6	26.6	31.6	40.0
0.1461	21.8	21.8	22.0	23.0	25.1	28.7	35.1
0.1651	21.9	21.9	22.1	22.7	24.3	27.2	32.3
0.1842	21.9	21.9	21.9	22.3	23.7	26.1	30.4
0.2033	21.6	21.6	21.6	21.9	23.1	25.3	28.9

4.5.1.2. Shroud temperature 375°C

Figure 4-21 provides temperature measurements at the surface of the shroud facing the wall from nine thermocouples at locations shown in Figure 4-15. Figure 4-22 provides temperature measurements on the surface of the wall facing the shroud from thermocouples at locations shown in Figure 4-8. The measurements shown in these figures are provided in tabular form at discrete times in Table 4-15 for the shroud and in Table 4-16 through Table 4-18 for the front face of the wall. Similar to the 272°C shroud temperature test, there's greater spread among temperatures for the wall than the shroud. Temperatures in tabular form at discrete times for embedded thermocouples is provided in Table 4-19 through Table 4-23 at locations A, B, C, D, and E as shown in Figure 4-9 and Figure 4-10, respectively.

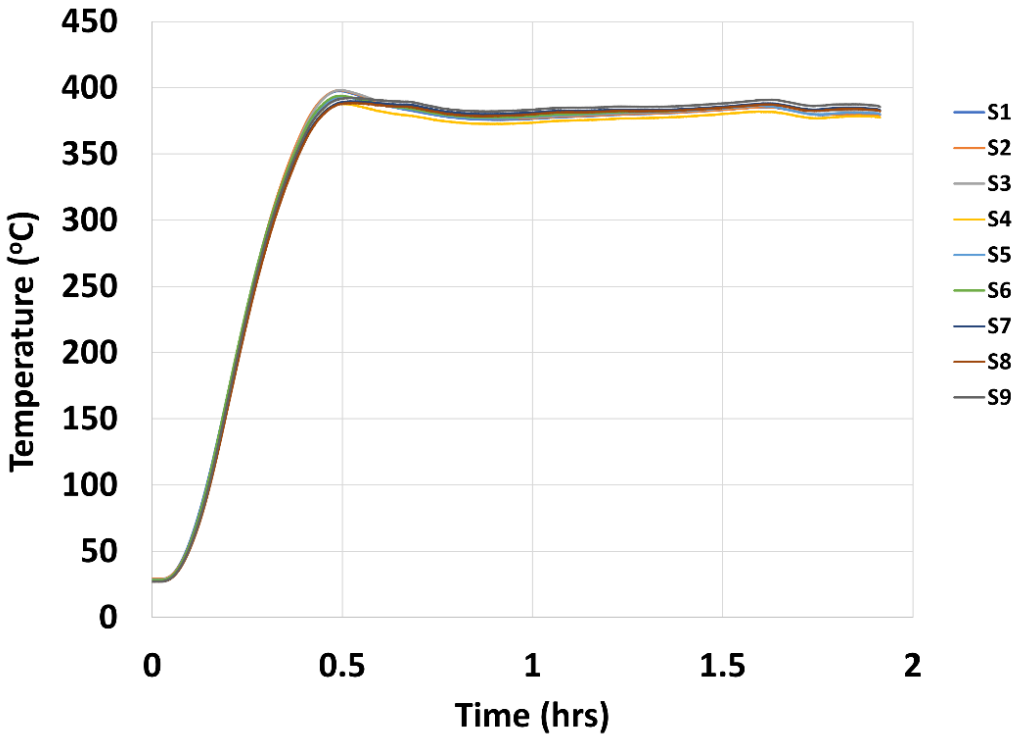

Figure 4-21: Formed wall shroud temperature 375°C: Temperature on surface of shroud at nine locations.

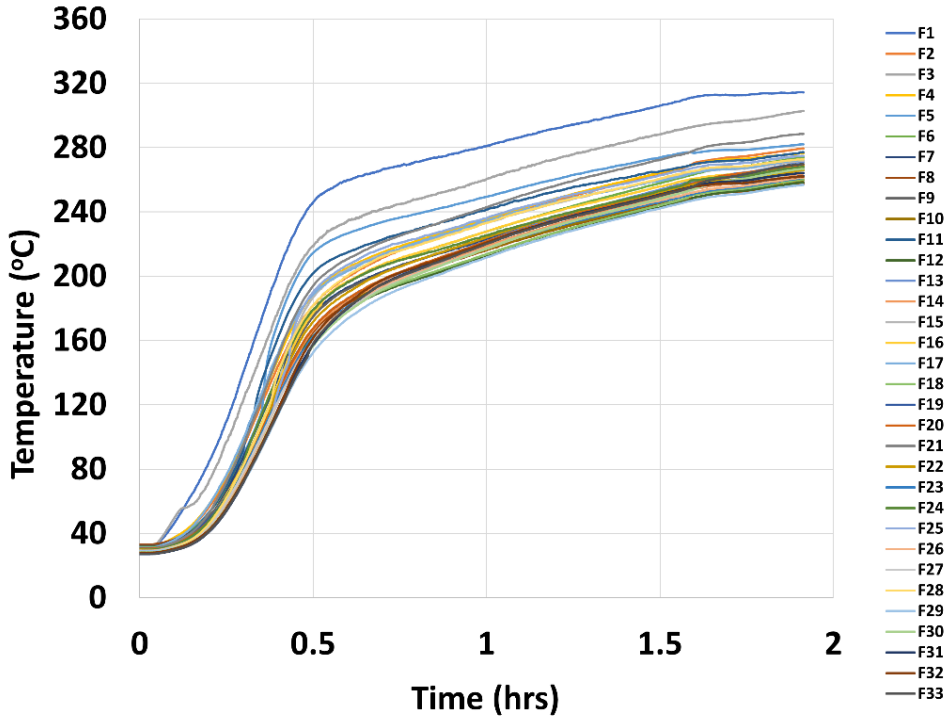

Figure 4-22: Formed wall shroud temperature 375°C: Temperature on wall surface facing shroud.

Table 4-15: Formed wall shroud temperature 375°C: Temperature on surface of shroud at nine locations

	Temperature (°C)								
	location								
Time (s)	S1	S2	S3	S4	S5	S6	S7	S8	S9
0	29.1	29.1	28.8	28.0	28.3	28.2	27.0	27.1	27.2
300	46.3	45.3	44.4	43.8	44.6	45.0	42.4	41.9	42.9
600	127.6	124.9	123.2	121.5	123.8	126.7	118.6	117.0	120.8
900	234.5	233.5	230.7	226.1	230.2	235.1	225.9	223.7	229.7
1200	321.8	322.1	319.3	311.5	316.1	320.3	312.0	310.3	316.1
1500	379.4	380.0	378.6	368.4	373.7	376.2	368.6	367.5	372.3
1800	397.4	397.9	398.1	387.8	393.0	393.7	389.1	387.9	391.7
2100	389.7	390.5	391.0	383.3	388.3	388.6	388.5	387.3	390.9
2400	383.5	384.4	384.8	379.3	384.1	384.8	387.2	385.8	389.5
2700	379.2	380.0	380.5	375.3	379.8	380.5	383.0	381.7	385.1
3000	376.5	377.3	377.9	373.0	377.2	378.1	380.4	378.9	382.5
3300	375.7	376.6	377.3	372.6	376.7	377.6	380.2	378.8	382.4
3600	376.6	377.1	377.8	373.6	378.0	378.6	381.4	379.9	383.4
3900	377.9	378.3	379.1	375.2	379.3	380.1	382.6	381.4	384.8
4200	378.8	379.1	379.9	375.7	380.1	380.8	382.9	381.8	385.2
4500	379.8	380.2	381.1	376.9	381.2	381.8	383.4	382.5	385.7
4800	380.6	380.8	381.7	377.3	381.7	382.2	383.3	382.5	385.6
5100	381.7	381.9	382.8	378.5	382.9	383.4	384.2	383.3	386.6
5400	383.2	383.3	384.3	380.2	384.5	384.9	385.8	384.8	388.2
5700	385.0	385.1	386.1	381.8	386.4	387.1	387.6	386.7	390.2
6000	383.6	383.8	386.1	380.3	383.7	386.5	386.5	385.8	389.5
6300	379.6	379.9	382.5	377.0	380.0	383.3	383.6	382.7	386.4
6600	380.2	380.0	383.1	378.2	381.0	384.3	384.9	383.9	387.4

Table 4-16: Formed wall shroud temperature 375°C: temperatures at wall surface facing heaters, F1 to F11

	Temperature (°C)										
	location										
Time (s)	F1	F2	F3	F4	F5	F6	F7	F8	F9	F10	F11
0	31.7	32.4	31.6	32.2	32.4	32.0	32.3	33.2	32.2	31.4	31.1
300	41.4	35.4	43.8	35.6	35.1	34.4	34.3	35.1	34.4	33.2	33.5
600	70.3	47.7	61.0	48.7	45.6	45.1	42.6	43.9	43.9	41.9	44.5
900	109.7	73.3	96.8	76.0	68.6	68.3	66.1	64.4	64.9	62.8	69.5
1200	162.1	111.2	141.7	114.3	105.2	103.5	103.6	96.4	99.2	96.7	118.8
1500	212.9	151.8	187.5	157.5	181.7	145.7	145.2	134.6	141.8	136.5	171.4
1800	245.8	181.8	218.7	188.7	214.5	178.8	176.4	165.1	174.8	167.0	201.8
2100	258.3	197.2	232.3	203.3	225.4	194.2	190.9	180.7	190.1	182.1	213.5
2400	264.2	207.8	239.8	212.0	231.6	203.3	199.7	190.5	199.0	191.7	220.4
2700	268.5	216.0	244.8	218.6	236.4	210.6	206.5	198.1	206.2	199.0	226.2
3000	272.9	222.5	250.0	224.4	240.4	216.4	212.3	204.6	212.4	205.0	231.4
3300	276.5	228.4	254.9	229.9	244.9	222.0	217.3	210.4	218.1	210.6	236.0
3600	280.9	234.4	260.3	235.3	249.4	227.8	222.7	216.2	223.8	216.4	241.4
3900	285.9	240.1	265.8	241.1	254.2	233.3	228.3	222.0	229.6	222.2	246.9
4200	290.4	245.3	271.1	246.3	258.7	238.7	233.3	227.2	234.5	227.4	251.2
4500	294.2	250.0	275.8	251.2	263.0	243.8	237.7	232.1	239.7	232.3	255.5
4800	298.0	254.6	279.9	255.8	266.5	248.5	242.0	236.3	244.1	236.9	258.5
5100	301.8	259.1	284.0	260.1	270.2	253.3	245.8	240.6	248.6	241.4	262.0
5400	306.1	263.6	288.3	264.4	273.8	257.9	250.1	244.6	252.8	245.9	265.2
5700	310.7	268.7	292.5	268.7	277.1	262.6	254.1	248.2	257.3	250.3	268.8
6000	312.7	272.9	295.4	272.0	278.3	266.5	256.8	251.5	261.2	253.2	271.5
6300	312.7	274.7	297.0	273.1	278.6	268.5	257.8	253.0	262.3	254.5	272.2
6600	313.8	277.1	299.9	274.9	280.4	271.3	260.1	255.3	264.7	257.3	274.8

Table 4-17: Formed wall shroud temperature 375°C: temperatures at wall surface facing heaters, F12 to F22

	Temperature (°C)										
	location										
Time (s)	F12	F13	F14	F15	F16	F17	F18	F19	F20	F21	F22
0	31.6	30.3	30.6	30.9	30.9	31.2	31.0	30.6	30.5	30.0	30.0
300	33.5	31.8	32.2	32.7	32.6	34.3	32.7	32.7	32.7	33.1	31.6
600	42.2	39.7	40.4	41.4	41.6	47.9	40.8	42.2	41.3	43.8	39.8
900	63.0	61.1	61.1	63.1	63.9	76.2	61.4	63.1	62.4	71.9	60.9
1200	95.9	95.4	94.0	96.9	99.1	117.5	93.7	97.0	96.6	113.7	94.4
1500	134.1	135.0	134.0	149.3	142.1	161.0	131.2	136.4	136.5	160.3	139.7
1800	162.7	166.8	166.4	186.9	177.1	188.7	161.1	167.5	167.3	194.0	171.6
2100	177.5	183.0	182.1	202.4	194.7	201.4	177.3	183.7	183.7	208.9	187.7
2400	187.2	193.7	192.5	210.7	204.3	210.3	188.0	194.2	194.5	218.0	198.5
2700	194.5	201.9	200.1	217.1	211.2	217.0	195.5	202.0	202.4	225.1	205.9
3000	200.4	208.9	206.4	222.3	216.6	223.0	201.7	208.4	209.1	231.2	212.1
3300	206.2	215.3	212.6	227.3	221.9	228.1	207.6	214.8	215.1	237.1	218.2
3600	212.2	221.8	218.6	233.2	227.7	234.4	213.7	221.0	221.7	243.0	224.2
3900	218.0	228.2	224.8	238.6	233.4	240.1	219.6	227.1	227.7	248.9	229.9
4200	223.6	233.9	230.1	243.6	238.3	244.4	225.2	232.6	233.0	254.3	235.0
4500	228.8	239.3	235.3	248.2	243.1	249.1	230.3	237.7	238.3	259.3	240.0
4800	233.7	244.4	240.0	252.2	247.3	252.2	235.2	242.4	243.2	263.9	244.2
5100	238.3	249.1	244.6	256.0	251.4	255.8	239.7	246.9	247.6	268.1	248.2
5400	242.7	253.8	249.3	260.3	255.8	259.3	244.2	251.4	252.2	272.4	252.0
5700	247.2	258.6	253.5	264.3	260.1	263.5	249.4	256.0	256.8	276.9	256.4
6000	251.6	262.4	256.7	266.3	262.6	266.3	252.9	260.5	261.8	281.8	259.1
6300	253.3	264.7	258.3	267.1	263.9	267.5	254.7	262.1	264.4	283.4	260.6
6600	255.9	267.9	261.2	269.8	266.5	270.0	257.7	264.5	267.2	286.4	263.2

Table 4-18: Formed wall shroud temperature 375°C: temperatures at wall surface facing heaters, F23 to F33

	Temperature (°C)										
	location										
Time (s)	F23	F24	F25	F26	F27	F28	F29	F30	F31	F32	F33
0	29.8	29.8	29.2	29.3	29.1	28.3	28.8	28.3	27.1	28.0	27.4
300	31.6	31.7	30.9	31.0	30.8	30.3	30.1	29.8	28.7	29.6	28.8
600	39.9	40.8	38.5	38.7	38.6	38.9	36.4	36.6	35.2	36.6	35.5
900	60.5	62.8	58.8	58.6	59.7	62.3	54.3	56.2	53.9	55.7	54.4
1200	94.1	104.4	91.6	91.5	92.7	98.5	85.1	87.9	86.8	87.6	85.8
1500	132.5	148.4	139.6	130.2	130.1	149.5	121.9	125.5	125.4	125.7	122.3
1800	162.4	179.1	190.0	160.8	160.0	181.8	152.5	156.5	157.3	161.5	157.9
2100	178.6	193.8	204.9	177.9	176.6	197.8	170.7	175.1	177.1	180.6	177.6
2400	189.9	203.6	214.8	189.8	188.4	208.7	183.2	187.9	190.8	193.5	190.7
2700	198.4	209.9	220.7	198.4	196.7	215.8	192.0	196.8	200.1	202.2	199.7
3000	205.1	215.1	225.5	204.8	203.8	221.3	199.0	203.7	207.3	208.4	206.7
3300	211.2	219.8	230.6	211.1	210.5	227.1	205.3	210.5	214.2	214.4	213.4
3600	217.5	225.4	236.2	217.6	217.1	233.2	211.6	217.3	220.8	220.8	220.1
3900	223.8	230.5	242.0	224.0	223.4	238.9	217.8	223.7	227.2	226.7	226.6
4200	228.7	235.6	246.2	229.1	229.1	243.8	223.4	229.1	232.7	232.2	231.9
4500	233.7	240.2	250.9	234.4	234.3	248.4	228.5	234.4	237.6	236.9	236.8
4800	237.9	244.5	254.9	238.8	239.0	252.4	233.3	239.1	241.8	241.4	241.2
5100	242.0	248.8	258.5	243.0	243.7	256.3	237.6	243.5	246.3	245.5	245.6
5400	246.1	253.1	262.8	247.0	248.2	260.6	242.1	248.3	250.9	250.4	250.1
5700	250.5	258.8	266.7	251.4	252.9	264.9	246.7	253.2	255.2	255.0	254.8
6000	254.0	261.2	269.4	254.8	257.5	267.8	249.9	258.4	258.5	257.4	260.6
6300	255.8	262.5	270.6	256.4	259.0	268.5	251.6	260.9	259.6	258.2	263.7
6600	258.5	265.8	273.0	258.9	261.9	270.9	254.7	264.3	262.3	260.4	267.6

Table 4-19: Formed wall shroud temperature 375°C: Thermocouples measurements at discrete times at distances from front surface at location A

Location A	Time (hrs)							
Distance from front surface (m)	0	0.25	0.5	0.75	1	1.25	1.5	1.75
	Temperature (°C)							
0.0000	32.3	66.1	176.4	206.5	222.7	237.7	250.1	257.8
0.0191	31.9	38.4	84.4	123.1	145.7	163.8	179.5	193
0.0381	32.2	33.3	50.7	79.9	103.6	122.3	138.4	152
0.0572	32.3	32.6	40.6	62.1	84.7	105.2	121.7	134
0.0762	32.4	32.5	36.7	53.4	74.1	94.7	112.2	126
0.1270	35.6	35.6	35.5	36.3	39.0	42.1	46.4	52
0.1461	35.5	35.5	35.4	35.7	37.2	39.6	42.7	47.1
0.1651	35.5	35.5	35.4	35.5	36.2	37.7	40.0	43.3
0.1842	35.7	35.6	35.5	35.5	35.9	37.0	38.9	41.7
0.2033	35.4	35.4	35.3	35.3	35.5	36.5	38.1	40.7

Table 4-20: Formed wall shroud temperature 375°C: Thermocouple measurements at discrete times at distances from front surface at location B

Location B	Time (hrs)							
Distance from front surface (m)	0	0.25	0.5	0.75	1	1.25	1. 5	1.75
	Temperature (°C)							
0.0000	32.2	64.9	174.8	206.2	223.8	239.7	252.8	262.3
0.0191	32.1	39.2	83.8	123.0	146.9	165.9	181.9	196
0.0381	32.2	33.6	50.8	80.5	105.3	124.7	140.5	154
0.0572	32.4	32.8	41.0	63.5	87.2	107.6	123.3	137
0.0762	32.5	32.5	38.2	57.5	79.9	99.9	116.1	130
0.1270	35.8	35.8	35.9	36.7	39.5	43.5	49.9	56.7
0.1461	35.7	35.6	35.6	36.0	37.8	40.6	45.3	50.9
0.1651	35.6	35.6	35.6	35.7	36.5	38.2	41.1	45.3
0.1842	35.7	35.6	35.6	35.6	36.0	37.3	39.6	43.1
0.2033	35.5	35.5	35.5	35.4	35.7	36.7	38.6	41.7

Table 4-21: Formed wall shroud temperature 375ºC: thermocouple measurements at discrete times at distances from front surface at location C

Location C	Time (hrs)							
Distance from front surface (m)	0	0.25	0. 5	0.75	1	1.25	1.5	1.75
	Temperature (ºC)							
0.0000	31.2	76.2	188.7	217.0	234.4	249.1	259.3	267.5
0.0191	31.3	38.6	83.9	122.4	146.6	165.7	182.1	196
0.0381	31.2	32.9	53.1	83.8	108.4	127.9	144.7	159
0.0572	31.5	31.9	41.8	65.5	89.4	110.5	127.0	140
0.0762	31.5	31.7	38.1	58.2	81.0	101.8	119.4	133
0.1270	34.7	34.7	34.7	35.0	36.8	39.3	42.8	47.2
0.1461	34.7	34.6	34.6	34.8	36.1	38.2	41.2	45.1
0.1651	34.7	34.7	34.6	34.7	35.4	37.0	39.4	42.7
0.1842	34.5	34.5	34.4	34.4	34.8	36.0	37.9	40.6
0.2033	34.6	34.6	34.6	34.6	34.8	35.8	37.4	39.9

Table 4-22: Formed wall shroud temperature 375ºC: thermocouple measurements at discrete times at distances from front surface at location D

Location D	Time (hrs)							
Distance from front surface (m)	0	0.25	0.5	0.75	1	1.25	1.5	1.75
	Temperature (ºC)							
0.0000	29.2	58.8	190.0	62.5	86.8	107.5	123.3	136.7
0.0191	29.6	35.5	77.2	54.5	76.7	97.3	113.5	127
0.0381	29.6	31.1	50.2	33.0	35.6	39.5	45.9	52.2
0.0572	29.5	29.9	39.2	32.5	33.8	36.2	40.3	45.3
0.0762	29.7	29.8	35.4	32.4	33.1	34.6	37.4	41.3
0.1270	32.3	32.3	32.3	32.4	32.8	33.9	36.0	39.3
0.1461	32.4	32.4	32.3	32.7	32.9	33.8	35.7	38.7
0.1651	32.5	32.5	32.4	215.8	233.2	248.4	260.6	268
0.1842	32.6	32.6	32.5	128.1	153.8	174.1	190.8	205
0.2033	32.7	32.7	32.7	88.8	115.3	136.4	153.7	169

Table 4-23: Formed wall shroud temperature 375ºC: thermocouple measurements at discrete times at distances from front surface at location E

Location E	Time (hrs)							
Distance from front surface (m)	0	0.25	0.5	0.75	1	1.25	1.5	1.75
	Temperature (ºC)							
0.0000	22.3	47.2	100.0	128.7	144.5	158.2	169.3	268.5
0.0191	22.3	34.2	67.3	94.8	112.7	127.8	140.7	205
0.0381	22.0	28.3	51.2	78.4	98.1	112.2	123.1	169
0.0572	22.6	26.6	44.5	70.3	91.5	107.3	117.4	149
0.0762	21.7	24.5	39.6	64.1	85.3	101.9	112.2	137
0.1270	21.6	21.7	22.0	23.6	26.6	31.6	40.0	51.8
0.1461	21.8	21.8	22.0	23.0	25.1	28.7	35.1	45.6
0.1651	21.9	21.9	22.1	22.7	24.3	27.2	32.3	42
0.1842	21.9	21.9	21.9	22.3	23.7	26.1	30.4	39.7
0.2033	21.6	21.6	21.6	21.9	23.1	25.3	28.9	38.3

4.5.1.3. Shroud temperature 444ºC

Figure 4-23 provides temperature measurements at the surface of the shroud facing the wall from nine thermocouples at locations shown in Figure 4-15. Figure 4-24 provides temperature measurements on the surface of the wall facing the shroud from thermocouples at locations shown in Figure 4-8. The measurements shown in these figures are provided in tabular form at discrete times in Table 4-24 for the shroud and in Table 4-25 through Table 4-27 for the front face of the wall. Similar to the other tests, there's greater spread among temperatures for the wall than the shroud. Temperatures in tabular form at discrete times for embedded thermocouples is provided in Table 4-28 through Table 4-32 at locations A, B, C, D, and E as shown in Figure 4-9 and Figure 4-10, respectively.

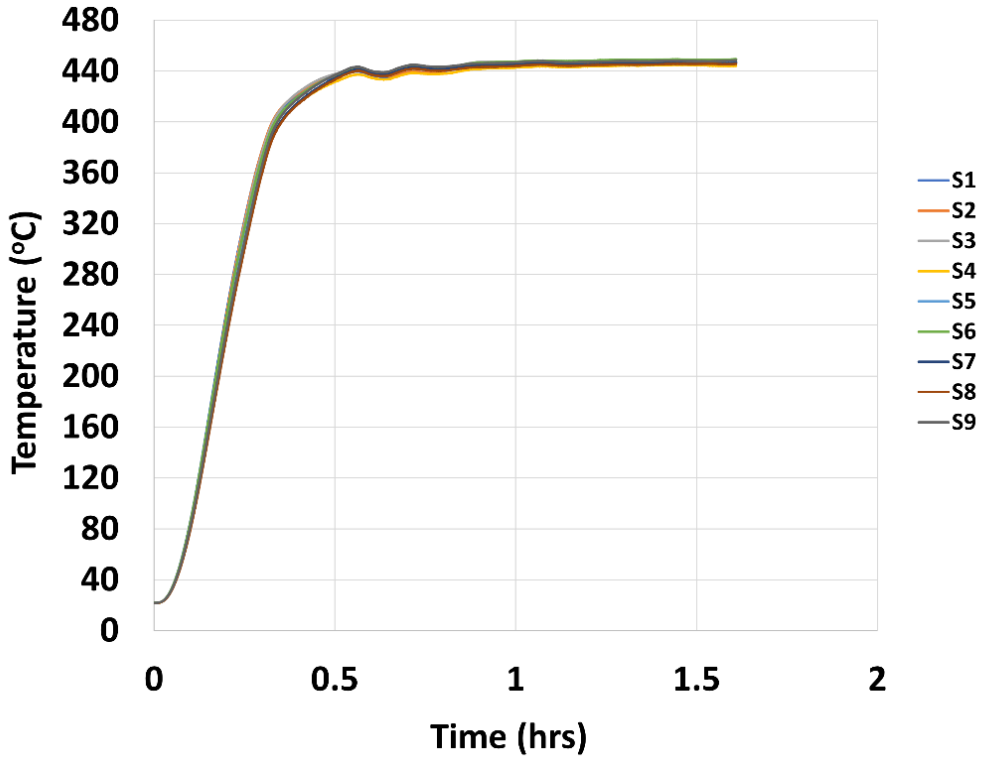

Figure 4-23: Formed wall shroud temperature 444°C: Temperature on surface of shroud at nine locations.

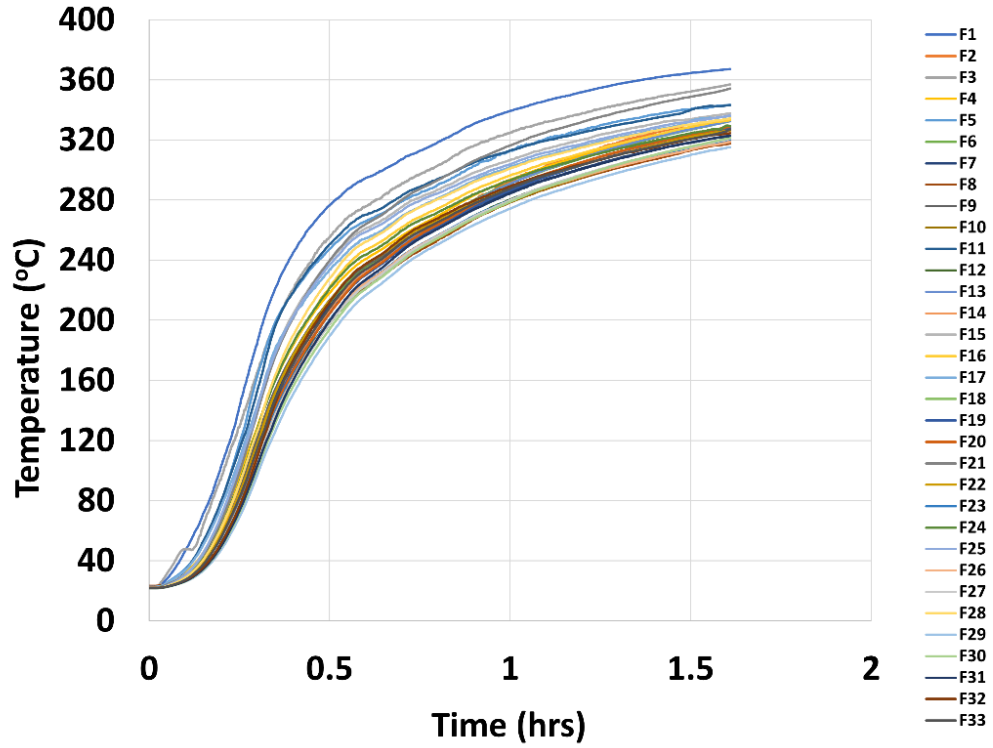

Figure 4-24: Formed wall shroud temperature 444°C: Temperature on wall surface facing shroud.

Table 4-24: Formed wall shroud temperature 444°C: Temperature on surface of shroud at nine locations

	Temperature (°C)								
	location								
Time (s)	S1	S2	S3	S4	S5	S6	S7	S8	S9
0	21.8	21.8	21.7	21.6	21.8	21.9	21.7	21.6	21.8
300	64.4	62.4	61.2	61.6	62.6	63.8	60.4	59.2	61.3
600	194.4	191.4	188.9	185.2	188.3	192.0	180.1	178.1	183.2
900	322.5	321.4	318.8	307.6	311.9	315.9	300.9	299.5	305.4
1200	402.7	403.5	402.3	392.1	398.1	399.2	391.3	390.2	395.7
1500	425.0	425.9	426.9	418.1	423.7	423.5	419.5	417.9	422.4
1800	435.4	436.1	437.6	431.4	436.5	436.6	434.3	433.1	436.8
2100	438.5	439.1	440.8	436.4	440.9	441.3	439.9	439.1	442.1
2400	436.4	436.9	438.7	434.9	439.7	440.1	439.3	438.1	441.3
2700	438.5	438.8	440.8	437.9	442.1	442.5	442.1	440.8	444.0
3000	441.7	441.7	443.7	439.0	443.5	444.0	442.5	441.2	444.2
3300	445.5	445.3	447.4	441.9	446.1	446.6	444.5	443.3	446.1
3600	445.7	445.4	447.5	442.7	446.6	447.3	445.1	444.0	446.8
3900	446.3	446.0	448.0	443.5	447.3	448.3	446.0	444.9	447.7
4200	446.1	445.7	447.8	443.2	446.8	448.0	445.3	444.2	446.8
4500	447.0	446.4	448.4	443.8	447.4	448.6	445.8	444.9	447.4
4800	447.2	446.5	448.5	444.1	447.7	448.8	446.1	444.9	447.7
5100	447.5	446.7	448.8	444.6	448.1	449.2	446.5	445.5	448.1
5400	447.3	446.4	448.6	444.6	447.7	449.0	446.2	445.5	447.8
5700	447.1	446.7	448.7	444.0	447.7	449.0	446.1	445.4	448.1

Table 4-25: Formed wall shroud temperature 444°C: temperatures at wall surface facing heaters, F1 to F11

	Temperature (°C)										
	location										
Time (s)	F1	F2	F3	F4	F5	F6	F7	F8	F9	F10	F11
0	22.1	22.1	22.3	22.4	22.2	22.4	22.5	23.3	22.5	22.0	21.8

	Temperature (°C)										
300	39.3	28.9	44.7	29.0	31.1	28.0	26.5	27.6	27.9	26.0	29.5
600	80.2	50.1	74.1	51.0	59.4	47.9	45.8	44.2	46.5	43.6	61.0
900	142.4	93.1	129.0	95.8	118.1	88.9	87.4	80.9	88.9	82.1	114.2
1200	211.3	142.5	189.3	151.4	188.9	143.6	141.0	133.2	144.9	133.1	183.7
1500	252.0	182.5	228.6	190.7	224.5	183.4	181.3	173.0	184.8	171.6	225.7
1800	276.4	209.9	255.5	218.2	247.4	211.7	209.7	199.3	213.4	199.7	250.6
2100	292.6	231.1	273.2	238.2	264.1	232.2	230.0	219.7	233.7	220.9	268.5
2400	302.4	244.8	286.1	250.8	274.0	246.1	242.7	233.3	246.4	234.3	278.1
2700	312.8	258.3	297.2	263.1	284.7	259.2	255.6	246.6	259.0	247.7	288.8
3000	322.5	269.5	307.6	274.2	293.7	270.6	266.4	257.7	269.7	258.7	297.5
3300	332.4	282.7	318.0	285.3	305.3	282.0	277.3	269.7	280.4	269.8	306.8
3600	339.3	292.4	324.7	293.7	312.8	291.0	285.6	278.6	288.9	278.6	313.0
3900	345.0	300.6	330.9	300.9	319.4	298.7	292.5	286.2	296.1	286.3	318.8
4200	349.8	308.6	336.0	307.2	324.9	305.4	298.7	292.3	302.3	292.8	323.0
4500	354.7	315.0	340.7	313.3	329.9	311.6	304.6	298.3	308.2	299.0	327.7
4800	358.7	320.9	344.9	318.7	333.9	317.3	309.7	303.4	313.5	304.5	331.5
5100	362.0	325.8	349.1	323.5	337.6	322.3	314.3	308.2	318.1	309.6	335.3
5400	364.6	328.2	352.2	327.9	340.5	326.9	318.4	313.1	322.3	314.2	340.0
5700	366.6	331.4	355.7	331.6	342.9	331.2	322.0	316.7	326.3	318.2	342.5

Table 4-26: Formed wall shroud temperature 444°C: temperatures at wall surface facing heaters, F12 to F22

	Temperature (°C)										
	location										
Time (s)	F12	F13	F14	F15	F16	F17	F18	F19	F20	F21	F22
0	22.34	21.85	21.91	22.12	22.18	22.63	22.4	22.17	22.18	21.93	21.89
300	27.1	25.3	26.1	28.3	26.9	30.4	26.4	26.8	26.6	27.9	26.2
600	44.2	41.8	43.9	52.6	46.4	58.1	42.4	44.0	43.4	49.7	43.7
900	80.6	80.3	84.8	102.7	90.8	107.7	78.7	82.8	81.0	98.7	84.5
1200	129.7	133.3	137.0	168.2	152.7	169.6	126.5	133.9	132.4	165.3	142.1
1500	171.2	174.8	177.5	211.7	191.1	208.8	167.8	174.5	173.9	209.8	184.1

	Temperature (°C)										
1800	200.3	206.0	207.3	239.5	221.9	233.8	197.5	204.4	204.5	239.8	213.0
2100	222.0	229.6	228.9	258.8	244.6	252.9	220.4	227.5	228.0	261.4	234.7
2400	235.9	244.6	242.9	270.0	256.4	263.6	234.7	241.9	242.4	274.2	247.7
2700	249.6	259.1	256.5	281.9	268.8	275.4	249.0	255.7	256.9	287.4	260.9
3000	260.5	270.5	267.5	290.4	278.7	285.0	260.1	266.7	268.0	297.5	270.4
3300	271.5	281.7	278.3	299.7	288.7	295.1	271.1	277.5	279.1	308.1	280.3
3600	280.4	290.8	287.1	306.6	296.4	302.3	279.9	286.4	288.2	316.4	288.1
3900	288.0	299.0	294.5	313.0	303.4	308.6	287.7	294.3	296.3	323.9	295.4
4200	294.3	305.7	301.2	318.4	308.9	313.7	294.2	300.8	303.0	329.7	301.1
4500	300.5	312.1	307.3	323.5	314.5	318.9	300.3	307.0	309.0	335.3	306.9
4800	306.0	317.6	312.5	327.7	319.4	323.1	305.7	312.4	314.5	340.3	312.2
5100	310.8	322.6	317.4	331.5	324.1	327.4	310.6	317.1	319.1	344.9	317.3
5400	315.2	327.1	321.8	333.8	328.8	332.6	315.1	321.5	323.7	348.8	322.1
5700	318.9	331.2	325.3	336.9	332.2	335.2	318.7	325.6	327.7	352.6	325.5

Table 4-27: Formed wall shroud temperature 444°C: temperatures at wall surface facing heaters, F23 to F33

	Temperature (°C)										
	location										
Time (s)	F23	F24	F25	F26	F27	F28	F29	F30	F31	F32	F33
0	21.72	21.76	21.8	21.87	21.82	21.85	21.98	21.67	21.78	21.92	21.75
300	25.6	27.0	27.5	25.6	25.4	26.4	24.7	24.7	24.9	25.3	25.4
600	40.8	47.2	52.5	40.4	40.7	46.8	37.3	38.4	38.9	40.1	42.8
900	77.4	92.0	103.9	76.2	76.7	91.3	68.9	71.7	73.2	76.2	81.9
1200	129.0	150.4	168.1	128.0	127.3	152.9	117.5	122.1	124.5	133.4	137.3
1500	170.7	192.5	209.4	169.1	168.0	197.7	158.6	163.5	168.0	181.2	178.4
1800	200.2	221.5	237.0	199.7	197.7	227.8	189.5	194.2	199.7	212.1	208.3
2100	222.4	241.6	257.0	222.1	220.6	250.0	213.4	218.0	224.0	234.7	231.2
2400	236.3	253.6	267.6	235.9	235.0	261.8	229.0	233.0	239.3	248.3	245.0
2700	250.0	266.6	279.6	249.9	249.4	275.3	243.7	248.0	254.3	262.3	259.2
3000	260.8	275.9	288.2	260.5	260.4	284.2	255.0	259.1	265.3	272.0	269.4

	Temperature (°C)										
3300	271.3	285.7	296.9	270.9	271.0	293.5	265.4	269.8	275.5	281.3	279.4
3600	279.9	293.2	303.9	279.2	279.9	301.1	274.3	278.9	284.4	289.2	287.6
3900	287.6	300.1	310.9	287.1	288.1	307.6	282.5	287.3	292.1	296.1	295.3
4200	294.0	305.7	315.8	293.4	294.6	312.8	288.8	293.8	298.3	302.0	301.2
4500	299.9	311.2	320.5	299.3	300.7	317.9	294.9	300.3	304.1	306.7	307.0
4800	305.1	315.9	325.0	304.4	306.0	322.7	300.3	306.1	309.5	311.9	312.1
5100	310.0	320.3	329.1	309.2	311.1	326.8	305.4	311.0	314.2	316.1	316.5
5400	315.0	324.4	332.3	313.7	315.4	330.4	310.1	315.7	318.1	320.6	320.7
5700	318.8	327.5	335.2	317.5	319.6	333.2	314.0	320.0	321.8	323.6	324.8

Table 4-28: Formed wall shroud temperature 444°C: thermocouples measurements at discrete times at distances from front surface at location A

Location A	Time (hrs)						
Distance from front surface (m)	0	0.25	0.5	0.75	1	1.25	1.5
	Temperature (°C)						
0.0000	22.5	87.4	209.7	255.6	285.6	304.6	318.4
0.0191	21.9	35.3	97.9	147.0	182.1	209.3	230.9
0.0381	22.0	24.6	52.1	89.2	122.4	151.2	174.6
0.0572	22.1	22.7	36.4	64.6	94.6	122.8	145.7
0.0762	22.1	22.2	30.0	52.9	80.3	106.3	128.3
0.1270	23.4	23.4	23.4	24.3	27.0	31.2	37.8
0.1461	23.3	23.2	23.2	23.6	25.2	28.1	32.8
0.1651	23.3	23.2	23.2	23.3	24.1	25.9	29.1
0.1842	23.4	23.3	23.3	23.3	23.8	25.1	27.6
0.2033	23.2	23.1	23.1	23.1	23.4	24.5	26.6

Table 4-29: Formed wall shroud temperature 444°C: Thermocouples measurements at discrete times at distances from front surface at location B.

Location B	Time (hrs)						
Distance from front surface (m)	0	0.25	0.5	0.75	1	1.25	1.5
	Temperature (°C)						
0.0000	22.5	88.9	213.4	259.0	288.9	308.2	322.3
0.0191	22.3	36.0	98.0	147.5	183.4	211.4	232.7
0.0381	22.3	25.2	52.4	90.1	124.3	153.1	175.9
0.0572	22.4	23.2	37.3	67.2	98.6	125.4	147.9
0.0762	22.4	22.7	32.8	59.3	88.8	113.7	137.3
0.1270	23.9	23.8	24.0	25.0	28.1	35.0	42.9
0.1461	23.7	23.6	23.6	24.1	26.1	30.6	37.1
0.1651	23.6	23.6	23.6	23.8	24.6	27.0	31.4
0.1842	23.7	23.6	23.6	23.7	24.2	25.8	29.2
0.2033	23.5	23.5	23.4	23.4	23.8	25.0	27.9

Table 4-30: Formed wall shroud temperature 444°C: Thermocouples measurements at discrete times at distances from front surface at location C

Location C	Time (hrs)						
Distance from front surface (m)	0	0.25	0.5	0.75	1	1.25	1.5
	Temperature (°C)						
0.0000	22.6	107.7	233.8	275.4	302.3	318.9	332.6
0.0191	22.4	36.4	99.8	149.1	184.6	211.7	232.9
0.0381	22.1	25.7	57.8	98.3	132.1	159.7	182.7
0.0572	22.3	23.4	39.7	70.9	102.3	126.9	150.9
0.0762	22.3	22.7	33.7	60.8	92.4	112.2	136.5
0.1270	23.5	23.5	23.5	24.1	26.2	32.3	39.2
0.1461	23.4	23.4	23.4	23.7	25.3	30.0	36.1
0.1651	23.5	23.5	23.4	23.6	24.5	27.5	32.3
0.1842	23.3	23.2	23.2	23.2	23.7	25.5	29.3
0.2033	23.5	23.4	23.4	23.4	23.8	25.2	28.5

Table 4-31: Formed wall shroud temperature 444ºC: Thermocouples measurements at discrete times at distances from front surface at location D

Location D	Time (hrs)						
Distance from front surface (m)	0	0.25	0.5	0.75	1	1.25	1.5
	Temperature (ºC)						
0.0000	21.8	103.9	237.0	279.6	303.9	320.5	332.3
0.0191	22.0	33.2	92.0	142.4	178.8	207.0	228.1
0.0381	21.9	24.9	54.6	94.5	129.6	158.7	180.9
0.0572	21.8	22.6	37.9	68.9	101.2	128.4	150.6
0.0762	21.9	22.2	32.0	58.1	87.6	112.9	135.8
0.1270	22.8	22.7	22.8	23.7	26.9	34.4	42.4
0.1461	22.8	22.8	22.7	23.1	24.6	28.7	34.8
0.1651	22.9	22.8	22.8	22.9	23.6	25.9	30.4
0.1842	22.9	22.9	22.8	22.8	23.2	24.8	28.2
0.2033	23.1	23.1	23.1	23.1	23.4	24.7	27.7

Table 4-32: Formed wall shroud temperature 444ºC: Thermocouples measurements at discrete times at distances from front surface at location E

Location E	Time (hrs)						
Distance from front surface (m)	0	0.25	0.5	0.75	1	1.25	1.5
	Temperature (ºC)						
0.0000	21.9	91.3	227.8	275.3	301.1	317.9	330.4
0.0191	22.1	36.8	104.2	156.9	193.7	221.8	242.6
0.0381	21.8	25.8	60.9	104.1	140.8	170.2	193.1
0.0572	22.4	23.7	43.7	79.2	113.8	141.8	166.0
0.0762	21.5	21.9	34.2	64.2	95.7	122.7	148.0
0.1270	23.1	23.0	23.1	24.1	27.5	35.2	41.9
0.1461	23.3	23.2	23.2	23.5	25.2	29.6	35.3
0.1651	23.4	23.3	23.3	23.5	24.4	27.0	31.4
0.1842	23.4	23.4	23.3	23.3	23.8	25.5	28.9
0.2033	23.0	23.0	23.0	23.0	23.3	24.5	27.4

4.5.2. Masonry wall

Figure 4-25 shows temperature measurements at the surface of the shroud facing the wall from nine thermocouples at locations shown in Figure 4-15. The measurements are also provided in tabular form at discrete times in Table 4-33 for the shroud. Figure 4-26 shows temperature measurements on the surface of the wall facing the shroud from thermocouples at locations shown in Figure 4-11 through Figure 4-13. Figure 4-27 shows temperatures at the webs and cores of the five blocks from embedded thermocouples. Table 4-34 provides temperatures at discrete times from thermocouples at the front and back faces for each of the five blocks. Temperatures in tabular form at discrete times for embedded thermocouples is provided in Table 4-35 through Table 4-37 at the front locations, Table 4-38 through Table 4-40 at the middle locations, and Table 4-41 through Table 4-43 at the back locations.

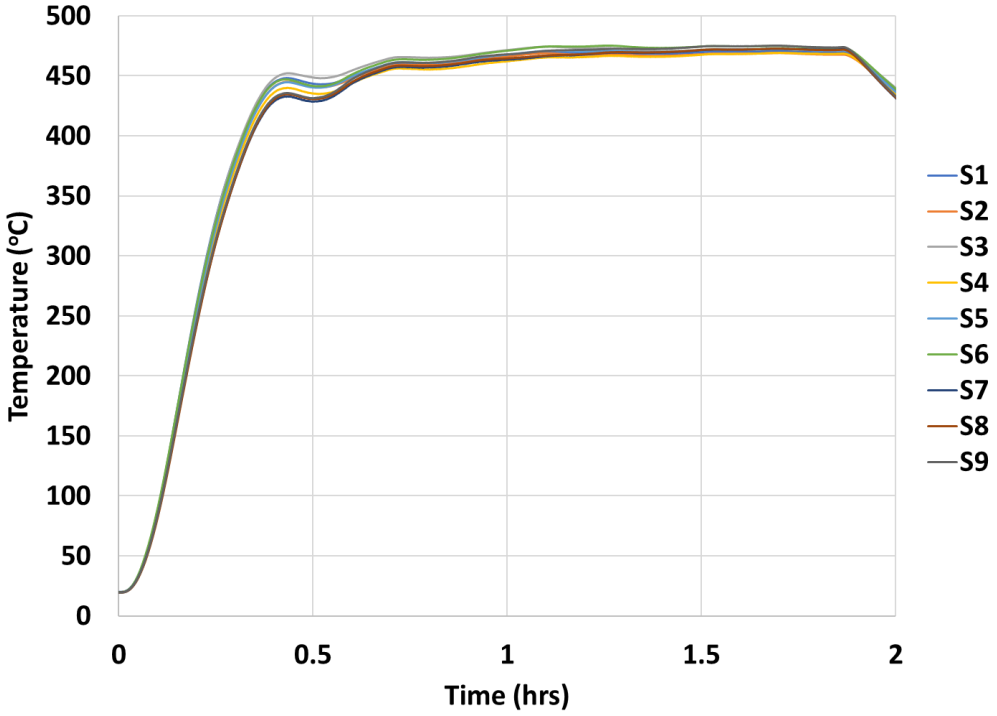

Figure 4-25: Masonry wall shroud temperature 470°C: Temperature on surface of shroud at nine locations.

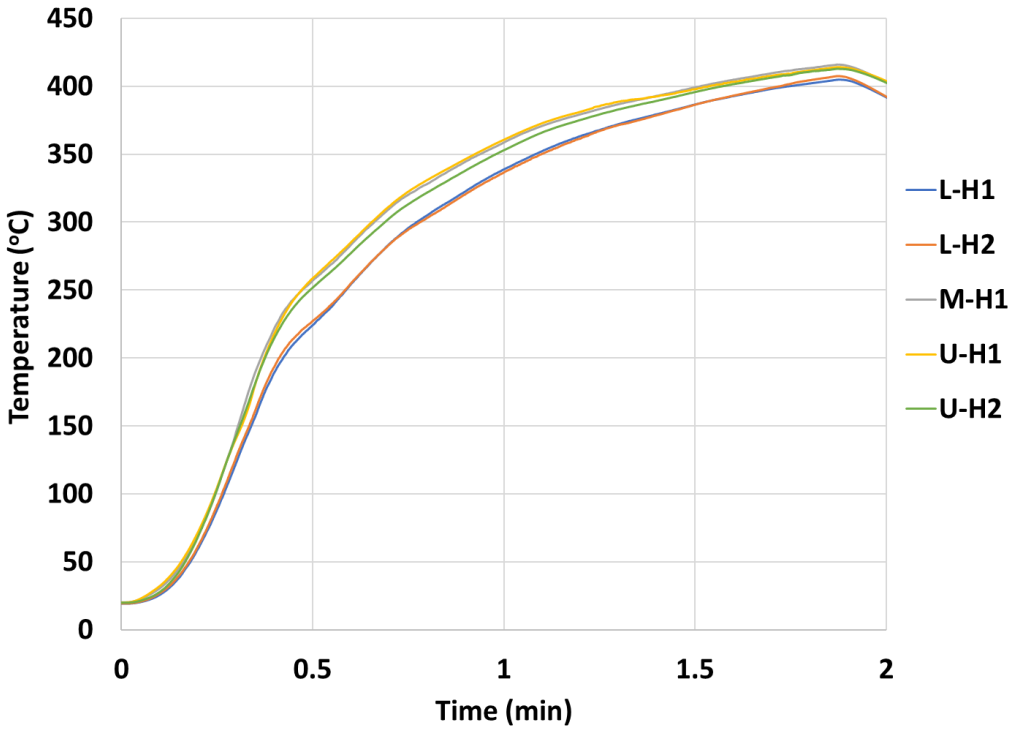

Figure 4-26: Masonry wall shroud temperature 470°C: Temperature on wall surface facing shroud.

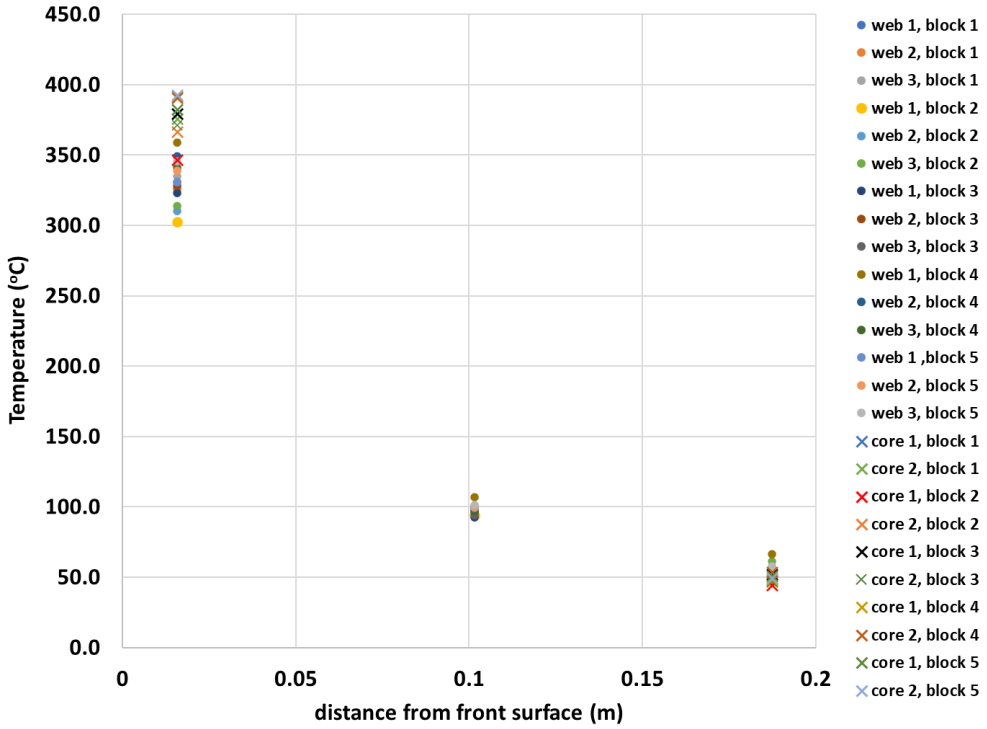

Figure 4-27: Masonry wall shroud temperature 470°C: In-depth temperature profiles at webs and cores.

Table 4-33: Masonry wall shroud temperature 470°C: Temperature on surface of shroud at nine locations

	Temperature (°C)								
	location								
Time (s)	S1	S2	S3	S4	S5	S6	S7	S8	S9
0	20.0	19.8	20.0	19.8	19.8	19.7	19.6	19.4	19.4
300	65.4	64.4	66.5	64.7	65.9	67.3	62.7	61.2	62.6
600	202.1	197.7	201.3	195.0	197.7	201.4	189.5	187.4	190.6
900	331.8	326.6	330.8	320.0	323.7	328.5	311.4	311.1	314.0
1200	411.7	407.5	412.9	401.8	406.5	410.3	393.6	394.1	396.2
1500	447.2	444.0	450.8	438.9	443.6	446.5	431.8	433.5	434.6
1800	443.5	440.8	448.6	435.3	440.3	441.6	428.6	430.6	431.5
2100	447.3	445.4	452.3	440.8	446.6	448.1	439.6	441.0	443.3
2400	457.0	455.3	461.8	452.1	457.3	459.7	452.9	454.2	456.8
2700	460.5	459.2	465.5	455.9	461.2	463.7	457.3	458.4	461.2
3000	460.3	459.4	465.4	455.8	461.3	464.0	457.7	458.8	461.6
3300	463.2	462.7	468.1	459.1	464.7	467.4	461.2	462.4	465.4
3600	466.7	466.0	471.4	462.2	467.7	470.9	463.6	464.6	467.9
3900	469.5	468.7	474.1	465.1	470.5	474.0	465.9	466.6	470.4
4200	469.1	467.8	473.4	465.4	470.4	474.4	467.1	467.7	471.5
4500	469.3	467.8	473.2	466.6	470.8	475.2	469.0	469.3	472.2
4800	468.6	467.0	471.6	466.0	470.0	473.8	469.2	469.6	472.4
5100	468.5	466.8	470.8	466.1	469.9	473.4	469.7	470.0	472.8
5400	469.7	468.0	471.8	467.6	471.2	474.5	471.4	471.6	474.4
5700	470.0	468.3	472.0	468.2	471.6	474.6	471.8	471.9	474.7
6000	470.4	468.8	472.2	468.8	472.0	474.8	472.4	472.4	475.0
6300	470.1	468.4	471.6	468.7	471.7	474.1	472.2	472.1	474.5

Table 4-34: Masonry wall shroud temperature 470°C: thermocouple temperatures at front and back surfaces of wall.

	Temperature (°C)									
	Front surface					Back surface				
Time (s)	L-H1	L-H2	M-H1	U-H1	U-H2	L-C1	L-C2	M-C1	U-C1	U-C2
0	19.2	19.3	20.1	20.1	19.9	19.2	19.2	20.0	20.0	19.9
300	23.3	24.1	27.3	28.7	24.9	19.2	19.2	20.0	20.0	19.9
600	44.5	45.9	52.2	54.6	50.0	19.1	19.2	20.0	20.0	19.9
900	88.4	91.6	103.2	104.7	103.3	19.1	19.2	20.0	20.0	20.0
1200	145.9	149.7	176.1	164.6	168.1	19.1	19.2	20.1	20.1	20.1
1500	197.3	202.2	230.6	227.4	223.3	19.1	19.1	20.1	20.2	20.1
1800	224.1	227.2	257.0	258.7	251.7	19.1	19.1	20.2	20.3	20.2
2100	248.7	249.6	278.4	280.5	272.7	19.1	19.1	20.3	20.4	20.3
2400	274.3	274.6	301.5	303.1	294.5	19.1	19.1	20.6	20.5	20.4
2700	295.6	294.5	320.2	322.4	313.2	19.2	19.2	21.2	20.7	20.7
3000	311.3	308.8	333.9	336.3	327.3	19.5	19.6	22.1	21.1	21.4
3300	325.7	323.6	347.2	349.0	340.7	20.0	20.5	23.2	21.8	22.7
3600	338.8	336.7	358.6	360.6	352.9	21.0	22.0	24.5	23.0	24.8
3900	350.2	348.1	369.1	371.0	364.0	22.5	24.0	26.1	24.8	27.4
4200	359.9	358.2	376.8	378.7	372.4	24.6	26.6	28.0	27.1	30.4
4500	367.7	367.1	383.2	385.4	379.3	27.2	29.6	30.2	30.2	33.7
4800	374.7	373.6	388.8	390.1	385.2	30.1	32.8	32.7	33.6	37.1
5100	380.5	379.9	393.9	393.4	390.3	33.1	36.0	35.3	37.1	40.5
5400	386.6	386.4	399.2	397.8	395.8	36.3	39.1	38.1	40.7	43.7
5700	391.7	392.1	403.9	402.4	400.6	39.4	42.1	41.0	44.2	46.8
6000	396.3	397.0	408.0	406.2	404.8	42.4	44.9	44.0	47.5	49.7
6300	400.2	401.8	411.6	409.3	408.2	45.1	47.6	47.0	50.7	52.5

Table 4-35: Masonry wall shroud temperature 470°C: front embedded thermocouple temperatures closest to shroud at lower level, L-F1 to L-F10

	Temperature (°C)									
	location									
Time (s)	L-F1	L-F2	L-F3	L-F4	L-F5	L-F6	L-F7	L-F8	L-F9	L-F10
0	19.6	19.7	19.7	19.7	19.8	19.6	19.6	19.7	19.6	19.5
300	20.0	20.2	20.1	20.0	20.1	19.9	19.8	20.0	19.9	19.8
600	24.6	25.3	24.8	24.2	24.5	23.3	22.8	23.8	23.7	22.8
900	39.0	41.3	39.3	37.9	38.4	33.8	33.3	35.8	36.2	33.1
1200	63.5	69.1	64.1	63.2	63.0	53.9	53.7	57.5	59.9	52.8
1500	92.5	101.9	93.1	95.1	93.1	80.0	82.9	84.7	91.5	79.2
1800	117.0	129.6	116.9	121.9	118.8	102.7	108.5	108.1	118.4	104.4
2100	136.7	153.6	137.7	145.1	140.6	120.8	127.0	126.9	140.5	124.9
2400	156.3	178.6	158.6	170.3	162.3	138.8	147.8	146.0	163.8	144.8
2700	176.1	203.7	179.1	195.9	184.0	157.3	170.3	165.1	187.7	164.9
3000	195.0	227.2	197.9	220.3	204.0	174.7	191.8	182.8	210.8	183.7
3300	212.5	248.6	215.1	242.7	222.1	190.8	212.0	199.0	232.5	200.8
3600	229.0	268.4	231.0	263.4	238.8	205.9	231.0	214.3	252.6	216.7
3900	244.1	286.4	245.7	282.2	254.2	220.0	248.5	228.7	271.0	231.3
4200	258.0	302.8	259.3	299.1	268.1	233.2	264.8	242.1	287.8	244.9
4500	270.7	317.9	271.5	314.5	280.5	245.4	279.7	254.5	303.0	257.2
4800	282.3	331.5	282.6	328.0	291.8	256.9	293.5	266.0	316.6	268.7
5100	292.6	343.2	292.6	339.8	301.9	267.4	306.0	276.3	328.8	279.2
5400	302.1	353.6	301.8	350.3	311.2	277.1	317.3	285.8	339.7	288.9
5700	310.9	363.1	310.4	359.7	319.7	286.3	327.8	294.7	349.7	297.8
6000	318.8	371.4	318.2	368.1	327.5	294.8	337.4	302.9	358.5	306.1
6300	326.0	378.9	325.4	375.6	334.7	302.7	346.2	310.5	366.5	313.6

Table 4-36: Masonry wall shroud temperature 470°C: front embedded thermocouple temperatures closet to shroud at middle level, M-F1 to M-F5

	Temperature (°C)				
	location				
Time (s)	M-F1	M-F2	M-F3	M-F4	M-F5
0	19.4	19.5	19.7	19.4	20.0
300	20.0	20.0	20.4	19.9	20.7
600	24.6	24.9	25.8	24.4	26.1
900	38.0	39.4	40.5	38.1	41.4
1200	61.9	66.4	66.1	64.1	68.1
1500	91.0	99.4	96.3	96.4	98.2
1800	116.6	126.6	120.5	122.6	122.8
2100	138.8	152.4	142.7	146.2	144.1
2400	159.7	178.9	164.1	170.2	165.0
2700	180.2	205.4	184.9	194.4	185.4
3000	199.1	230.2	204.0	217.6	204.1
3300	216.2	252.6	221.2	239.1	221.2
3600	232.0	273.0	237.0	259.1	237.1
3900	246.6	291.2	251.6	277.5	251.7
4200	259.8	307.6	264.9	294.3	265.1
4500	271.5	322.0	276.7	309.2	277.0
4800	282.2	334.6	287.3	322.6	288.0
5100	291.7	345.6	296.8	334.5	297.9
5400	300.4	355.3	305.6	345.2	307.1
5700	308.5	364.1	313.8	354.9	315.8
6000	316.0	371.9	321.3	363.6	323.7
6300	322.9	378.9	328.2	371.4	330.9

Table 4-37: Masonry wall shroud temperature 470°C: front embedded thermocouple temperatures closest to shroud at upper level, U-F1 to U-F10

	Temperature (°C)									
	location									
Time (s)	U-F1	U-F2	U-F3	U-F4	U-F5	U-F6	U-F7	U-F8	U-F9	U-F10
0	20.1	20.4	21.0	20.2	19.7	19.4	19.9	19.7	19.7	19.8
300	22.6	22.0	22.4	21.7	20.9	20.3	20.7	20.4	20.5	20.4
600	37.2	32.6	31.2	30.8	28.8	27.5	27.5	26.7	27.9	26.7
900	65.4	55.4	52.2	53.0	48.8	45.7	46.2	45.6	50.1	46.9
1200	102.1	90.7	85.0	88.7	80.9	75.4	78.7	76.6	86.2	81.0
1500	139.1	126.3	119.4	125.9	115.2	106.8	112.1	107.9	120.7	115.7
1800	173.8	159.6	149.1	158.6	144.6	132.3	140.0	133.3	152.1	145.4
2100	199.8	186.9	174.0	185.6	168.3	155.3	166.4	156.8	179.9	169.5
2400	222.2	212.3	196.1	210.9	189.8	176.4	192.0	178.2	206.3	191.2
2700	242.5	236.8	216.8	235.4	210.1	196.4	217.1	198.7	231.9	211.6
3000	259.5	258.8	235.0	257.3	227.9	214.2	240.2	217.3	255.0	229.6
3300	274.2	278.4	251.1	277.0	243.7	230.0	261.1	234.0	275.6	245.6
3600	287.7	296.5	266.1	295.2	258.4	244.7	280.3	249.5	294.5	260.6
3900	300.0	313.0	279.9	311.9	272.0	258.4	297.8	263.9	311.8	274.5
4200	311.1	327.9	292.4	327.1	284.2	271.0	313.5	277.1	327.2	287.1
4500	320.6	340.7	303.3	340.3	294.6	282.1	327.3	288.7	340.4	298.1
4800	328.8	351.9	313.1	351.2	304.1	292.1	339.5	299.1	352.1	308.0
5100	335.7	361.7	321.4	360.8	312.6	301.1	350.0	308.3	362.1	316.9
5400	342.1	370.4	328.9	369.4	320.5	309.4	359.5	316.8	371.1	324.9
5700	348.2	378.3	336.2	377.3	327.9	317.2	368.0	324.8	379.1	332.4
6000	353.8	385.1	342.9	384.2	334.6	324.3	375.6	332.1	386.2	339.3
6300	358.9	391.2	349.1	390.4	340.9	331.0	382.4	338.8	392.4	345.5

Table 4-38: Masonry wall shroud temperature 470°C: middle embedded thermocouple temperatures at lower level, L-M1 to L-M6

	Temperature (°C)					
	location					
Time (s)	L-M1	L-M2	L-M3	L-M4	L-M5	L-M6
0	19.6	19.6	19.7	19.6	19.6	19.5
300	19.6	19.6	19.7	19.6	19.6	19.5
600	19.6	19.6	19.7	19.6	19.6	19.5
900	19.6	19.6	19.7	19.6	19.6	19.5
1200	19.8	19.7	19.8	19.7	19.8	19.7
1500	20.3	20.2	20.4	20.1	20.4	20.3
1800	21.7	21.2	22.1	21.2	22.0	21.7
2100	25.2	23.8	26.5	23.7	26.2	25.5
2400	32.8	29.6	34.9	29.6	36.6	34.6
2700	43.2	38.5	45.4	38.3	51.0	50.4
3000	54.3	49.4	55.9	47.7	64.0	68.4
3300	64.1	59.8	64.9	56.3	73.1	79.7
3600	72.0	68.4	72.1	63.7	78.9	86.0
3900	78.1	75.0	77.7	69.9	82.7	89.3
4200	82.8	79.8	81.8	75.0	84.8	91.2
4500	86.3	83.3	85.0	79.3	86.8	92.4
4800	89.2	86.0	87.5	82.8	88.5	93.1
5100	91.4	88.2	89.6	85.8	90.2	93.7
5400	93.0	90.3	91.3	88.3	91.8	94.5
5700	94.3	92.0	92.9	90.5	93.4	95.8
6000	95.8	93.7	94.5	92.4	94.9	97.8
6300	97.8	95.4	96.5	94.2	96.7	100.4

Table 4-39: Masonry wall shroud temperature 470°C: middle embedded thermocouple temperatures at middle level, M-M1 to M-M3

	Temperature (°C)		
	location		
Time (s)	M-M1	M-M2	M-M3
0	19.0	19.7	19.9
300	19.0	19.7	19.9
600	18.9	19.7	19.9
900	18.9	19.7	20.0
1200	19.1	19.9	20.1
1500	19.5	20.3	20.6
1800	20.8	21.4	21.9
2100	23.9	24.2	25.9
2400	30.4	30.8	34.4
2700	39.1	41.0	45.2
3000	48.9	52.7	56.8
3300	58.8	63.2	66.7
3600	67.8	71.7	74.4
3900	75.1	77.9	80.1
4200	80.4	82.4	84.1
4500	84.1	85.3	86.8
4800	86.7	87.6	88.7
5100	88.4	89.4	90.2
5400	89.7	91.0	91.4
5700	90.7	92.5	92.4
6000	91.7	94.0	93.2
6300	92.6	95.4	94.1

Table 4-40: Masonry wall shroud temperature 470°C: middle embedded thermocouple temperatures at upper level, U-M1 to U-M6

	Temperature (°C)					
	location					
Time (s)	U-M1	U-M2	U-M3	U-M4	U-M5	U-M6
0	19.7	20.1	19.8	19.5	19.6	19.3
300	19.7	20.1	19.8	19.5	19.6	19.3
600	19.7	20.1	19.8	19.5	19.6	19.3
900	19.8	20.1	19.7	19.5	19.5	19.3
1200	20.4	20.3	19.9	19.7	19.7	19.4
1500	23.2	21.0	20.4	20.5	20.4	20.2
1800	29.4	22.6	21.8	22.3	22.2	22.5
2100	39.4	27.0	25.3	28.0	29.5	31.2
2400	50.4	35.6	32.3	38.2	43.3	45.0
2700	60.1	46.5	41.7	49.9	58.4	58.8
3000	68.0	57.6	52.2	60.7	70.6	69.3
3300	74.2	67.4	62.0	69.7	78.7	76.3
3600	79.0	75.0	70.1	76.7	83.6	80.8
3900	82.9	80.7	76.3	82.0	86.9	83.9
4200	86.4	84.7	81.1	85.9	89.0	86.2
4500	89.4	87.6	84.8	88.9	90.6	88.2
4800	92.0	89.9	87.7	91.4	91.9	90.0
5100	94.1	91.7	90.0	93.1	93.0	91.7
5400	96.3	93.4	91.8	94.2	94.2	93.3
5700	99.2	95.2	93.3	95.2	95.6	95.2
6000	102.9	97.2	95.0	96.8	97.4	97.8
6300	107.0	99.7	97.3	99.3	99.6	101.1

Table 4-41: Masonry wall shroud temperature 470°C: back embedded thermocouple temperatures at lower level, L-R1 to L-R10

	Temperature (°C)									
	location									
Time (s)	L-R1	L-R2	L-R3	L-R4	L-R5	L-R6	L-R7	L-R8	L-R9	L-R10
0	19.6	19.3	19.6	19.5	19.5	19.3	19.4	19.2	19.3	19.3
300	19.6	19.3	19.6	19.5	19.5	19.3	19.4	19.2	19.4	19.3
600	19.6	19.3	19.6	19.5	19.5	19.3	19.4	19.2	19.3	19.3
900	19.6	19.3	19.6	19.5	19.5	19.3	19.4	19.2	19.3	19.3
1200	19.6	19.3	19.6	19.5	19.5	19.3	19.4	19.2	19.3	19.2
1500	19.6	19.3	19.6	19.5	19.5	19.3	19.4	19.2	19.3	19.3
1800	19.6	19.4	19.6	19.5	19.5	19.3	19.4	19.2	19.3	19.3
2100	19.7	19.4	19.7	19.6	19.7	19.4	19.4	19.2	19.3	19.3
2400	19.8	19.6	19.8	19.7	20.1	19.7	19.5	19.3	19.4	19.3
2700	20.2	20.0	20.0	20.0	20.9	20.4	19.9	19.6	19.8	19.4
3000	21.3	20.9	20.5	20.7	22.3	21.5	20.7	20.3	20.6	19.9
3300	23.3	22.1	21.5	21.9	24.2	23.2	21.9	21.7	22.0	20.7
3600	26.0	23.7	23.2	23.3	26.6	25.3	23.3	23.8	23.7	22.3
3900	29.2	25.6	25.5	25.1	29.4	27.7	25.0	26.5	25.8	24.8
4200	32.8	27.8	28.4	27.2	32.6	30.4	26.8	30.2	28.3	28.4
4500	36.5	30.3	31.7	29.6	35.9	33.4	28.9	33.4	30.9	33.1
4800	40.3	32.9	35.2	32.2	39.3	36.5	31.1	37.2	33.8	38.4
5100	43.9	35.7	38.7	34.9	42.7	39.7	33.5	40.7	36.7	43.7
5400	47.5	38.6	42.2	37.7	46.0	42.9	36.0	44.1	39.8	48.8
5700	50.8	41.6	45.5	40.6	49.3	46.1	38.6	47.3	43.0	53.4
6000	54.0	44.5	48.6	43.6	52.4	49.3	41.4	50.3	46.2	57.5
6300	57.0	47.5	51.6	46.5	55.4	52.4	44.2	53.1	49.4	61.1

Table 4-42: Masonry wall shroud temperature 470°C: back embedded thermocouple temperatures at middle level, M-R1 to M-R5

	Temperature (°C)				
	location				
Time (s)	M-R1	M-R2	M-R3	M-R4	M-R5
0	20.0	20.0	19.9	19.7	19.9
300	20.0	20.0	19.9	19.7	19.9
600	20.0	20.0	19.9	19.7	19.9
900	20.0	20.0	19.9	19.7	19.9
1200	20.0	20.0	19.9	19.7	19.9
1500	20.0	20.0	19.9	19.8	19.9
1800	20.1	20.1	20.0	19.9	19.9
2100	20.2	20.2	20.1	19.9	20.0
2400	20.3	20.3	20.2	20.0	20.1
2700	20.7	20.7	20.4	20.5	20.4
3000	21.3	21.6	21.0	21.5	20.9
3300	22.5	22.9	22.0	22.7	22.0
3600	24.2	24.7	23.7	24.2	23.5
3900	26.7	26.9	26.0	25.9	25.6
4200	29.8	29.4	29.1	27.8	28.2
4500	33.6	32.2	32.6	30.0	31.2
4800	37.8	35.2	36.5	32.5	34.5
5100	42.0	38.4	40.5	35.2	37.9
5400	46.0	41.8	44.5	38.0	41.4
5700	49.7	45.2	48.3	41.0	44.8
6000	53.0	48.7	52.0	44.1	48.1
6300	56.1	52.1	55.4	47.2	51.3

Table 4-43: Masonry wall shroud temperature 470°C: back embedded thermocouple temperatures at upper level, U-R1 to U-R10

	Temperature (°C)									
	location									
Time (s)	U-R1	U-R2	U-R3	U-R4	U-R5	U-R6	U-R7	U-R8	U-R9	U-R10
0	19.3	19.0	19.0	19.8	19.8	19.9	20.2	20.1	19.8	20.1
300	19.3	19.0	19.1	19.8	19.9	19.9	20.2	20.1	19.8	20.2
600	19.3	19.0	19.0	19.8	19.9	19.9	20.2	20.1	19.8	20.2
900	19.3	19.0	19.1	19.8	19.9	19.9	20.3	20.1	19.8	20.2
1200	19.3	19.1	19.1	19.8	20.0	19.9	20.3	20.1	19.8	20.2
1500	19.3	19.1	19.1	19.8	20.0	19.9	20.4	20.1	19.8	20.2
1800	19.5	19.1	19.2	19.8	20.1	19.9	20.4	20.2	20.0	20.3
2100	20.2	19.2	19.2	19.9	20.1	20.0	20.5	20.3	20.1	20.5
2400	21.7	19.3	19.2	19.9	20.2	20.2	20.8	20.5	20.5	20.7
2700	24.2	19.8	19.6	20.0	20.5	20.6	21.7	21.0	21.4	21.2
3000	27.5	20.6	20.2	20.4	21.2	21.6	23.0	22.2	22.8	22.4
3300	31.2	21.8	21.2	21.1	22.4	23.3	24.6	24.2	24.4	24.4
3600	35.2	23.2	22.9	22.2	24.4	25.7	26.5	27.0	26.2	27.3
3900	39.3	25.0	25.3	24.0	27.1	28.5	28.7	30.3	28.2	30.8
4200	43.3	27.1	28.3	26.3	30.1	31.6	31.2	34.0	30.5	34.5
4500	47.2	29.5	31.9	29.1	33.4	34.9	33.8	37.7	32.9	38.3
4800	50.9	32.2	35.7	32.3	36.9	38.2	36.6	41.3	35.5	42.0
5100	54.4	35.2	39.7	35.7	40.4	41.6	39.4	44.8	38.2	45.5
5400	57.7	38.4	43.6	39.2	43.8	45.0	42.3	48.1	41.0	48.8
5700	60.9	41.7	47.3	42.6	47.1	48.2	45.2	51.2	43.8	51.9
6000	63.9	45.1	50.9	45.8	50.3	51.2	48.0	54.1	46.6	54.9
6300	66.6	48.4	54.3	48.9	53.2	54.2	50.8	56.8	49.4	57.6

This page left blank

5. COMPARISONS AND DISCUSSION

In this section the measurements of each experiment within a series are consolidated into tables to provide a summary of the data and to facilitate comparison of the fuels for discussion.

5.1. Jet fires

Table 5-1 provides the mass flow rate, average SEP, and average dimensions for each jet fire experiment. The results indicate that ethylene has the highest average SEP among the fuels and is about 20% and 14% greater than ethane and isopentane, respectively. The mass flow rate for isopentane is the highest among the fuels and is about 34% and 26% higher than ethylene and ethane, respectively. All experiments have subsonic flow rates and tend to be dominated by momentum forces as the fuel exits causing the initial portion of the flame to be horizontal, but then tilts vertically due to buoyancy forces.

Table 5-1: Measurements of mass flow rate, SEP, and dimensions for jet fire experiments.

Measurement	ethane	ethylene	isopentane
Mass flow rate (kg/s)	3.1 ± 0.09	2.9 ± 0.08	3.9 ± 0.1
Mass flow rate at exit* (kg/s)	1.9 ± 0.05	1.7 ± 0.05	2.3 ± 0.06
Average SEP (kW/m^2)	158.4 ± 12.4	190.5 ± 9.0	166.8 ± 12.8
Average projected horizontal length** (m)	12.5 ± 2.3	13.8 ± 1.8	17.3 ± 1.4
Average projected vertical height*‡ (m)	7.7 ± 2.6	8 ± 1.8	9.8 ± 2.6

*Assumes a discharge coefficient of 0.6.
**Projected onto north-south axis.
‡From ground.

Table 5-2 provides average wind speed and direction at different heights for the jet fire experiments. The wind speed and direction for ethane and ethylene are the most similar among the fuels, whereas the wind conditions for isopentane are very different. Due to similar wind conditions the heat flux gauge measurements can be compared for ethane and ethylene. Figure 5-1 shows a comparison of heat flux measurements from the gauges for these two fuels. The heat flux for ethylene is greater than that of ethane at most locations. Note that heat flux gauges that failed during experiments are not included in Figure 5-1. The higher heat flux for ethylene is expected based on the comparison of the average SEP.

Table 5-2: Wind conditions for jet fire experiments.

Height (m)	ethane	ethylene	isopentane
	Average wind speed (m/s)		
2	1.9 ± 0.2	2.2 ± 0.3	2.9 ± 0.6
5	2.2 ± 0.3	2.7 ± 0.4	3.5 ± 0.8
7.6	2.3 ± 0.2	3.1 ± 0.5	3.8 ± 0.8
	Average wind direction (deg)		
2	107.1 ± 3.7	106.3 ± 6.3	227.0 ± 9.6
5	108.7 ± 3.8	110.2 ± 3.6	226.3 ± 0.8
7.6	111.1 ± 4.2	115.2 ± 3.8	228.2 ± 0.8
Average among heights	109.0 ± 3.9	110.6 ± 4.5	227.2 ± 9.0

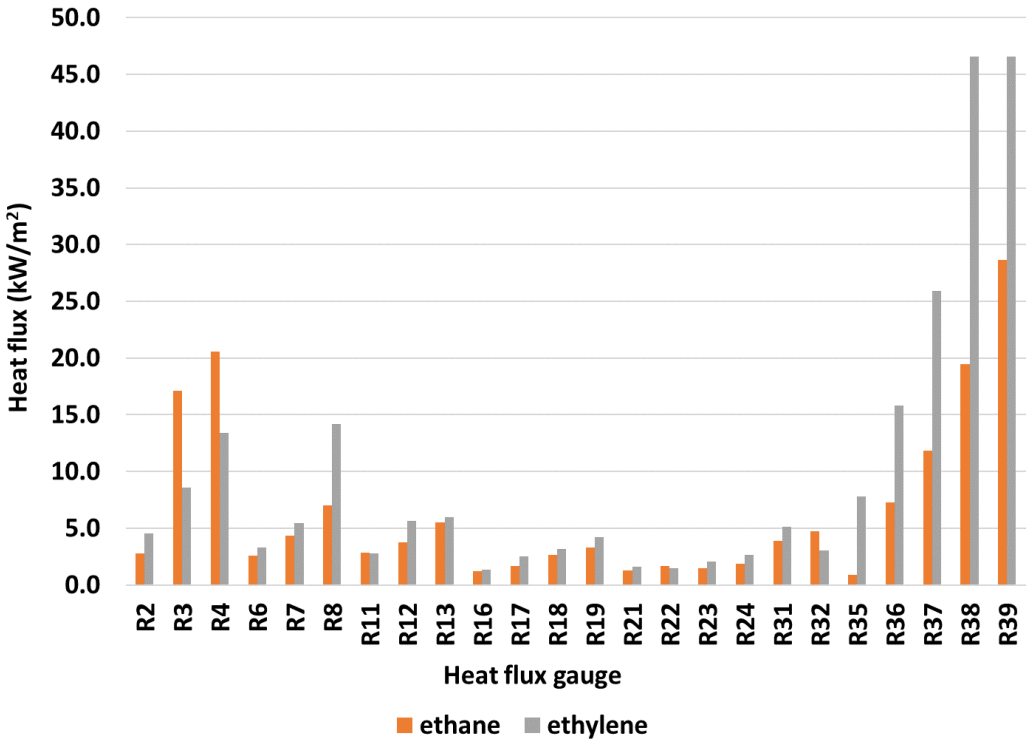

Figure 5-1: Heat flux gauge measurements for the ethane and ethylene jet fires

The horizontal flame length for all jet fires is compared to a correlation by Bradley, et al [12]. The correlation is derived from the analysis of numerous datasets of jet flame measurements. The correlation uses the following equations.

$$U^* = \left(\frac{u}{S_L}\right) Re_L^{-0.4} \left(\frac{P_e}{P_{atm}}\right) \quad \text{Eq. 5.1.1}$$

$$Re_L = \frac{S_L D}{\upsilon} \quad \text{Eq. 5.1.2}$$

$$\frac{H}{D} = 81 U^{*0.46} \quad \text{Eq. 5.1.3}$$

Where, u is the exit velocity, S_L is the laminar burning velocity, P_e is the exit pressure, P_{atm} is the atmospheric pressure, and υ is the kinematic viscosity. The parameters used to calculate the horizontal flame length are provided in Table 5-3. Table 5-4 provides a comparison of the horizontal flame length between the correlation (eq. 5.3) and experiment. The comparison indicates that the correlation overpredicts the length by about 15% for ethane and underpredicts 18% for ethylene and 6% for isopentane which is fairly good agreement overall.

Table 5-3: Parameters for calculated flame length using correlation [12]

	ethane	ethylene	isopentane
S_L (m/s) [13]	0.27	0.3	0.399
D (m)	0.0762	0.0762	0.0762
υ(m2/s)	2.10E-07	2.29E-07	4.63E-07
ρ (kg/m3)	485	519	643
P_e	712918	537791	732918
P_{atm}	81317	81030	81520
u	19	17	18
Re_L	9.79E+04	9.98E+04	6.56E+04
Flow rate (kg/s)	1.86	1.74	2.34

Table 5-4: Comparison of horizontal jet flame length to correlation [12]

Projected horizontal distance	ethane	ethylene	isopentane
correlation	14.4	11.3	16.3
experiment	12.5 ± 2.3	13.8 ± 1.8	17.3 ± 1.4

The radiative power of the jet fires is compared to data presented in ref. [14] which provides guidance on hazard assessment regarding jet fires based on the compilation of experimental studies. The radiative power is the product of the SEP and the surface area of the flame. Determining the surface area is difficult since the jet fires displayed highly contorted flame shapes that cannot be represented by a simple geometry. Numerous cameras at different view angles including a view from above are needed to determine the surface area. Thus, this comparison is presented as a range based on the single IR camera used for the jet fire experiments. Based on an image in which all camera frames are

averaged, the area encompassing temperatures above 1150 K is determined for each jet fire. The temperature of 1150K is used since it is the threshold temperature used to determine the average SEP. To determine the radiative power the measured average SEP is then multiplied by this area.

The area from the average image is projected and captures only one view of the flame. Thus, it is underestimated by at least a factor of two and most likely three. Thus, to carry out the comparison the area is multiplied by a factor of two for a lower range and three for an upper range for the radiative power. This range is compared to data in ref. [14] which is provided in a plot of radiative power versus power based on the heat release rate. The comparison is provided in Table 5-5 and indicates that the estimated powers are within the range of data presented in ref. [14]. Note that most studies by other researchers have not measured SEP using an IR camera, but rather have inferred it based on radiometer measurements and idealized flame shapes. Thus, direct comparison of SEP measurements is not presented.

Table 5-5: Comparison of power to data presented in ref. [14] for the jet fires.

Fuel	Heat release rate (MW)	Power (MW)		Power from ref. [14] (MW)	
		Lower range	Upper range	Lower range	Upper range
Ethane	80	18	28	13	47
Ethylene	90	20	29	10	40
Isopentane	103	37	55	14	50

5.2. Pool fires

Table 5-6 provides the average mass flow rate and release temperature for each pool fire experiments over time periods of steady wind speeds. The mass flow rate for the ethane pool fire experiment is the highest among the tests by approximately 40% for both ethylene and propane, and 268% for isopentane. In performing the first experiment, the propane pool fire, the diptubes indicated that a liquid layer of at least ½" did not form within the pool. Initially, it was believed that the diptubes malfunctioned, but subsequent to the propane experiment they proved to be functioning correctly by performing a small test using diesel fuel. Thus, to reduce evaporation during filling a plastic sheet was installed on top of the 5-m pool for the next experiment, the ethane pool fire. Despite the installation of the plastic sheet a liquid layer greater than ½" failed to develop. Once the ethane was ignited the mass flow rate was increased in an attempt to form a detectable liquid layer which still did not form. Given these findings, the mass flow was set at a lower rate for the ethylene pool fire. Thus, this is the reason why the mass flow rate of ethane is higher than the ethylene and propane pool fire experiments.

Since the fire encompassed the entire pool area for each of these fuels, a liquid layer did form, however, not enough to be detectable by the diptubes. A liquid layer of about 3" formed during the isopentane pool fire. Thus, its fuel regression rate is driven by the heat transferred from the fire to the pool rather than being controlled as with the other pool fire experiments.

Table 5-6: Average mass flow rate and release temperature for pool fire experiments.

Measurement	Ethane		Ethylene		Propane	Isopentane
	Period 72-100 s	Period 129-156 s	Period 320-346 s	Period 433-462 s	Period 328-378 s	Period 356-383 s
Mass flow rate (kg/s)	3.2 ± 0.08	3.0 ± 0.07	2.3 ± 0.1	2.3 ± 0.1	2.2 ± 0.05	0.87 ± 0.02
Temperature (°C)	-64.5 ± 0.1	-65.2 ± 0.1	-84.0 ± 0.01	-84.2 ± 0.03	-18.2 ± 0.01	0.1 ± 0.01

Table 5-7 provides the average flame length and average tilt with respect to the vertical direction for each pool fire experiments over time periods of steady wind speeds. The ethylene pool fire resulted in the highest average flame tilt since it was performed in the highest wind speed (~4-5 m/s) among the tests as indicated in Table 5-8. The ethane and iso-pentane pool fires were performed in the lowest wind speed (~1 m/s) and the propane pool fire in an intermediate wind speed (~3 m/s).

Table 5-7: Average flame length and tilt angle for the pool fire experiments.

Measurement	Ethane		Ethylene		Propane	Isopentane
	Period 72-100 s	Period 129-156 s	Period 320-346 s	Period 433-462 s	Period 328-378 s	Period 356-383 s
	Station 1 (south)					
Length (m)	25.3 ± 2.8	25.7 ± 3.0	16.7 ± 2.3	16.9 ± 3.2	21.0 ± 3.6	10.3 ± 1.6
Tilt Angle (deg)	12.4 ± 2.6	0.7 ± 7.8	52.4 ± 6.2	51.3 ± 6.3	40.9 ± 6.9	-18.3 ± 5.3
	Station 2 (west)					
Length (m)	20.9 ± 2.9	23.2 ± 3.6	6.1 ± 1.3	7.3 ± 1.4	10.1 ± 1.4	11.6 ± 2.2
Tilt Angle (deg)	10.4 ± 2.7	10.7 ± 4.4	-18.5 ± 11.3	-27.3 ± 12.7	23.9 ± 7.9	-13.7 ± 6.2

Table 5-8: Average wind conditions for the pool fire experiments.

	Ethane		Ethylene		Propane	Isopentane
	Period 72-100 s	Period 129-156 s	Period 320-346 s	Period 433-462 s	Period 328-378 s	Period 356-383 s
Height (m)	Average wind speed (m/s)					
2	1.0 ± 0.04	1.2 ± 0.04	3.37 ± 0.13	4.16 ± 0.14	2.57 ± 0.10	1.40 ± 0.07
5	0.9 ± 0.03	1.3 ± 0.03	3.80 ± 0.15	4.88 ± 0.13	2.77 ± 0.12	1.45 ± 0.03
7.6	1.0 ± 0.04	1.2 ± 0.04	3.96 ± 0.15	5.11 ± 0.15	2.90 ± 0.10	1.44 ± 0.05
	Average wind direction (deg)					
2	255.0 ± 5.0	268.9 ± 8.6	225.9 ± 7.3	239.0 ± 4.8	277.4 ± 12.3	99.5 ± 3.9
5	283.7 ± 5.8	285.7 ± 13.6	222.6 ± 6.1	239.3 ± 6.5	278.5 ± 11.4	96.4 ± 4.0
7.6	291.4 ± 8.0	288.4 ± 8.5	221.2 ± 5.0	241.7 ± 1.5	279.0 ± 12.3	99.7 ± 3.7
Average direction among heights	276.7 ± 19.8	281.0 ± 13.3	223.2 ± 2.4	240.0 ± 1.4	278.3 ± 12.0	98.6 ± 1.9

Table 5-9 provides the temporally and spatially averaged SEP among the experiments averaged over periods of steady wind conditions. Table 5-10 provides the temporally and spatially averaged SEP among the experiments averaged over the entire test duration. The results indicate that the ethylene pool fire resulted in the overall highest average SEP over the entire test duration. The average SEP for the ethane and propane pool fires is not significantly lower and are within 10 kW/m^2 to that of ethylene. The average SEP for the isopentane pool fire test is about 30 kW/m^2 lower than ethylene. Based on visual observations, all pool fire experiments produced significant amounts of smoke except for the ethane pool fire which produced relatively minor amounts of smoke.

Table 5-9: Surface emissive power for pool fire experiments averaged over periods of steady wind conditions.

SEP*† (kW/m^2)					
Ethane		Ethylene		Propane	Isopentane
Period 72-100 s	Period 129-156 s	Period 320-346 s	Period 433-462 s	Period 328-378 s	Period 356-383 s
Station 1 (south)					
167.3 ± 13.1	170.7 ± 13.5	188.4 ± 11.5	188.3 ± 10.0	185.9 ± 13.4	154.4 ± 9.5
Station 2 (west)					
175.2 ± 13.2	182.2 ± 14.6	185.7 ± 8.9	185.9 ± 9.2	200.2 ± 12.9	162.6 ± 12.7

*Spatially averaged
†Corrected for atmospheric attenuation

Table 5-10: Surface emissive power for pool fire experiments averaged over entire test duration.

SEP*† (kW/m^2)			
Ethane	**Ethylene**	**Propane**	**Isopentane**
Entire test duration			
Station 1 (south)			
171.2 ± 14.9	186.3 ± 13.3	178.6 ± 16.0	155.0 ± 10.3
Station 2 (west)			
184.8 ± 16.3	188.2 ± 10.9	189.1 ± 14.1	162.9 ± 11.5

*Spatially averaged
†Corrected for atmospheric attenuation

It should be noted that for an equivalent comparison of the pool fire experiments reported here to experiments performed by other researchers, the fuels should be of similar composition. One notable example in which comparison could erroneously be made is for propane. The propane pool fire used almost pure propane (99.0%+), whereas past Liquified Petroleum Gas (LPG) pool fire experiments have used a mixture of fuels. For instance, a 20-m diameter pool fire performed by Mizner and Eyre [15] used a mixture of propane, propene, methane, and ethane. They report that during the time of stabilized burning the composition of the pool was 60% propane and 40% propene after the methane and ethane burned off first due to their lower boiling points. They calculated an average SEP of 48 kW/m^2 based on using heat flux gauge measurements and a solid flame model representing the flame as a tilted cylinder. Significant amount of smoke covering the luminous portion of the flame was reported.

For pool fires, smoke production plays a key role in affecting the average SEP and flame emissivity. If a fire is optically thick, the flame emissivity will be approximately equal to one. For most heavy hydrocarbons, fires greater than about 3 m in diameter will emit thermal radiation from the outer portion of the flame envelope originating at a layer near the surface and not within the flame's interior. This criterion defines the condition for a fire to be considered optically thick. Optically thin fires will emit thermal radiation predominantly from product gases, mainly water and carbon dioxide. For optically thin fires, the flame is considered transparent. However, for optically thick fires, the local soot production becomes saturated to the point that local radiation emission is absorbed within the flame envelope except within a relatively thin layer compared to the volume of the fire near the plumes surface.

For optically thick fires, the SEP, which is the energy emitted per unit time per unit area, is a function of the surface area of the flame and not the volume as for optically thin fires which have lower SEP values due to the predominance of gas band radiation. For increasing diameters, the combustion process becomes increasingly incomplete due to radiative losses and limited oxygen supply to its interior with the result that increasing levels of soot and smoke are produced. Soot particles at temperatures above ~600°C are responsible for the luminosity of the fire. If they are not oxidized within the flame, they will escape the flame envelope and cool and become part of the smoke from the fire. Smoke is made up of a mixture of gases, condensable aerosols, and particulate matter from a fire. Carbon particulates, or soot, is included as a particulate matter of smoke and is the black clouds often seen around fires. A sufficient layer of black smoke will absorb a sizable portion of the radiation emitted from the flame, resulting in a much lower emission to the surroundings and hence reduced

thermal hazard distances. Large hydrocarbon fires on the order of 10's of meters or greater will generate copious quantities of smoke. A relatively small portion of the flame will be persistently visible near the base of the fire, with the rest shrouded in black smoke. Thus, with increasing pool diameter the average SEP over the flame will first increase with increasing fire diameter due to reaching the optically thick limit and then decrease with further increases in fire diameter due to the increasing smoke layer coverage [16].

A comparison of the burn rate with various fuels and pool diameters is provided in Figure 5-2. Although the fuel was controlled for ethane, ethylene, and propane pool fires, their rates are plotted for reference. The burn rate of the isopentane pool fire is within the range of other fuels. Note that the burn rates of the ethane, ethylene, and propane pool fires are similar to that measured for large scale tests burning LNG and LPG.

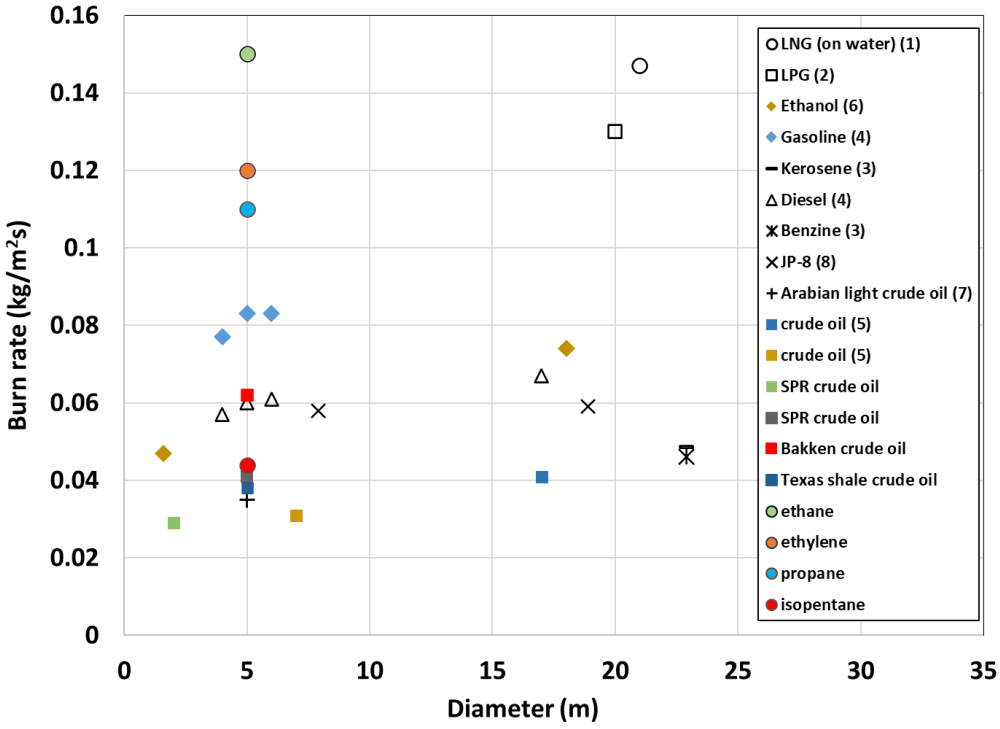

Figure 5-2: Burn rates for various fuels and pool diameters

In Figure 5-3 measured average flame length is compared to a commonly used correlation for flame height developed by Heskestad [17]. The correlation is based upon theoretical and experimental observations and is of the following form.

$$\frac{L}{D} = 3.7Q^{*2/5} - 1.02 \qquad \text{Eq. 5.2.1}$$

Q* is a dimensionless heat release rate and is defined as,

$$Q^* = \frac{\dot{m}H_c}{\rho_a T_a C_{p_a}\sqrt{gD}D^2} \qquad \text{Eq. 5.2.2}$$

where $\dot{m}$ is the mass release rate (kg/s), H_c is the heat of combustion, ρ_a (kg/m^3) is the density at atmospheric conditions, T_a is the atmospheric temperature (K), C_{p_a} is the specific heat at atmospheric conditions, g (m/s^2) is the gravity constant, and D (m) is the pool diameter. Dimensional flame height correlations offer the advantage of being able to predict the flame height of large-scale pool fires using gas burners at fixed diameters of small-scale. With gas burners the mass flow rate can be controlled, allowing for the measurement of flame height over a range of Q* values. This correlation does not include the effect of wind which tends to shorten a flame. Thus, the comparison is most applicable to the ethane and isopentane pool fires since they were performed in nearly quiescent conditions. The comparison indicates that the correlation slightly under predicts the average flame height by about 4% for the ethane and propane pool fires, and over predicts for the ethylene and isopentane pool fires by about 22% and 24%, respectively. However, given the outdoor conditions of the pool fire experiments the correlation provides good agreement overall.

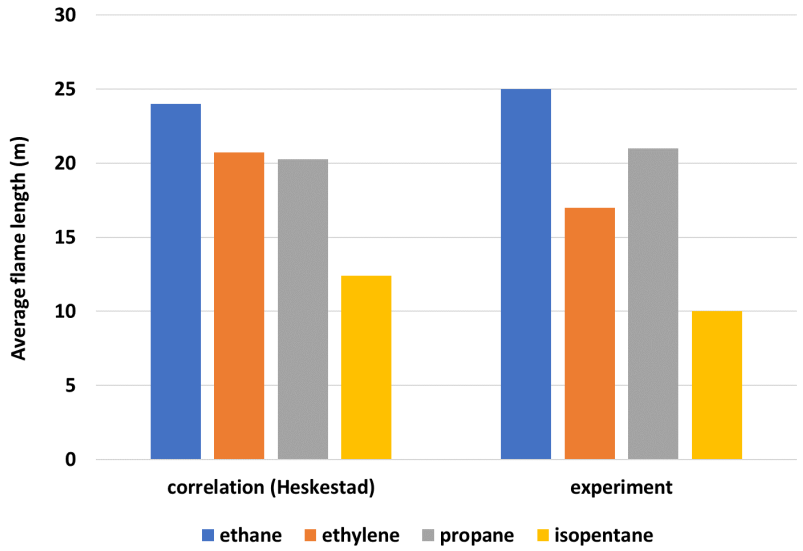

Figure 5-3: Comparison of measured average flame length to correlation

A comparison of average surface emissive power with other experiments using different fuels for various pool diameters is provided in Figure 5-4. The average SEP of 5-m diameter pools illustrates how it can significantly differ depending on the fuel. Overall, the average SEP of ethane, ethylene, propane, and isopentane is about a factor of 2.5 greater than that of diesel, gasoline, and crude oils. Heavier hydrocarbons will produce more smoke than lighter hydrocarbons such as the pure fuels used in the present experiments.

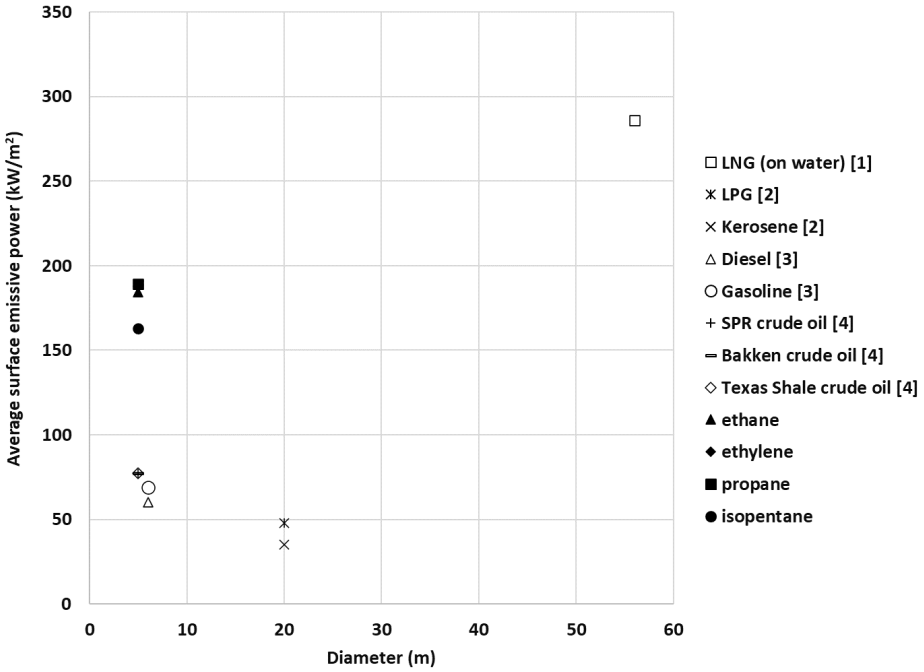

Figure 5-4: Average SEP for various fuels and pool diameters (fuels: 1- ref. [18], 2 – ref. [15], 3 – ref. [19], 4 –ref. [20]).

5.3. Fireballs

Table 5-11 provides the conditions of the fuel within the test tank just prior to release for each experiment. The mass released is similar among all tests and release pressures are within 15 psig of each other. The temperature is much lower for ethane and ethylene since they are cryogens. The temperature of isopentane is a result of heating the tank to bring the isopentane to a thermodynamic state for the fuel to flash upon release. If the isopentane was released at atmospheric temperatures a significant amount of fuel would spill on the ground and would burn similar to a pool fire due to its liquid state.

Table 5-12 provides the weather conditions for each fireball experiment. The ethane has the highest wind speeds of about 4 m/s, whereas for ethylene and isopentane there was low wind speeds of about 0.8 m/s and 1 m/s, respectively.

Table 5-11: Conditions of fuel within test tank for fireball experiments.

Condition	Ethane	Ethylene	Isopentane
Tank pressure (psig)	181	175	164
Temperature (°C)	-32.8	-59.4	114
Amount of fuel (kg)(gallons)	1157 (656)	1153 (613)	1150 (481)
Density (kg/m3)	466	497	509

Table 5-12: Weather conditions for fireball experiments.

Height (m)	ethane	ethylene	isopentane
	Average wind speed (m/s)		
2	3.8 ± 0.4	0.88 ± 0.02	1.11 ± 0.1
5	4.2 ± 0.4	0.81 ± 0.03	0.81 ± 0.06
7.6	4.5 ± 0.4	0.75 ± 0.02	0.94 ± 0.1
	Average wind direction (deg)		
2	229.5 ± 7.5	56.9 ± 10.4	101.2 ± 11.2
5	237.1 ± 21.4	47.7 ± 13.4	107.8 ± 15.3
7.6	231.8 ± 13.2	60.0 ± 9.0	126.1 ± 17.1
Average among heights	232.8 ± 21.4	54.9 ± 10.9	111.8 ± 14.6

Measurements of SEP, effective diameter, height, and timing is provided in Table 5-13. Also provided are derived quantities based on measurement such as power and the power-fractional height product. Note that height is measured from the center of the fireball to the ground. The results indicate that isopentane has the highest maximum average SEP of 381 kW/m^2, followed by ethane with an intermediate value of 350 kW/m^2, and ethylene with the lowest value of 299 kW/m^2. This is in contrast to the results for the jet fire and pool fire experiments where ethylene had the highest average SEP among the fuels.

The thermal dose derived from the heat flux measurements shown in Figure 5-5 indicates that ethane and isopentane fireballs are almost a factor of two higher than that of the ethylene fireball. Note that in comparing the quantities in Table 5-13, the maximum power and maximum power-fractional height product both reflect the trend of the thermal dose.

Table 5-13: Measurements averaged between south and east stations for fireball experiments

Measurement	Ethane	Ethylene	Isopentane
Time at maximum power (s)	2.9	6.3	1.7
Maximum power (MW)	1404	692	1171
Total energy (MJ)	3796	4806	4869
Average SEP at maximum power*† (kW/m^2)	341	260	373
Maximum average SEP*†	350	299	381
Time at maximum average SEP (s)	3.3	0.9	2.3
Height at maximum average SEP (m)	62	15	61
Effective diameter at maximum average SEP (m)	74	34	62

Measurement	Ethane	Ethylene	Isopentane
Maximum SEP** † (kW/m^2)	667	751	756
Time to maximum SEP (s)	3.1	4.1	2.3
Effective diameter at maximum power (m)	76	64	67
Maximum effective diameter (m)	78	78	67
Maximum rise height (m)	139	173	164
Height at maximum power (m)	55	109	44
Maximum P(1-h/h_{max}) (MW)	921	387	855
Time at Maximum P(1-h/h_{max}) (MW)	2.2	2.2	1.7
Height at maximum P(1-h/h_{max}) (m)	42	37	44
Effective diameter at maximum P(1-h/h_{max}) (m)	74	53	67
Time at total burnout (s)	8.0	13.0	10.0

*Spatially averaged
**Local maximum
†Corrected for atmospheric attenuation

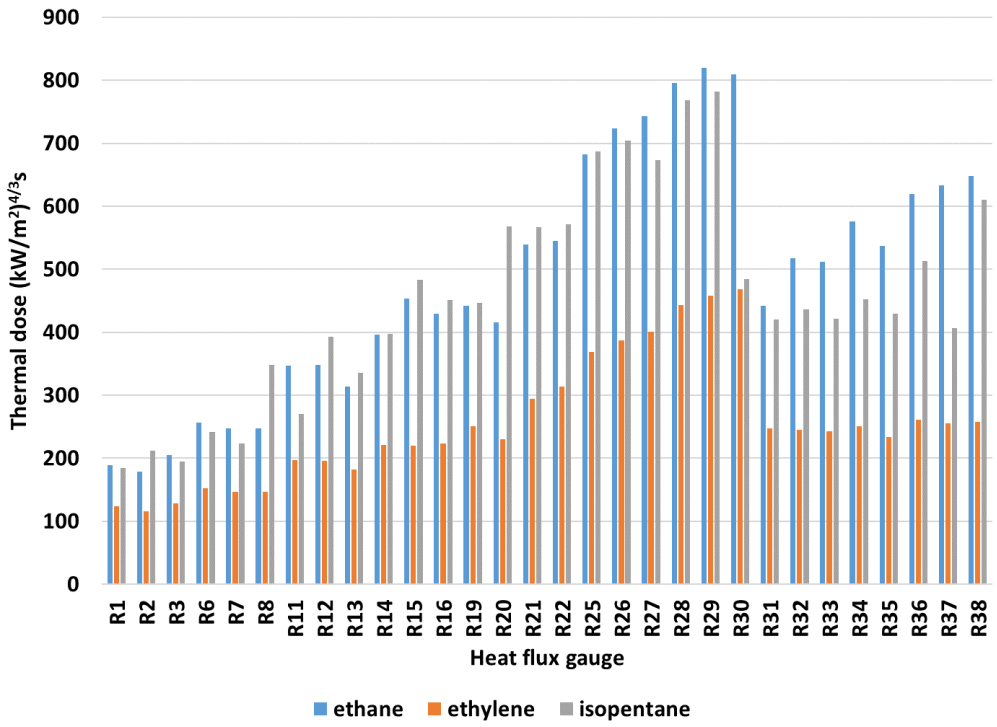

Figure 5-5: Thermal dose calculated from heat flux gauges for fireball experiments

A time sequence of each fireball experiment is shown in Figure 5-6. The ethane fireball produces the least smoke among the fuels, whereas ethylene appears to produce the most. This is evident in comparing the remnant smoke rings of ethylene and isopentane. The ethane fireball did not produce

a smoke ring. The images also show how the ethylene fireball persists for longer than the other fireballs and forms a growing toroidal shape. This persistence is reflected in the plateu of the heat flux gauge measurements following a peak as mentioned is section 3.3.3.

Figure 5-6: Time sequence of each fireball experiment

In Figure 5-7 the maximum effective diameter versus fuel mass for the fireball experiments is compared to data by other researchers. The diameter is termed 'effective' since it is calculated by using area measurements to determine an equivalent diameter assuming a perfect circle. The comparison indicates that maximum effective diameter for ethane and ethylene is higher than other fuels for similar masses, whereas isopentane is similar. The maximum effective diameter is also compared to a correlation in ref. [21] in which the maximum diameter is given by $D=5.5m^{1/3}$, where m is the fuel mass (kg). Figure 5-8 provides a comparison of Robert's correlation with experimental data and indicates overall good agreement with results from the present experiments.

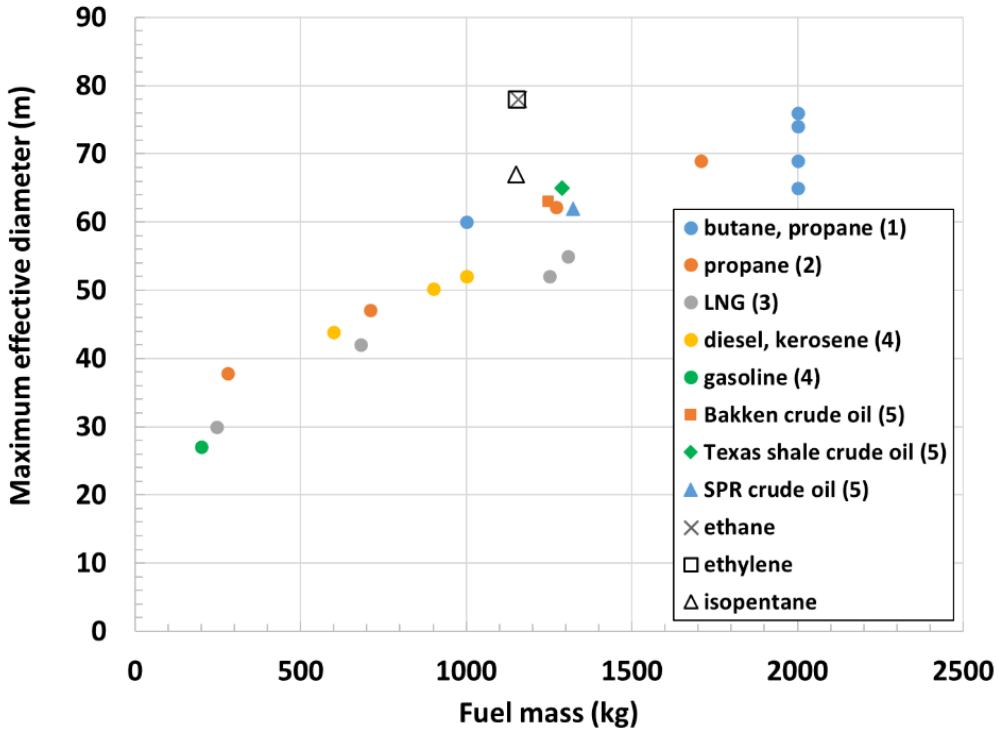

Figure 5-7: Comparison of maximum effective diameter as a function of fuel mass (1 – ref. [22], 2 - [23], 3 – ref. [24], 4 – ref. [25], 5 – ref. [20])

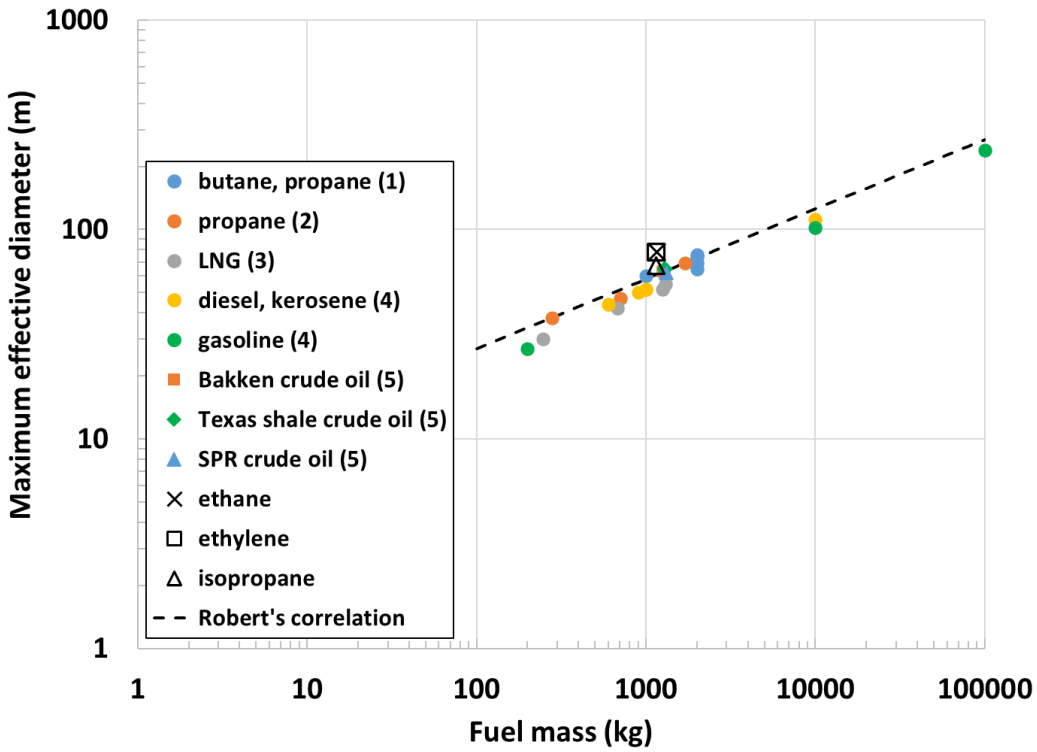

Figure 5-8: Comparison of maximum effective diameter with Robert's correlation (1 – ref. [22], 2 - [23], 3 – ref. [24], 4 – ref. [25], 5 – ref. [20])

A comparison of maximum rise height versus fuel mass to other experimental studies is provided in Figure 5-9. The maximum rise height is defined as the height at which the fireball starts to break up. Since the criteria defining breakup are not provided in these studies, this is an approximate comparison. The comparison indicates that the maximum rise heights of the ethane, ethylene, and isopentane are much higher than those of the other fuels. This can be attributable to the different test configuration. In the present tests, the fuel was directed only in the upward vertical direction, whereas in the other studies with exception of the crude oils the fuel was released in a semi-spherical pattern with horizontal and vertical trajectories due to how the tank was failed. This type of configuration results in the fireball first expanding along the ground and then lifting off to form a spherical shape.

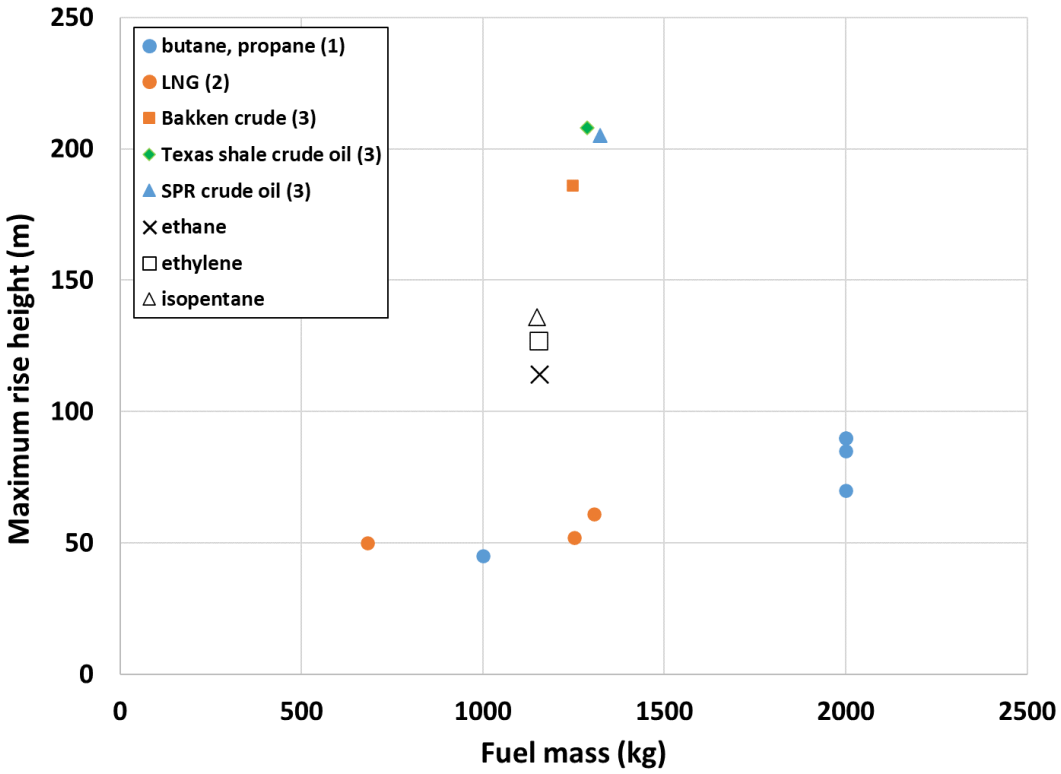

Figure 5-9: Comparison of maximum rise height versus fuel mass (1 – ref. [22], 2 – ref. [24], 3 – ref. [20])

A comparison of duration until extinction versus fuel mass with experiments performed by other researchers is provided in Figure 5-10. The definition for extinction used in previous studies is the time at which visible thermal radiation ceases. The comparison indicates ethylene has the longest duration among the experiments, while ethane and isopentane are within the range of crude oils and one LNG experiment reported in ref. [24]. Note, however, that results can differ by up to 50% among repeat tests as shown in ref. [22].

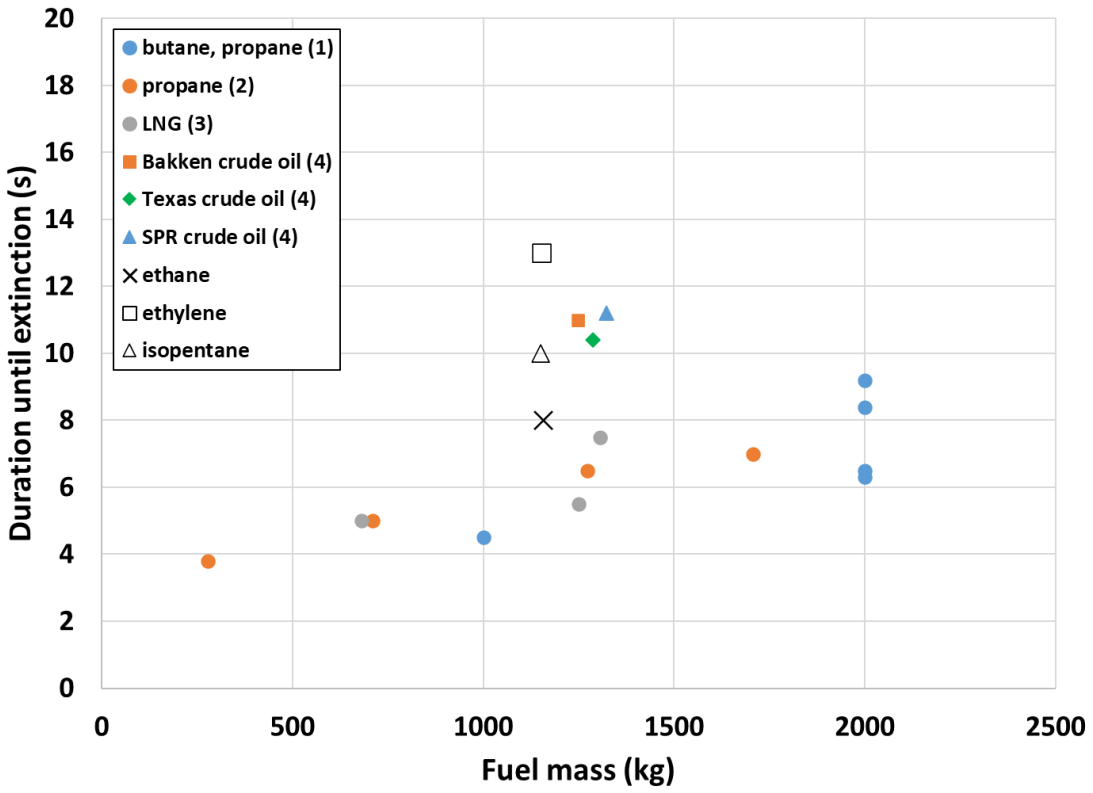

Figure 5-10: Comparison of fireball duration (1 – ref. [22], 2 – ref. [23], 3 – ref. [24], 4– ref. [20])

A comparison of the maximum average SEP of the fireball experiments with data by other researchers is provided in Figure 5-11. This comparison is approximate in that the criteria differ among the studies. For instance, in ref. [22] the spatially averaged SEP is averaged over the duration in which the fireball size is nearly constant. In ref. [23] the spatially averaged SEP at maximum power and at maximum area is reported. In ref. [24], the spatially averaged SEP 3 seconds after rupture is reported. In ref. [25] a range of spatially averaged SEP values that appear to be based on the maximum energy released is reported. The values for the experiments reported here are based on the maximum value of the average SEP based on the IR camera measurements. The comparison indicates that the fireballs from the present tests are within the range of values previously found for propane and butane fireballs of similar fuel masses.

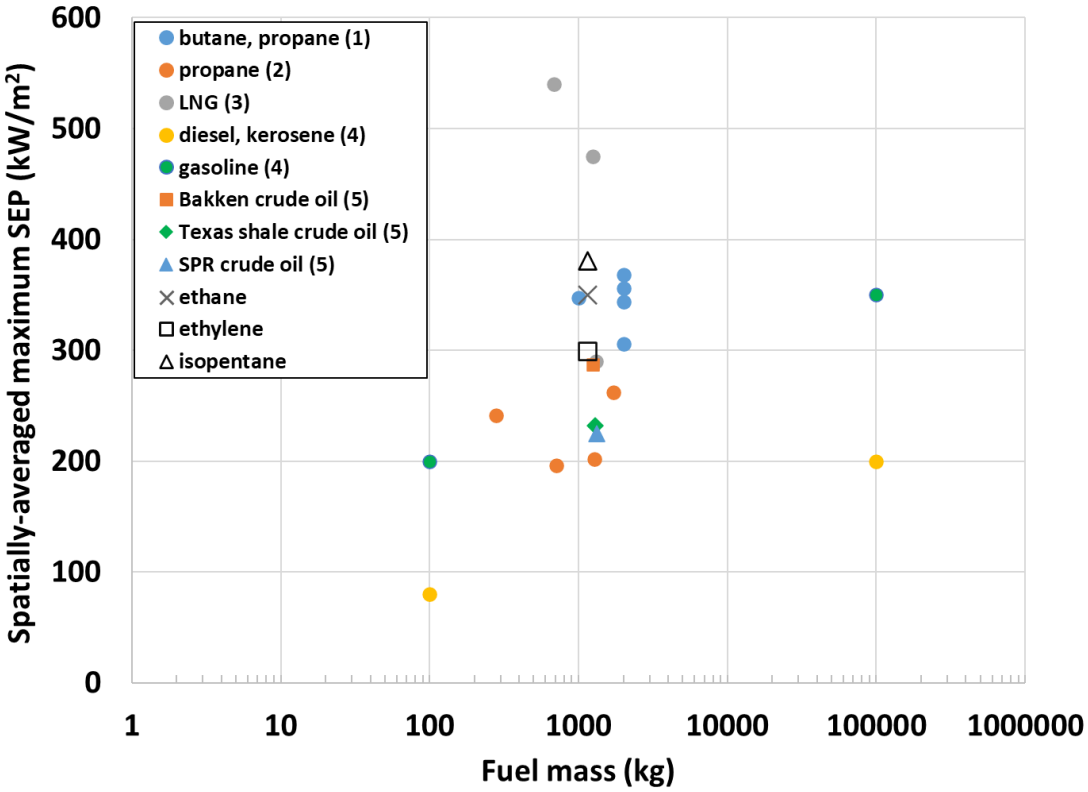

Figure 5-11: Comparison of maximum average SEP (1 – ref. [22], 2 – ref. [23], 3 – ref. [24], 4 – ref. [25], 5 – ref. [20])

6. SUMMARY AND CONCLUSIONS

1. Data sets are extensive and are provided with uncertainty values. Data can be used to compare with simulation results.
2. All fuels produced significant amounts of smoke with the exception of ethane which produced relatively little smoke.
3. For the jet fire experiments, the average projected flame lengths ranged from 12.5 m to 17.3 m for exit mass flow rates ranging from 1.7 kg/s to 2.3 kg/s.
4. For the 5-m diameter pool fire experiment, average flame lengths range from 10.3 m to 25.7 m for exit mass flow rates ranging from 0.87 kg/s to 3.2 kg/s.
5. For the fireball experiments, the maximum effective diameter ranged from 67 m to 78 m with maximum rise heights ranging from 139 m to 164 m .
6. For a given fuel, the average SEP significantly increases by a factor of up to 2.4 for the fireball experiments compared to the jet and pool fire experiments.
7. The highest average SEP among the fuels for the jet and pool fire experiments resulted from ethylene with a value of approximately 190 kW/m^2 for both types of fires. The maximum average SEP of the ethylene fireball is 299 kW/m^2.
8. The average SEP of the ethane jet fire and pool fire differed with values of about 158 kW/m^2 versus 177 kW/m^2, and the maximum average SEP for the ethane fireball is 350 kW/m^2.
9. The average SEP of the isopentane jet fire and pool fire differed with values of about 167 kW/m^2 versus 158 kW/m^2. The highest maximum average SEP among the fuels for the fireball experiments resulted from isopentane with a value of 381 kW/m^2.
10. The average SEP of the propane pool fire is about 185 kW/m^2 which is 4.3% higher and 2.7% lower compared to the ethane and ethylene pool fires, respectively, and 15% higher than the isopentane pool fire.
11. The thermal dose for the ethane and isopentane fireballs are almost a factor of two higher than that of the ethylene fireball. The maximum power and maximum power-fractional height product both reflect the trend of the thermal dose.

This page left blank

REFERENCES

[1] A. Luketa, "Model Evaluation Protocol for Fire Models Involving Fuels at Liquefied Natural Gas Facilities," Sandia National Laboratories, SAND2022-6812, Albuquerque, NM, May 2022.

[2] R. Corlett, "Gas Fires with Pool-like Boundary Conditions: Further Results and Interpretations," *Combustion and Flame,* vol. 14, pp. 351-360, 1970.

[3] D. L. Brenchley, "Assessment of Research and Development (R&D) Needs in Ammonia Safety and Environmental Controls," Pacific Northwest Laboratory, sec. 5.4, September 1981.

[4] J. Nakos, "Uncertainty Analysis of Steady State Incident Heat Flux Measurements in Hydrocarbon Fuel Fires," Sandia National Laboratories, SAND2005-7144, Albuquerque, NM, December 2005.

[5] S.R Campos, et al., "Orifice plate meter field performance: Forumulation and Validation in Multiphase Flow Conditions," *Experimental Thermal and Fluid Science,* vol. 58, pp. 93-104, 2014.

[6] R. Corlett, "Gas fires with pool-like boundary conditions," *Combustion and Flame,* vol. 12, no. 1, pp. 19-32, Feb. 1968.

[7] K. McGrattan, et al., "Fire Dynamics Simulator Techical Reference Guide Volume 3: Validation," NIST Special Publication 1018-3, Sixth Edition, April 4, 2025.

[8] O. W. Blodgett, Design of Welded Structures, James F. Lincoln Arc Welding Foundation, 1972.

[9] J. Nakos, J. Pantuso and J. Bentz, "Final Report - Summary of Thermal Testing of the Furnace Characterization Unit (FCU) for the Coast Guard," Sandia National Laboratories, SAND2000-1534, Albuquerque, NM, 2000.

[10] ASTM 549-23, *Standard Specification for Perlite Loose Fill Insulation,* 2023.

[11] E. King, S. Todd and K. Kelley, "Perlite: Thermal Data and Energy Required for Expansion. Report of Investigation," Bureau of Mines, Washington, D.C., 1948.

[12] D. Bradley, P. Gaskell, X. Gu and A. Palacios, "Jet flame heights, lift-off distances, and mean flame surface density for extensive ranges of fuels and flow rates," *Combustion and Flame,* vol. 164, pp. 400-409, 2016.

[13] A. Gosh, N. Munoz-Munoz, K. P. Chatelain and D. Lacoste, "Laminar burning velocity of hydrogen, methane, ethane, ethylene, and propane flames at near-cryogenic temperatures," *Applications in Energy and Combustion Science,* vol. 12, pp. 1-10, 2022.

[14] B. Lowesmith, G. Hankinson, M. Acton and G. Chamerlain, "An Overview of the Nature of Hydrocarbon Jet Fire Hazards in the Oil and Gas Industry and a Simplified Approach to Assessing the Hazards," *Trans IChemE,* vol. 85, no. Part B, pp. 207-220, May 2007.

[15] G. Mizner and E. J. A., "Large-Scale LNG and LPG pool fires," EFCE Publication Series (European Federation of Chemical Engineering) 25, 147-163., 1982.

[16] H. Koseki and G. Mulholland, "The Effect of Diameter on the Burning of Crude Oil Pool Fires," *Fire Technology,* pp. 54-65, Feb. 1991.

[17] G. Heskestad, "Fire Plumes," in *SFPE Handbook of Fire Protection Engineering (2nd ed.)*, NFPA and SFPE, 1995, pp. 2-9 - 2-19.

[18] T. Blanchat, P. Helmick, R. Jensen, A. Luketa, R. Deola, J. Suo-Anttila, J. Mercier, T. Miller, A. Ricks, R. Simpson, B. Demosthenous, S. Tieszen and M. Hightower, "The Pheonix Series Large Scale LNG Pool Fire Experiments," Sandia National Laboratories, Albuquerque, NM, 2010, SAND2010-8676.

[19] M. Munoz, J. Arnaldos, J. Casal and E. Planas, "Analysis of the geometric and radiative characteristics of hydrocarbon pool fires," *Combustion and Flame,* vol. 139, pp. 273-277, 2004.

[20] A. Luketa, B. Blanchat, D. Lord, J. Hogge, A. Cruz-Cabrera and R. Allen, "Pool Fire and Fireball Experiments in Support of the US DOE/DOT/TC Crude Oil Characterization Research Study," Sandia National Laboratories, Albuquerque, NM, SAND2019-9189, August 2019.

[21] A. Roberts, "Thermal radiation from releases of LPG from pressurised storage," *Fire Safety Journal,* vol. 4, pp. 197-212, 1982.

[22] D. Johnson and M. Pritchard, "Large scale experimental study of Boiling Liquid Expanding Vapour Explosions (BLEVEs)," *GASTECH (1990): International LNG/LPG Conference and Exhibitiion Conference Papers,* vol. 1, no. 14, pp. session 3, paper 3.3, 1990.

[23] T. Roberts, A. Gosse and S. Hawksworth, "Thermal Radiation from Fireballs on Failure of Liquefied Petroleum Gas Storage Vessels," *Trans IChemE,* vol. 78, no. Part B, pp. 184-192, 2000.

[24] S. Betteridge and L. Phillips, "Large scale pressurised LNG BLEVE experiments," *Institution of Chemical Engineers Symposium,* no. 160, paper 35, pp. 353-364, 2015.

[25] S.B. Dorofeev, et al., "Fireballs from Deflagration and Detonation of Heterogeneous Fuel-rich Clouds," *Fire Safety Journal,* vol. 25, pp. 323-336, 1995.

APPENDIX A. LIVERY SYSTEM, INVESTIGATIONS, AND COMPOSITIONS

A.1. Delivery system for jet and pool fire experiments

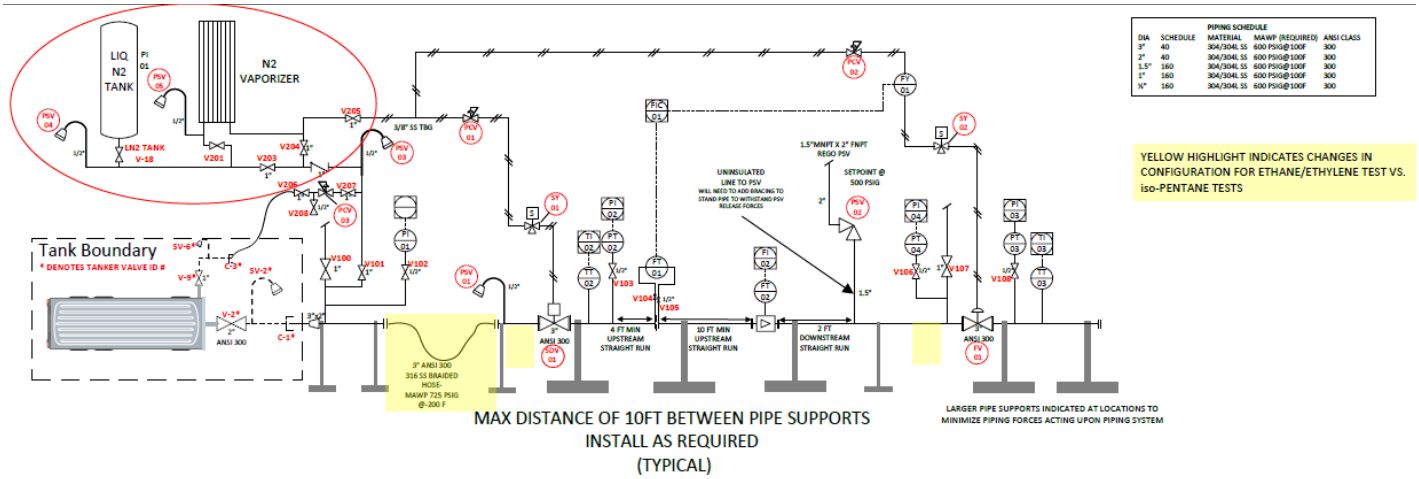

Figure A-1. Jet fire testing configuration ethane/ethylene.

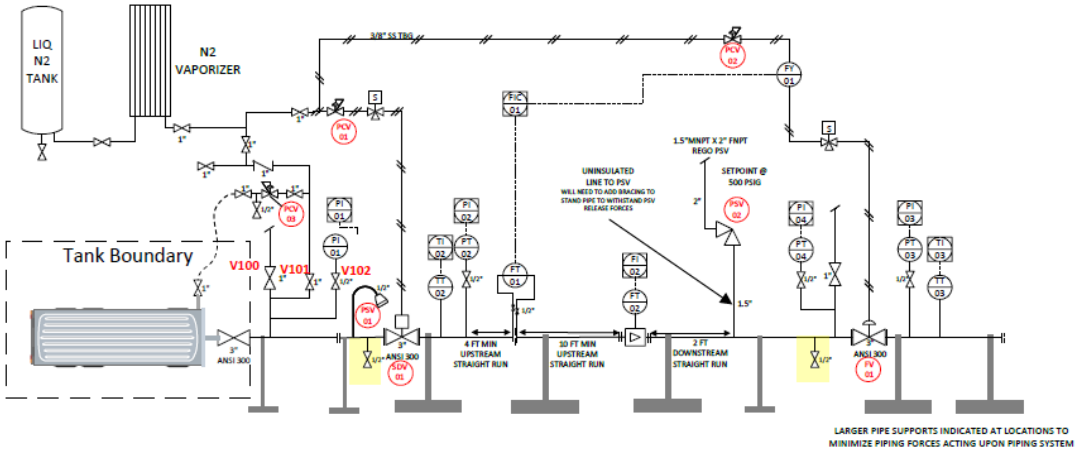

Figure A- 2. Jet fire testing configuration iso-pentane.

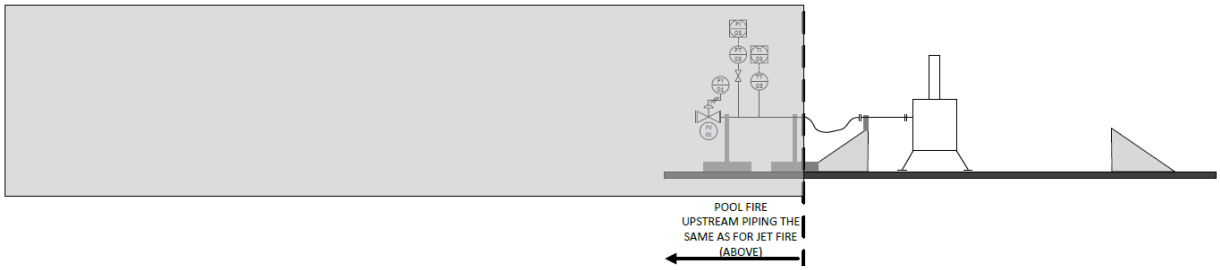

Figure A- 3. Pool fire testing configuration.

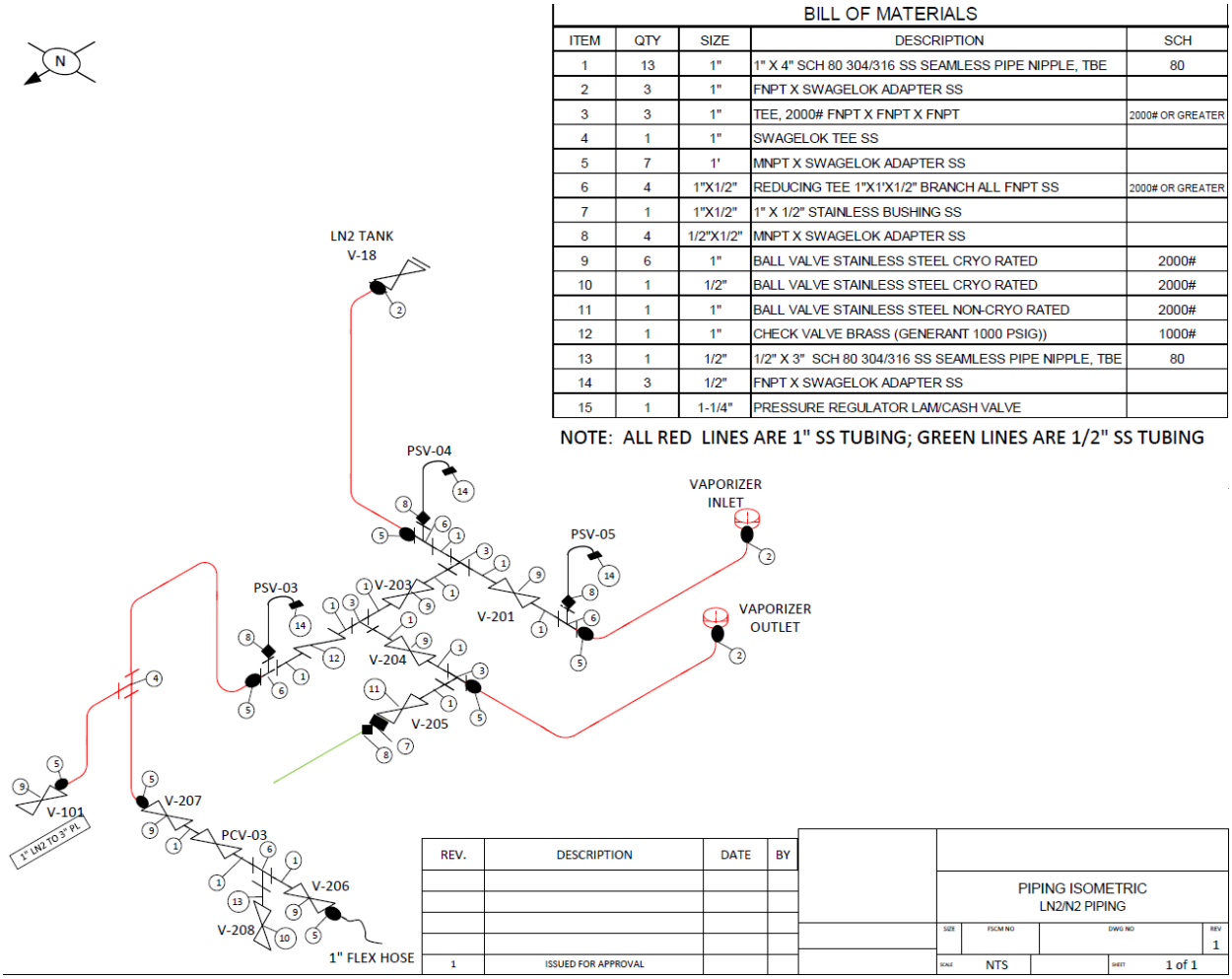

BILL OF MATERIALS

ITEM	QTY	SIZE	DESCRIPTION	SCH
1	13	1"	1" X 4" SCH 80 304/316 SS SEAMLESS PIPE NIPPLE, TBE	80
2	3	1"	FNPT X SWAGELOK ADAPTER SS	
3	3	1"	TEE, 2000# FNPT X FNPT X FNPT	2000# OR GREATER
4	1	1"	SWAGELOK TEE SS	
5	7	1'	MNPT X SWAGELOK ADAPTER SS	
6	4	1"X1/2"	REDUCING TEE 1"X1'X1/2" BRANCH ALL FNPT SS	2000# OR GREATER
7	1	1"X1/2"	1" X 1/2" STAINLESS BUSHING SS	
8	4	1/2"X1/2"	MNPT X SWAGELOK ADAPTER SS	
9	6	1"	BALL VALVE STAINLESS STEEL CRYO RATED	2000#
10	1	1/2"	BALL VALVE STAINLESS STEEL CRYO RATED	2000#
11	1	1"	BALL VALVE STAINLESS STEEL NON-CRYO RATED	2000#
12	1	1"	CHECK VALVE BRASS (GENERANT 1000 PSIG))	1000#
13	1	1/2"	1/2" X 3" SCH 80 304/316 SS SEAMLESS PIPE NIPPLE, TBE	80
14	3	1/2"	FNPT X SWAGELOK ADAPTER SS	
15	1	1-1/4"	PRESSURE REGULATOR LAM/CASH VALVE	

NOTE: ALL RED LINES ARE 1" SS TUBING; GREEN LINES ARE 1/2" SS TUBING

Figure A- 4. Liquid nitrogen and vaporizer configuration.

A.2. Anhydrous ammonia investigation

To confirm previous researcher's findings regarding the inability for anhydrous ammonia to maintain a flame, a small-scale test is performed using a square gas burner. The anhydrous ammonia is tested in gaseous rather than liquid form to allow for immediate termination of its release if the fuel cannot be ignited or maintain a stable flame. In such an event a liquid test would pose the risk of vapor

dispersion which must be prevented due to ammonia's high toxicity. The American Conference of Governmental Industrial Hygienists recommend a threshold limit value (TLV) of 25 ppm averaged over 8 hours and 35 ppm as a short-term exposure limit. Exposure to a concentration at and above 300 ppm is considered immediately danger to life or health.

A 2.5 quart of anhydrous ammonia (99.995%) is used to supply gaseous ammonia to the gas burner as shown in Figure A- 5. The square gas burner is 1'x1'x1' and is of basic construction where an inlet allows introduction of the ammonia, and a square board placed above the inlet acts to diffuse the gas evenly. A screen is placed above the diffuser to support crushed rock which further enhances even dispersal across the surface of the burner. The inlet, diffuser, and supportive screen is show in Figure A- 6.

Two propane torches are positioned towards the burner for ignition as shown in Figure A- 7 . The test is carried out by first activating the propane torches followed by the release of the ammonia into the gas burner. Once the ammonia ignited the propane torches are deactivated. Several tests are performed to evaluate two fuel release pressures of 10 psi and 40 psi.

In all the tests the ammonia ignites but once the torches are terminated the flame extinguishes between 5-10 seconds afterwards. Thus, a flame could not be sustained for any of the experiments.

Figure A- 5: Ammonia 2.5-quart container.

Figure A- 6: Top view of gas burner showing (a) inlet (b) diffuser, and (c) screen to support crushed rock.

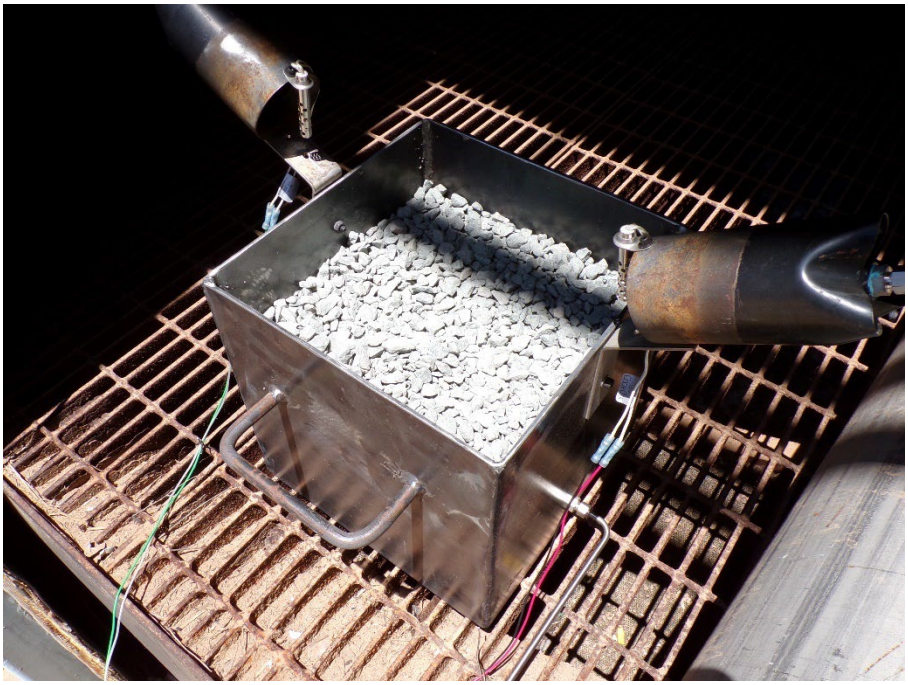

Figure A- 7: Gas burner with propane torches.

A.3. Composition of fuels

GAS INNOVATIONS

CERTIFICATE OF CONFORMANCE
ETHANE
REFRIGERANT

Guaranteed Specifications		Typical Analysi
95.0% +	Ethane	99.0% +
Sum of all impurities to	Propane	< 0.97 %
Be < 5 %	Methane	< 0.03 %
Sulfur < 1 PPM	Nitrogen	< 100 PPM
Moisture < 5 PPM	Oxygen	< 20 PPM
	CO + CO2	< 20 PPM
	Moisture	< 5 PPM
	Sulfur	< 0.50 PPM

Certified by: Christopher Pelc Date: 11/27/2024

** Liquid Phase Analysis – Reported in More Per Cent **

SO# 00219866

Cylinder Serial Number(s)
BULK LOAD – GI ISO
GSIN 000002-2

Batch Number
ETA-112724-REF

GAS INNOVATIONS

CERTIFICATE OF CONFORMANCE
ETHYLENE
REFRIGERANT GRADE

Guaranteed Specifications		Minimal Purity
99.5 % +	Ethylene	99.5 % +
Sum of all impurities to	Acetylene	< 5 PPM
be < 0.5 %	Carbon Dioxide	< 5 PPM
Water < 5 PPM	Carbon Monoxide	< 1 PPM
	Ethane	< 800 PPM
	Methane	< 200 PPM
	Nitrogen	< 300 PPM
	Oxygen	< 100 PPM
	Water	< 3 PPM
	Alcohols	< 1 PPM

"This document certifies that the contents of this finished goods container conform to the specifications listed. This confirmation is based upon analysis of the source raw material and does not reflect analysis of the finished goods container."

Certified by: Christopher Pelc Date: 11/27/2024

SO# 00219866

Cylinder Serial Number(s)
BULK LOAD – GI ISO
FTIU 535-053-6

Batch Number
ETY-112724-C

GAS INNOVATIONS

CERTIFICATE OF CONFORMANCE
PROPANE
C.P. GRADE

Guaranteed Specifications		Minimum Purity
99.0 % +	Propane	99.0 % +
Sum of all impurities to	Methane	< 0.05 %
be < 1.00 %	Ethane	< 0.05 %
Sulfur < 0.50 PPM	Propylene	< 0.20 %
Water < 5 PPM	Butanes	< 0.50 %
	Pentanes	< 0.20 %
Liquid Phase Analysis	BTEX	Not Detected
	Water	< 5 PPM
	Sulfur	< 0.50 PPM

Certified by: Christopher Pelc Date: 10/15/2024

SO# 00219866

GAS INNOVATIONS

CERTIFICATE OF CONFORMANCE
ISOPENTANE
C.P. GRADE

Guaranteed Specifications		Minimal Purity
99.0 % +	Isopentane	99.00 % +
Sum of all impurities to	Pentanes	< 0.60 %
be < 1.00 %	Propane	< 0.10 %
Sulfur < 0.50 PPM	Propylene	< 0.10 %
Water < 5 PPM	Butanes	< 0.20 %
Liquid Phase Analysis	Benzene	Not Detected
	Water	< 5 PPM
	Sulfur	< 0.50 PPM

Certified by: Christopher Pelc Date: 10/15/2024

SO# 00219866

Cylinder Serial Number(s)
BULK LOAD – GI ISO
242057-4

Batch Number
ISP-101524-C

DISTRIBUTION

Email—Internal

Name	Org.	Sandia Email Address
Michael Starr	08533	mjstarr@sandia.gov
Carlos Lopez	01532	carlope@sandia.gov
Technical Library	1911	sanddocs@sandia.gov

Email—External

Name	Company Email Address	Company Name
Scott Davis	Scott.G.Davis@gexcon.com	Gexcon
Bjorn Erling	Bjorn.Erling.Vembe@dnv.com	DNV
Jason Floyd	Jason.Floyd@ul.org	Underwriters Laboratory Fire Safety Research Institute
Bryant Hendrickson	bhendrickson@blueeandc.com	BLUE Engineering and Consulting
Andrew Kohout	Andrew.Kohout@ferc.gov	Federal Energy Regulatory Commission
Kevin McGrattan	kevin.mcgrattan@nist.gov	National Institute of Standards and Technology
Thach Nguyen	thach.d.nguyen@dot.gov	Pipeline and Hazardous Materials Safety Administration
James Stewart	James.Stewart@hse.gov.uk	Health and Safety Executive

This page left blank

Sandia National Laboratories

Sandia National Laboratories is a multimission laboratory managed and operated by National Technology & Engineering Solutions of Sandia LLC, a wholly owned subsidiary of Honeywell International Inc. for the U.S. Department of Energy's National Nuclear Security Administration under contract DE-NA0003525.